# STRUCTURE AND DYNAMICS OF BIOMOLECULES IN THE GAS PHASE USING VIBRATIONALLY AND ROTATIONALLY RESOLVED ELECTRONIC SPECTROSCOPY

by

**Jessica Anne Thomas**

B.S.Ed., Indiana University of Pennsylvania, 2002

Submitted to the Graduate Faculty of

Arts and Sciences in partial fulfillment

of the requirements for the degree of

Doctor of Philosophy

University of Pittsburgh

2011

UNIVERSITY OF PITTSBURGH

ARTS AND SCIENCES

This dissertation was presented by

Jessica Anne Thomas

It was defended on

April 1, 2011

and approved by

Committee Members:

Lillian Chong, Assistant Professor
Department of Chemistry, University of Pittsburgh

Sunil Saxena, Associate Professor
Department of Chemistry, University of Pittsburgh

Michel Mons, Researcher
Laboratoire Francis Perrin, CEA Saclay

Dissertation Advisor:

David W. Pratt, Professor
Department of Chemistry, University of Pittsburgh

**STRUCTURE AND DYNAMICS OF BIOMOLECULES IN THE GAS PHASE USING VIBRATIONALLY AND ROTATIONALLY RESOLVED ELECTRONIC SPECTROSCOPY**

Jessica Anne Thomas, Ph.D.

University of Pittsburgh, 2011

Rotationally resolved electronic spectroscopy is used to determine the rotational constants of small aromatic molecules. These rotational constants, when compared to calculated low energy structures, provide a precise description of the structure of the molecule. In addition, by comparing rotational constants for the structure in the ground and excited electronic states, as well as those associated with various vibronic transitions, an understanding of the dynamics of the molecule can be obtained. In this work, molecules containing double rings, including 1,3-benzodioxole, coumaran, and 1-phenylpyrrole, were studied using rotationally resolved electronic spectroscopy to determine their structures, low frequency vibrational motions, and changes in electronic distribution upon electronic excitation.

Laser ablation, a technique used to produce gas phase samples of moderately sized biomolecules with significantly less decomposition than with thermal vaporization, was used to obtain gas phase samples of short peptide sequences. These molecules were studied using a IR/UV double resonance technique which enabled the collection of IR spectra with resolved transitions in the amide A and OH stretch regions. Specifically, several short sequences found in a folding nucleus of β-lactoglobulin were compared to calculated structures in order to identify intramolecular interactions that stabilize the structures.

## TABLE OF CONTENTS

## LIST OF TABLES

## LIST OF FIGURES

## LIST OF SCHEMES

## LIST OF ABBREVIATIONS

| | |
|---|---|
| $0_0^0$ | electronic origin |
| $39_1^2$ | vibronic transition originating in $v''_{39}=1$ and terminating in $v'_{39}=2$ |
| $^1L_a$, $^1L_b$ | excited singlet states in Platt's notation |
| 1PP | 1-phenylpyrrole |
| Ac-Trp-$NH_2$ | acetyl-tryptophanamide |
| Ac-Trp-Tyr-$NH_2$ | acetyl-tryptophan-tyrosinamide |
| Ac-Trp-Tyr-Ser-$NH_2$ | acetyl-tryptophan-tyrosine-serinyl-amide |
| Ala | alanine |
| BDO | 1,3-benzodioxole |
| cc-pvdz | correlation-consistent polarized valence double-zeta basis set |
| $cm^{-1}$ | wavenumbers |
| $C_n$ | n-membered ring formed by a hydrogen bond in a peptide backbone |
| COU | coumaran |
| CT | charge transfer |
| CW | continuous wave |
| DFT-D | density functional theory with disperson |
| DMABN | 4,4-dimethylaminobenzonitrile |
| freq | frequency |
| FWHM | full width at half maximum |
| $\hat{H}$ | Hamiltonian |
| HOMO | highest occupied molecular orbital |
| ICT | intramolecular charge transfer |
| IR | infrared |
| J | total rotational angular momentum quantum number |
| JB95 | spectral fitting program |
| $K_a$, $K_c$ | component of total rotational angular momentum along *a*, *c*-axis |
| LE | locally excited state |
| Leu | leucine |
| LIF | laser induced fluorescence |
| LUMO | lowest unoccupied molecular orbital |
| MHz | megahertz |
| MP2 | second order Møller-Plesset |
| NATA | N-acetyl-tryptophanamide |
| $Nd^{3+}$:YAG | neodymium yttrium aluminum garnet laser |
| NH | nitrogen-hydrogen bond |
| NH-π | interaction between an NH bond and the π-electrons of an aromatic ring |
| $NH_2^{anti}$ | antisymmetric stretches of the two bonds in an $NH_2$ group |
| $NH_2^{sym}$ | symmetric stretches of the two bonds in an $NH_2$ group |
| OMC | observed minus calculated |
| OH | oxygen-hydrogen bond |

| | |
|---|---|
| OPO | optical parametric oscillator |
| P-branch | region of a spectrum containing transitions with $\Delta J = -1$ |
| pbe GGA | Perdew-Burke-Ernzerhof generalized gradient approximation |
| PES | potential energy surface |
| PICT | planar intramolecular charge transfer |
| PMT | photomultiplier tube |
| Q-branch | region of a spectrum containing transitions with $\Delta J = 0$ |
| R-branch | region of a spectrum containing transitions with $\Delta J = +1$ |
| Ser | serine |
| $S_0$ | ground electronic state |
| $S_1$ | first excited electronic state |
| $S_1$-$S_0$ | electronic transition between $S_0$ and $S_1$ |
| TICT | twisted intramolecular charge transfer |
| TM | transition dipole moment |
| TOF-MS | time of flight mass spectrometry |
| Trp | tryptophan |
| Tyr | tyrosine |
| UV | ultraviolet |
| β-turn | a 180° turn in the backbone of a peptide chain, also called $C_{10}$ |
| γ-turn | intramolecular interaction in the backbone of a peptide, also called $C_7$ |
| μ | permanent dipole moment |
| $\mu_i$ | component of permanent dipole moment along *i*-axis |

# PREFACE

It would be impossible to have completed this work without the support of many people. As a new graduate student I learned how to use the equipment and analyze results from my fellow students. The most influential were those with whom I was able to spend the most time: John Yi, Leonardo Alvarez-Valtierra, Diane Miller, and Philip Morgan. Leo became a mentor to me for which I am grateful. Later, I had very helpful discussions with newer members of the group, particularly Adam Fleisher, Justin Young, and Ryan Bird. I am grateful to fellow graduate student Matthew Kofke who synthesized Ac-Trp-NH(Me) during the summer he worked in the Pratt group. I hope that I was a good mentor to Casey Clements with whom I spent many hours in the lab and office.

During the last seven years, I have made many requests of the staff of the electronic and machine shops, and my work could not have been completed without Bob Muha, Chuck Fleishaker, Dennis Sicher, and Tom Gasmire. I am also grateful to Fran Nagy for putting up with me as I checked and double checked the departmental requirements for progress towards graduation.

Early in my studies here at Pitt I was influenced by talks given by Michel Mons about the study of small peptides. Subsequent conversations with him and his colleague, François Piuzzi, helped me to design a laser ablation device for use in one of our labs. They were generous enough to open their lab to me for four months to broaden my horizons by learning a new type of experiment and studying a set of molecules I found very interesting. While there, I had the pleasure of working with Eric Gloaguen with whom I am pleased to have been able to continue our acquaintance at various conferences.

At times it was necessary to get assistance with calculations to support my experimental work. Drs. Daniel Schofield and Lillian Chong provided ongoing help with the 1,3-benzodioxole and peptide projects, respectively. A fellow graduate student in Dr. Ken Jordan's group, Glen Jenness, taught me how to use Orca after first learning how to use it himself. Pitt's Center for Molecular and Materials Simulations provided computational resources, classes, and assistance that greatly increased the speed of my calculations.

I was also fortunate to be able to communicate with Dr. Michael Hollas regarding the 1,3-benzodioxole project. It was an honor to share my work with the man who literally wrote the book on high resolution spectroscopy.

I thank the professors of my core classes, Drs. Coalson, Petoud, Pratt, and Saxena, for preparing me for my subsequent years of research. Of these, Dr. Pratt deserves special recognition. I have always enjoyed conversations with him, beginning with my campus visit, and this was a major component in my decision to join his research group. He has helped me in many ways including teaching me physical chemistry, mentoring me as a research advisor, and giving me opportunities as a teaching assistant. I am grateful to him for his encouragement and confidence. I also learned a lot from Dr. Peter Siska and was proud to serve as his teaching assistant for several years before his death in 2009.

I could not have completed this work without support at home. My husband, Douglas Thomas, has learned to put up with my long days, the uncertainty in my graduation date, and my use of the word "lase". We are also both lucky to have supportive and understanding families.

Finally, I will miss the friends that I made through Phi Lambda Upsilon who gave me an excuse to have fun.

# 1.0 INTRODUCTION

> "It is the behavior and distribution of the electrons around the nucleus that gives the fundamental character of an atom: It must be the same for molecules." C. A. Coulson, 1951

One of the first things a student of chemistry learns is how the number and distribution of electrons in an atom determines its properties. The periodic table is a beautiful schematic for organizing elements based on their electronic character and resulting properties. In the quote above, Coulson is certainly correct in his extension of the cause-and-effect relationship between electronic distribution and atomic properties to molecules and their electrons. We model this using VSEPR, MO theory, and by using arrows to represent the movement of electrons in mechanisms of chemical reactions.

When molecules are excited from their ground electronic state into higher energy levels, a redistribution of electrons and a change in the equilibrium structure of the molecule results. In this work, several experimental methods are used to determine the distribution of electrons in molecules. The information extracted from these experiments gives insight into not just the structure of a molecule, but also its dynamics.

The experiments in Chapters 2-5 were performed under the supervision of David W. Pratt in the Chemistry Department at the University of Pittsburgh. For the past two decades the Pratt group has primarily used laser induced fluorescence (LIF) to study the gas phase electronic

spectra of molecules. Two experimental set-ups are utilized for this purpose. The first is a vibrationally resolved experiment employing a pulsed laser and pulsed valve sample nozzle. The linewidths of transitions in the resulting spectra are on the order of a wavenumber. The second experiment produces rotationally resolved electronic spectra of individual bands observed in the first experiment. For this a CW laser and continuous nozzle are used. The laser has been modified to conduct stable scans over approximately four wavenumbers. The resulting spectrum has linewidths on the order of 10 - 100 MHz due to Doppler and Lorentzian broadening and is linearized and calibrated using an interferometer and $I_2$ spectrum.

In Chapters 2 and 3, rotationally resolved electronic spectroscopy is used to determine the gas phase structure of 1,3-benzodioxole (BDO) and coumaran (COU), respectively, by determining the rotational constants about each principal axis of the molecule. Each of these molecules contains a five-membered ring that shares one side with a benzene ring. BDO contains two oxygen atoms in the five-membered ring resulting in a plane of symmetry that bisects both rings. COU, however, contains only one oxygen atom and has $C_1$ symmetry. Chapter 2 focuses on distinguishing among conflicting assignments in the literature of the vibrational motions of BDO while Chapter 3 examines the importance of the symmetry of the electron distribution by contrasting BDO and COU.

In Chapter 4, charged plates are added to the rotationally resolved electronic spectroscopy experiment to utilize the Stark effect to determine the permanent dipole moment of 1-phenylpyrrole (1PP) in both the ground and first excited state. 1-Phenylpyrrole has previously been identified as a dual-fluorescent molecule that emits a red-shifted fluorescence when studied in polar solvents. Unexpectedly, the dipole moment of the excited state gas phase molecule is oriented in the direction opposite to that in the ground state, indicating a significant movement of

electrons from one ring to the other even in the absence of solvent. In the supplementary information, the ground state rotational constants of several bands are compared revealing information about assignments in the vibrationally resolved spectrum.

Chapter 5 details the addition of a laser ablation source to the vibrationally resolved electronic spectroscopy set-up used by the Pratt group, enabling the study of the electronic and vibronic transitions of larger molecules that tend to decompose when heated. This source is based on the one used at CEA/Saclay and was developed based on conversations with Drs. François Piuzzi and Michel Mons. The source was tested on molecules previously studied in the Pratt lab then used to take spectra of the protected amino acids acetyl-tryptophan-amide (Ac-Trp-$NH_2$) and acetyl-tryptophan-methylamide (Ac-Trp-NH(Me)). These experiments are the basis for larger systems explored in the final chapter.

These experiments of Chapter 6 differ from those of the previous chapters in that they involve a double resonance experiment where the electronic excitation makes it possible to do a gas phase IR experiment. These experiments were performed with Drs. Michel Mons and François Piuzzi at CEA/Saclay. The molecules of interest are short peptides consisting of amino acids found in a folding nucleus of β-lactoglobulin. Each amino acid in the chain affects the overall shape of the molecule as detected by studying shifts of NH and OH stretch frequencies from their typical values. These shifts provide information about intramolecular interactions in the molecules. Comparisons are made between the capped amino acid tryptophan of Chapter 5 and two larger molecules; acetyl-tryptophan-tyrosine-amine (Ac-Trp-Tyr-$NH_2$) and acetyl-tryptophan-tyrosine-serinyl-amine (Ac-Trp-Tyr-Ser-$NH_2$).

## 2.0 RE-EXAMINATION OF THE ROTATIONALLY RESOLVED SPECTRA OF THE ELECTRONIC ORIGIN AND SEVERAL VIBRONIC BANDS OF 1,3-BENZODIOXOLE

Jessica A. Thomas[a], Leonardo Alvarez-Valtierra[b], and David W. Pratt[a]

[a]Department of Chemistry, University of Pittsburgh, Pittsburgh, PA 15260, USA
[b]Division de Ciencias e Ingenierias, Universidad de Guanajuato, Leon, Gto. 37150, Mexico

### 2.1 ABSTRACT

The structure and vibrations of 1,3-benzodioxole are reinterpreted using rotational constants and inertial defects obtained from high resolution electronic spectroscopy. Results are examined in light of previously published theoretical calculations and conclusions are drawn regarding vibrational assignments for transitions to the excited state. Compared to the ground state, the excited $S_1$ state has a significantly more nonplanar geometry, owing to an enhanced anomeric effect involving the oxygen lone pair electrons.

*Chem. Phys. Lett*. **490** (2010) 109 – 115.

JAT and LAV performed the experimental measurements; JAT analyzed the spectra and wrote the paper.

## 2.2 INTRODUCTION

1,3-Benzodioxole (BDO) has been studied extensively by several spectrographic and theoretical methods owing to its propensity for large amplitude motion.[1-3] Currently, it is believed that the molecule has a nonplanar structure in its electronic ground state ($S_0$). While the aromatic ring is planar, the five-membered ring is puckered, with the oxygen atoms and the -$CH_2$ group on opposite sides of the aromatic plane. Careful microwave measurements performed and analyzed by Caminati, *et al.*[2] showed that the puckering is controlled by a double minimum potential with a barrier of ~130 $cm^{-1}$.

Several methods have been used to study the first electronically excited state ($S_1$) of BDO.[4-8] It has been shown that this state has a larger barrier to puckering than the $S_0$ and is less planar. But conflicting vibrational assignments for the excited state have been published. Pietraperzia, *et al.*[5] determined the rotational constants for several vibronic transitions and identified an inconsistency in one of the assignments, but did not suggest an alternative. More recently, Emanuele and Orlandi[8] described analytical expressions for the 2D potential energy surfaces spanned by the puckering and flapping vibrations in both the $S_0$ and $S_1$ states.

Here, BDO is re-examined using rotationally resolved electronic spectroscopy. Fits of these spectra yield inertial parameters that are interpreted in light of the recent theoretical work.[8] By so doing, ambiguities among the vibrational assignments made by previous authors are resolved.

## 2.3 EXPERIMENTAL

BDO (99%) was purchased from Sigma Aldrich and used without further purification. The experimental set-up has been described elsewhere,[9] and will be summarized here. Vibrationally resolved excitation spectra were collected by a photomultiplier tube at the intersection of a pulsed supersonic jet expansion and a UV laser beam produced by frequency doubling the output of an Nd:YAG pumped dye laser. The vapor from a liquid BDO sample was seeded into ~900 Torr of argon. The jet expansion was produced by expanding the BDO/Ar mixture into a $10^{-5}$ Torr vacuum chamber through a General Valve Series 9 nozzle with a 1.0 mm orifice.

High resolution spectra were recorded using a molecular beam machine and a high resolution CW laser. The molecular beam was formed in a differentially pumped vacuum chamber where a sample of BDO was heated to ~100 $^{0}$C, expanded in argon gas (~760 Torr) through a ~200 μm orifice in the quartz sample holder, and then skimmed to produce a collimated beam ~3 cm downstream of the nozzle. The source chamber and buffer chamber were independently evacuated by two diffusion pumps. UV light (FWHM ~1 MHz) generated by the CW laser was then directed to cross the molecular beam at right angles about 10 cm downstream of the nozzle. When tuned to the appropriate wavelength, this light was absorbed by the sample, producing fluorescence that was detected by collection optics and a photomultiplier tube to record a spectrum. An iodine absorption spectrum and frequency markers were collected simultaneously during the scan to calibrate the recorded data according to the previously published iodine spectrum.[10]

The rotationally resolved spectra of BDO were fit using the jb95 least squares fitting program.[11] The rigid rotor Hamiltonian,

$$\hat{H} = AP_a^2 + BP_b^2 + CP_c^2 \qquad 2.1$$

where A, B, and C are rotational constants ($A = \hbar^2/2I_a$, *etc.*) and $P_a$, $P_b$, and $P_c$ are the components of the rotational angular momentum vector in the inertial coordinate system, was used for both electronic states. Typically, *ab initio* calculations[12] were used to determine initial values of the rotational constants from the optimized geometries of both states; these were later modified during the course of the fit, using refined values from the fit and/or other experimental values. Each recorded band was first subjected to an autocorrelation analysis[13] to assess whether multiple sub-bands might be present in the spectrum.

## 2.4 RESULTS

The vibrationally resolved spectrum of BDO from 34700 to 35900 $cm^{-1}$ is shown in Figure 2.1. Additional low intensity bands lie to the blue of this region. For this work seven bands were studied at high resolution; the origin at 34785.5 $cm^{-1}$ and bands located at +93.2, 101.6, 204.2, 290.8, 353.9 and 383.6 $cm^{-1}$ above the origin. These are marked by arrows in Figure 2.1.

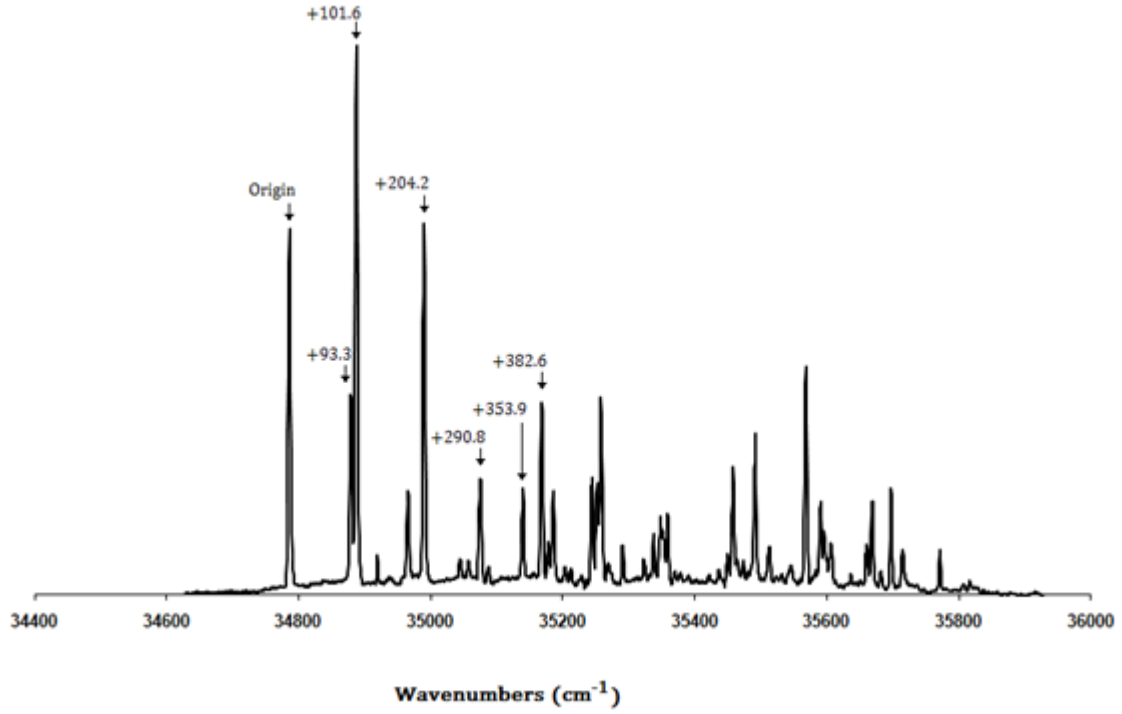


**Figure 2.1. Vibrationally resolved spectrum with the origin located at 34785.5 $cm^{-1}$. The bands studied in high resolution are indicated with arrows.**

Figure 2.2 shows the rotationally resolved electronic spectrum of the origin band of BDO in its entirety, a portion of the P branch at full resolution, and a simulation of this portion using the rotational constants obtained from the fit. Immediately apparent in this spectrum are the large number of transitions observed at high resolution. These fall into three classes; P, Q, and R, with $\Delta$ J = -1, 0, and +1, in order of increasing frequency. The relative intensity of these different branches depends on the orientation of the $S_1$-$S_0$ electronic transition moment; the relative intensity of the lines within the branches depends on the populations of the individual rovibronic levels in the $S_0$ state and their respective Hönl-London factors.[14] Finally, each observed line is in most cases a superposition of several rovibronic transitions owing to the simultaneous contributions of lifetime and Doppler broadening.

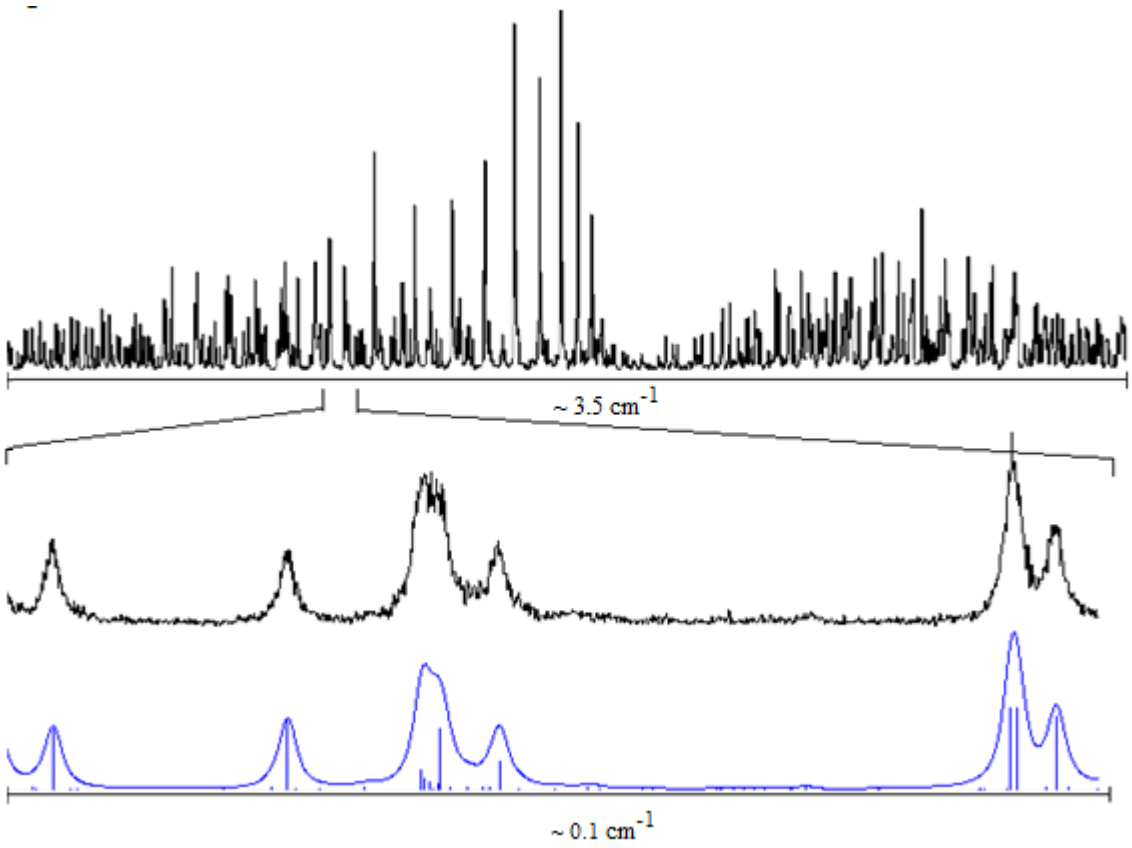


**Figure 2.2. Vibrationally resolved spectrum with the origin located at 34785.5 $cm^{-1}$. The bands studied in high resolution are indicated with arrows.**

The spectrum in Figure 2.2 spans approximately 3.5 $cm^{-1}$ and contains >4000 transitions of significant intensity of which 203 were assigned for an observed-minus-calculated (OMC) value of 3.04 MHz. The relative intensities of the transitions indicated a rotational temperature of 9 K. The spectrum was fit entirely with *a*-type transitions; thus, the $S_1$-$S_0$ transition moment lies along the *a*-axis of the molecule, bisecting both rings (Scheme 2.1). Individual rovibronic lines exhibited widths (FWHM) of 39 MHz; these were fit with a Voigt profile to yield a Gaussian width (due to the Doppler effect) of 15 MHz and a Lorentzian width (due to excited state decay)

of 24 MHz. The corresponding lifetime is 3.3 ns. No evidence of a tunneling splitting was found in the spectrum.

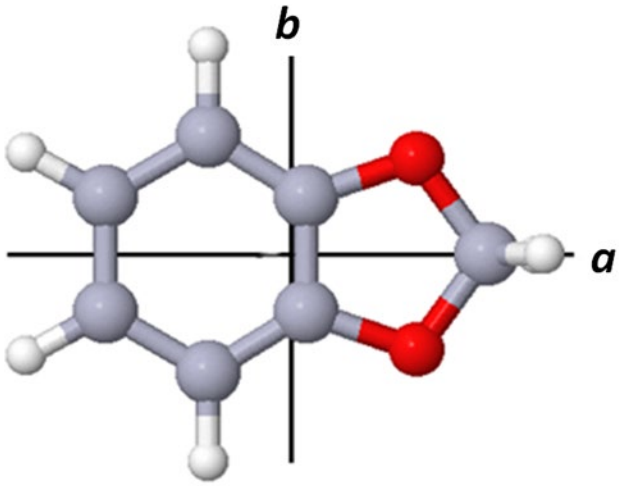


**Scheme 2.1. Structure of 1,3-benzodioxole.**

Table 2.1 lists the rotational constants obtained from the fit of the $S_1$-$S_0$ origin band in BDO. The constants determined by Pietraperzia, *et al.*,[5] when the ground state values are constrained to be equal to the more accurately determined values from the microwave experiment,[2] are provided for comparison. The $S_1$ rotational constants determined in this work by allowing both the ground and excited state constants to vary differ by only 0.4 MHz for A and agree within error with those of Pietraperzia, *et al.*[5] Also listed are a set of MP2 theoretical values computed using the 6-311g(d,p) basis set. The rotational constants of the $S_0$ level of the

origin band are in good agreement with those determined by the microwave experiment,[2] differing by 0.2 MHz for A and agreeing within error for B and C. The *ab initio* calculation, on the other hand, underestimates A and overestimates the other rotational constants.

**Table 2.1. Comparison of rotational constants obtained in this work with previously published results and *ab initio* calculations.**

| | This Work | Caminati, *et al*.[2] | MP2/6-311g(d,p) |
|---|---|---|---|
| A" (MHz) | 3795.2 | 3795.00 | 3769.9465 |
| B" (MHz) | 1621.0 | 1621.032 | 1627.4132 |
| C" (MHz) | 1147.9 | 1147.979 | 1152.6225 |
| | This Work | Pietraperzia, *et al*.[5] | |
| A' (MHz) | 3628.8 | 3628.42 | |
| B' (MHz) | 1628.4 | 1628.40 | |
| C' (MHz) | 1136.4 | 1136.44 | |

The examined vibronic bands of BDO all showed profiles similar to that of the origin with moderately intense P, Q, and R branches; each was fit entirely with *a*-type transitions. Representative spectra are displayed in Figure 2.3. Each spectrum spans about 3 $cm^{-1}$; in each case, approximately 100 – 200 of the lines were fit at a rotational temperature of 7 – 9 K. All of the fits had OMC's of less than 7 MHz, except for the +290.8 $cm^{-1}$ spectrum which had a lower signal-to-noise ratio and an OMC of 16.2 MHz. The linewidths of the +101.6 $cm^{-1}$ and higher energy bands are slightly larger (140 MHz) than the origin and +93.2 $cm^{-1}$ bands because of a

slight misalignment of the beams. There was no evidence of a tunneling splitting in any of the observed vibronic bands.

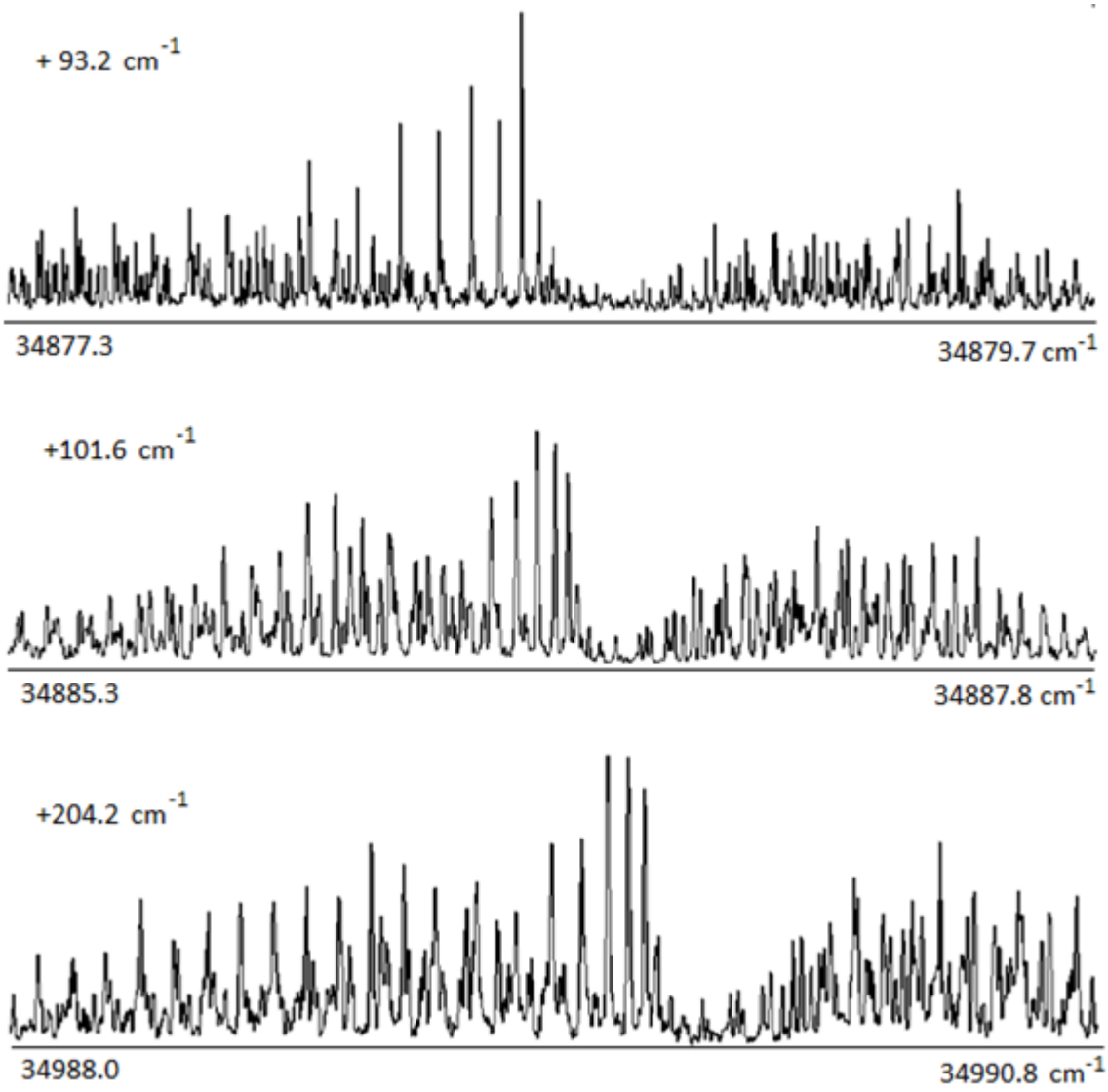


**Figure 2.3. Rotationally resolved spectra of some of the vibronic bands studied in this work.**

Table 2.2 lists the rotational constants obtained from the fits of the six vibronic bands of BDO. Notably, the ground state values for all bands are nearly the same, except possibly for the

+93.2 and +353.9 $cm^{-1}$ bands, where the measured values are significantly different. This may mean that these two transitions originate in some thermally populated level of the ground state. Previous work has identified the +93.2 $cm^{-1}$ band as a hot band.[5,6] The origin band and the bands at +101.6, +204.2, +290.8, and +382.6 $cm^{-1}$ clearly originate in the v=0 level of the $S_0$ state. In contrast, all observed bands terminate in different vibrational levels of the $S_1$ state. Except for the +353.9 $cm^{-1}$ band, the observed excited state values agree with those previously published by Pietraperzia, *et al*.[5] within ±0.9 MHz for A and ±0.3 MHz for B and C. Their values for the +353.9 $cm^{-1}$ band are A = 3618.5, B = 1632.2, and C = 1141.0 MHz.[5]

**Table 2.2. Rotational constants for the electronic origin and selected vibronic bands of 1,3-benzodioxole. The numbers in parentheses indicate the uncertainty in the last decimal place.**

| | origin | +93.2 | +101.6 | +204.2 | +290.8 | +353.9 | +382.6 |
|---|---|---|---|---|---|---|---|
| A" (MHz) | 3795.2 (1) | 3792.1 (1) | 3794.6 (7) | 3796.1 (7) | 3794.9 (7) | 3791.8 (7) | 3795.6 (7) |
| B" (MHz) | 1621.0 (1) | 1622.4 (1) | 1620.7 (2) | 1621.1 (2) | 1620.8 (2) | 1621.9 (2) | 1621.1 (2) |
| C" (MHz) | 1147.9 (1) | 1149.2 (1) | 1148.1 (1) | 1147.9 (1) | 1148.1 (1) | 1148.7 (1) | 1147.9 (1) |
| ΔI" (amu·Å$^2$) | -4.68 (0.06) | -5.02 (0.06) | -4.83 (0.10) | -4.61 (0.10) | -4.81 (0.10) | -4.91 (0.10) | -4.65 (0.10) |
| A' (MHz) | 3628.8 (1) | 3620.9 (1) | 3619.8 (7) | 3616.0 (7) | 3614.5 (7) | 3612.2 (7) | 3618.7 (7) |
| B' (MHz) | 1628.4 (1) | 1630.0 (1) | 1630.9 (2) | 1631.7 (2) | 1632.0 (2) | 1632.3 (2) | 1630.5 (2) |
| C' (MHz) | 1136.4 (1) | 1138.0 (1) | 1139.0 (1) | 1139.1 (1) | 1141.2 (1) | 1140.4 (1) | 1138.5 (1) |
| ΔI' (amu·Å$^2$) | -4.91 (0.06) | -5.52 (0.06) | -5.80 (0.10) | -5.83 (0.10) | -6.63 (0.10) | -6.37 (0.10) | -5.73 (0.10) |
| # Lines Assigned | 203 | 225 | 121 | 146 | 199 | 125 | 136 |
| OMC (MHz) | 3.04 | 4.04 | 3.19 | 2.81 | 16.2 | 6.59 | 5.22 |

## 2.5 DISCUSSION

The inertial defect,

$$\Delta I = I_c - I_a - I_b \qquad (2.2)$$

is a useful measure of the planarity of a molecule; if a molecule is planar in its equilibrium configuration, $\Delta I = 0$. The data in Table 2.1 show that BDO in its ground electronic state has $\Delta I = -4.75 \pm 0.10$ amu·Å$^2$. A methyl group with one hydrogen atom eclipsing a planar structure has an inertial defect of approximately -3.4 amu·Å$^2$, as found in 1-methylindole.[15] Thus, the larger magnitude of $\Delta I$ in the BDO ground state requires that the two hydrogen atoms of the $CH_2$ group and one or more of the heavy atoms are out-of-plane in the vibrationally averaged structure. This agrees with the puckered and flapped structure proposed by Caminati.[2] The magnitude of the inertial defect of the origin band increases from -4.75 to -4.91 amu·Å$^2$ upon electronic excitation, showing that the molecule is less planar in the excited state. In the excited state, all of the vibronic bands have an inertial defect of larger magnitude than the origin.

Figure 2.4 shows the two-dimensional potential energy surfaces (PES's) of both the ground and first excited electronic states of BDO that were recently calculated by Emanuele and Orlandi[8] using the CASSCF procedure followed by second-order perturbation theory (CASPT2). The three lowest frequency motions in the ground state are a twisting motion involving both rings ($\nu_{20}$), the flapping motion of the five-membered ring with respect to the benzene ring ($\nu_{38}$), and the pucker of the five-membered ring ($\nu_{39}$) (See Scheme 2.2). The calculated PES's shown in Figure 2.4 span two of these modes, the puckering and flapping vibrations. The ground state is predicted to have a double minimum potential along the puckering coordinate with a barrier of 125.7 cm$^{-1}$ and minima at $\pm 22.47^0$, and only a slight contribution from the flapping motion. This

is in good agreement with Caminati's microwave results.[2] Upon excitation to the $S_1$ state, the barrier height increases to a calculated 190.4 $cm^{-1}$ with pucker minima at $\pm 22.8^0$ and flap minima at $\pm 10.6^0$. Orlandi's excited state calculations predict a larger flap angle than in the ground state. We therefore expect an increase in the magnitude of the inertial defect in the $S_1$ state compared to the $S_0$ state, as the equilibrium structure moves further away from a planar one. The calculated inertial defects of these two structures are -4.66 amu·Å$^2$ for the ground state and -5.55 amu·Å$^2$ for the excited state, illustrating an observable difference in structure.

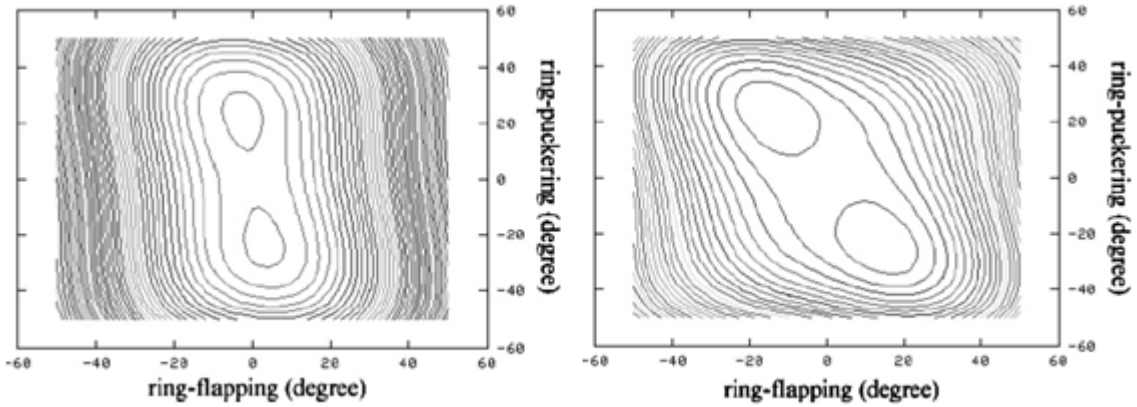


**Figure 2.4. Potential energy surfaces from Ref. 8 by Emanuele and Orlandi for the $S_0$ state, left, and $S_1$ state, right, of 1,3-benzodioxole.**

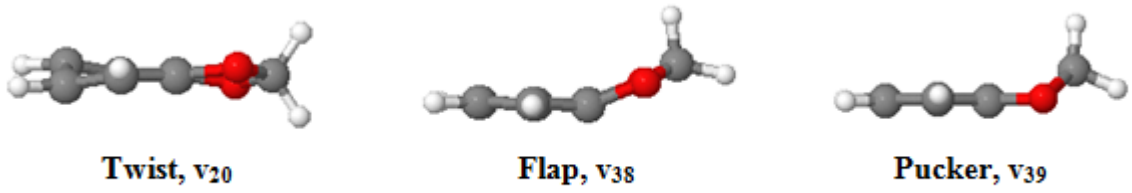


**Scheme 2.2. Low energy vibrational modes of BDO.**

Comparison of the two PES's shown in Figure 2.4 provides important insights into the origins of the vibrational structure in the $S_1$-$S_0$ spectrum of BDO. If there were no change in the equilibrium geometry of the molecule on electronic excitation, then the strongest band in the spectrum would be the $0_0^0$ band, with only small contributions from other vibrations. However, if the excited state PES is shifted along some coordinate relative to the ground state, a progression of bands involving that vibration would appear. (According to the Franck-Condon principle, the most intense of these bands would occur at the frequency where there is the largest overlap between the ground and excited state wavefunctions.) And, if there is a shift of the two states along two or more coordinates, then the spectrum will contain progressions in two or more vibrations. Thus, based on the data shown in Figure 2.4, we expect vibrational activity along at least two coordinates, the flap ($\nu_{38}$) and the pucker ($\nu_{39}$), in the $S_1$-$S_0$ electronic spectrum of BDO[a].

There is agreement in the literature that the band in the spectrum of BDO located at 34,785.5 $cm^{-1}$ is the origin[4-6,8] and that the intense band at +101.6 $cm^{-1}$ above the origin is the $39_0^2$ transition.[3,8,16] (The selection rule $\Delta$ v = 0, 2, 4, … applies, since vibrations 20, 38, and 39 are all non-totally symmetric modes.) Upon visual inspection of the vibrationally resolved spectrum, Figure 2.1, there seems to be a Franck-Condon progression present in the low frequency region; in fact, the strongest bands occur at +101.6 and +204.2 $cm^{-1}$ with approximately equal spacing. Indeed, the +204.2 $cm^{-1}$ band has previously been assigned to the transition by Hassan and Hollas.[b] The +101.6 $cm^{-1}$ band has the highest intensity and the

---

[a] Similar arguments would apply to the SVLF spectra of BDO.[3,4]

[b] The transitions that were originally assigned as twisting vibrations by Hassan and Hollas[4] have been reassigned as puckering vibrations.[16]

intensities of the origin and +204.2 $cm^{-1}$ bands also are significant, so it is surprising that no bands appear at +306 and +408 $cm^{-1}$. Alternate assignments for the +204.2 $cm^{-1}$ band are $38_0^2$, suggested by Orlandi[8] (mode 38 is the flapping vibration) and $38_0^1 39_0^1$, suggested by Laane *et al.*[2]

Rotational constants obtained from fits of high resolution spectra also are sensitive to vibrational motion. Thus, in the earlier study of vibrational satellites of BDO by microwave spectroscopy, it was found that there was a "zigzag" behavior of the observed rotational constants upon excitation of the v = 0, v = 1, v = 2, and v = 3 levels of the puckering motion, showing that this motion is controlled by a double minimum potential. Similar alternating shifts were found for the observed centrifugal distortion constants and for the component of the dipole moment along the *a* axis.[10]

In the excited state, there is no alternation in the values of the inertial defect as was observed by Caminati for the ground state. If the origin, +101.6 and +204.2 $cm^{-1}$ bands did form a progression, then such an alternation would be expected due to the double well in the excited state with a barrier to the pucker motion that is comparable to that of the ground state. This lack of alternation along with the lack of bands at +306 and +408 $cm^{-1}$ indicates that Hollas' assignment of the +204.2 $cm^{-1}$ band as $39_0^4$ and a member of a progression of the pucker mode is incorrect. Also, Hollas had predicted that the harmonic progression would be planar with respect to the puckering coordinate,[4] but the high resolution data show that this is not the case. The two remaining assignments for the +204 $cm^{-1}$ band are Laane's $38_0^1 39_0^1$ and Orlandi's $38_0^2$. Both originate in v=0 and are therefore in agreement with the experimental ground state rotational constants. But more information is needed to distinguish between these assignments.

To gain this information, we next consider the data for other bands including the intense hot band occurring at +93.2 $cm^{-1}$. The fact that the ground state rotational constants for this band differ from those of all the other bands confirms its identification as a hot band. Laane's assignment of $39_1^2$ can be dismissed because a transition from v = 1 in the ground state to v = 2 in the excited state is forbidden by selection rules. Also, if the +93.2 and +101.6 $cm^{-1}$ transitions terminate in the same level, they should have the same excited state rotational constants, which they do not. Hollas and Orlandi both assigned the +93.2 $cm^{-1}$ band to $38_0^1 39_1^0$. If the origin, +93.2, and +204.2 $cm^{-1}$ bands correspond to a progression of mode 38 in the excited state, $0_0^0$, $38_0^1 39_1^0$, and $38_0^2$ respectively, then an alternation of the inertial defects might initially be expected. However, since the increase in the barrier to planarity, which can be almost entirely attributed to the flap motion, is on the order of 65 $cm^{-1}$, all of the excited vibrational levels would lie above the barrier. Thus, the assignment made by Hollas and Orlandi of the +93.2 $cm^{-1}$ band to the $38_0^1 39_1^0$ transition is consistent with the experimental data.

The band occurring at +290.8 $cm^{-1}$ has not been previously examined in high resolution. This band has been assigned to $38_0^1 39_1^2$ by Laane and to $38_0^1 39_0^3$ by Orlandi. In Table 2.2, the ground state rotational constants of 290.8 $cm^{-1}$ match those of the origin band; thus, the transition originates in both $v_{38}$=0 and $v_{39}$=0. This rules out Laane's assignment but is consistent with that of Orlandi.

Now that the hot band at +93.2 $cm^{-1}$ is identified as a transition to the excited state $v_{38}$=1 level and the band at +290.8 $cm^{-1}$ as a transition to $v_{38}$=1, $v_{39}$=3, their rotational constants can be compared with those of the +204.2 $cm^{-1}$ band to distinguish between $38_0^1 39_0^1$ and $38_0^2$. If Laane's

assignment of $38_0^1 39_0^1$ is correct, then the bands occurring at +93.2, +204.2, and +290.8 $cm^{-1}$, which all terminate in $v_{38}$=0 and also in $v_{39}$=0, 1, and 3, respectively, should show a linear trend in the upper state inertial defects. Conversely, if Orlandi's assignment is correct, then the origin, +93.2, and +204.2 $cm^{-1}$ transitions, where $v_{39}$=0 and $v_{38}$= 0, 1, and 2, respectively, should show such a trend. When the inertial defects are plotted *versus* the energy difference of the bands, the series +93.2, +204.2, and +290.8 $cm^{-1}$ produce non-linear results whereas the inertial defects of the origin, +93.2, and +204.2 $cm^{-1}$ transitions are related linearly (not shown). The linearity is an indication that the transitions all belong to the same vibration as is seen in the case of the torsional motion of 1-naphthoic acid.[17] Therefore, the +204.2 $cm^{-1}$ band shall be assigned to the $38_0^2$ transition in agreement with the theoretical work of Orlandi.

Lastly, the assignment of the +204.2 $cm^{-1}$ band as $38_0^2$ can be used in the assignment of the band at +383.6 $cm^{-1}$. For this band Laane's assignment was $38_0^2$ which is now seen to be invalid. This leaves Orlandi's assignment of $37_0^1 38_0^1$, where $v_{37}$ is a complicated motion involving the deformation of the benzene ring with a calculated frequency of over 310 $cm^{-1}$. Of the bands studied in high resolution, the +353.9 $cm^{-1}$ band remains unassigned. It was identified as $38_0^2 39_0^2$ by Orlandi and as $37_0^1 39_0^1$ by Laane. It is difficult to distinguish these assignments using the present results, but it seems that the relatively high magnitude of the excited state inertial defect, -6.37 amu·$Å^2$, supports Orlandi's assignment of two quanta each in the pucker and flap modes rather than Laane's of one quantum each of benzene deformation and puckering.

Summarizing this discussion, we find excellent agreement between the vibrational assignments that can be derived from our high resolution data and those proposed by Emanuele

and Orlandi,[8] and listed in Table 2.3. The calculated vibrational frequencies also agree with those measured for the $S_1$-$S_0$ spectrum calibrated using the iodine spectrum.[10]

**Table 2.3. Selected published vibronic assignments for BDO made by J. Laane, J. M. Hollas, and G. Orlandi. The experimental work presented in this article is consistent with the assignments made by Orlandi and coworkers.**

| Position relative to origin ($cm^{-1}$) | Laane[3,6] | Hollas[4,15] | Orlandi[8] |
|---|---|---|---|
| +93.2 | $39_1^2$ | $38_0^1 39_1^0$ | $38_0^1 39_1^0$ |
| +101.6 | $39_0^2$ | $39_0^2$ | $39_0^2$ |
| +204.2 | $38_0^1 39_0^1$ | $39_0^4$ | $38_0^2$ |
| +290.8 | $38_0^1 39_1^2$ | - | $38_0^1 39_0^3$ |
| +353.9 | $37_0^1 39_0^1$ | - | $38_0^2 39_0^2$ |
| +382.6 | $38_0^2$ | - | $37_0^1 38_0^1$ |

BDO is an unusual molecule because it is found to be less planar in the excited state than the ground state. Most molecules are more planar in the excited state, owing to the delocalization of electrons. But in BDO, the lone pairs of electrons on the oxygen atoms have the ability to either conjugate with the $\pi$ electrons of the benzene ring or interact with the $\sigma^*$ orbital of the adjacent -$CH_2$ group. This interaction, known as the anomeric effect, is stabilizing and leads to a puckering of the five-membered ring.[18] 1,3-Dioxole contains the same five-membered ring as BDO and exhibits the anomeric effect. Laane reported that the barrier to puckering in BDO is significantly lower than that in 1,3-dioxole[3] indicating that the anomeric effect is somewhat quenched due to the competition from the conjugation with the aromatic ring.

Figure 2.5 shows the calculated frontier orbitals of BDO, as described from MP2/6-311g(d,p) calculations. Clearly, excitation of the HOMO-LUMO transition moves electron density into the benzene rings, and results in a decrease in the conjugation between the rings. With diminished conjugation comes the dominance of the anomeric effect and the resulting lack of planarity as evidenced by the increase in the magnitude of the inertial defect. The populated LUMO orbital also allows for an increased distortion along the flapping coordinate since the portions of the orbital located on the two sides of the molecule are bonding with respect to one another.


**Figure 2.5. Calculated frontier orbitals for benzodioxole. MP2/6-311g(d,p).**

## 2.6 CONCLUSION

Rotationally resolved electronic spectroscopy was used to determine the vibrational assignments of several electronic transitions of 1,3-benzodioxole. Previous conflicting assignments had been made by Hollas, Laane, and Orlandi using various methods. This work

supports the assignments made by Orlandi in all cases examined. Using the ground state rotational constants determined by Caminati using microwave spectroscopy, the hot band at +93.2 $cm^{-1}$ above the origin was assigned to the $38_0^1 39_1^0$ transition where $v_{38}$ is the flap mode of one ring with respect to the other and the $v_{39}$ mode is the pucker of the five-membered ring. The same technique was used to assign the band at +290.8 $cm^{-1}$ to $38_0^1 39_0^3$ rather than $38_0^1 39_1^2$. Once those transitions were assigned, there was enough data available to assign the +204.2 $cm^{-1}$ band to $38_0^2$. This eliminated the possibility of $38_0^2$ for the +383.6 band, leaving the assignment of $37_0^1 38_0^1$. Thus, the strong bands in the low frequency region of the vibrationally resolved spectrum do not form a Franck-Condon progression of the pucker mode as originally assigned. Rather, the $38_0^2$ transition is coincidently located at approximately twice the frequency of the $39_0^2$ transition and the pucker and flap modes interact in several of the other transitions.

## 2.7 POSTSCRIPT

Through further discussion with Michael Hollas after the publication of this letter it was determined that the alternation in intensities of transitions in the Q-branch of each rotationally resolved spectrum gives additional evidence to the assignments. In the origin band the Q-branch transitions with $K_a$ = odd are more intense than the neighboring $K_a$ = even values. On the other hand, this trend is reversed in the +93.2 $cm^{-1}$ band where the $K_a$ = even bands are more intense. All bands originating in the zero-point level of the $S_0$ state should have the same wavefunctions and the same nuclear spin statistical weights. The fact that the alternation in intensities is

reversed for the +93.2 $cm^{-1}$ band confirms the assignment of this band as a hot band because the ground state wavefunctions have different symmetries.

## 2.8 REFERENCES


1. J. A. Duckett, T. L. Smithson and H. Wieser, *Chem. Phys. Lett.* **1979**, *64*, 261.
2. W. Caminati, S. Melandri, G. Corbelli, L. B. Favero and R. Meyer, *Molec. Phys.* **1993**, *80*, 1297.
3. S. Sakurai, N. Meinander, K. Morris and J. Laane, *J. Am. Chem. Soc.* **1999**, *121*, 5056.
4. K. H. Hassan and J. M. Hollas, *Chem. Phys. Lett.* **1989**, *157*, 183.
5. G. Pietraperzia, A. Zoppi, M. Becucci, E. Droghetti and E. Castellucci, *Chem. Phys. Lett.* **2004**, *385*, 304.
6. J. Laane, E. Bondoc, S. Sakurai, K. Morris, N. Meinander and J. Choo, *J. Am. Chem. Soc.* **2000**, *122*, 2628.
7. Z. Kisiel, L. Pszczolkowski, G. Pietraperzia, M. Becucci, W. Caminati and R. Meyer, *Phys. Chem. Chem. Phys.* **2004**, *6*, 5469.
8. E. Emanuele and G. Orlandi, *J. Phys. Chem. A* **2005**, *109*, 6471.
9. W. A. Majewski, J. F. Pfanstiel, D. F. Plusquellic and D. W. Pratt in *High resolution optical spectroscopy in the ultraviolet, Vol. XXIII* Eds.: A. B. Myers and T. R. Rizzo), John Wiley & Sons, Inc., **1995**.
10. S. Gerstenkorn and P. Luc, *Atlas du spectroscopie d'absorption de la molecule d'iode*, CNRS, Paris, **1978/1982**.
11. D. F. Plusquellic, R. D. Suenram, B. Mate, J. O. Jensen and A. C. Samuels, *J. Chem. Phys.* **2007**, *115*, 3057.
12. M. J. Frisch, *et al*., *Gaussian03, Revision C.02*, Gaussian, Inc., Wallingford, CT, **2004**.
13. R. M. Helm, H.-P. Vogel and H. J. Neusser, *Chem. Phys. Lett.* **1997**, *270*, 285.
14. R. N. Zare, *Angular Momentum*, Wiley-Interscience, New York, **1988**.
15. T. M. Korter and D. W. Pratt, *J. Phys. Chem. B* **2001**, *105*, 4010.
16. J. M. Hollas, personal communication, **2009**.
17. S. Jagannathan and D. W. Pratt, *J. Chem. Phys.* **1994**, *100*, 1874.
18. J. M. Hollas, *High resolution spectroscopy*, Butterworths, Boston, **1982**.
19. E. Juaristi and G. Cuevas, *The anomeric effect*, CRC Press, Boca Raton, **1995**.

# 3.0 COUMARAN: COMPARISON WITH 1,3-BENZODIOXOLE

Jessica A. Thomas[a], Leonardo Alvarez-Valtierra[b], and David W. Pratt[a]

[a]Department of Chemistry, University of Pittsburgh, Pittsburgh, PA 15260, USA
[b]Division de Ciencias e Ingenierias, Universidad de Guanajuato, Leon, Gto. 37150, Mexico

## 3.1 ABSTRACT

Coumaran (2,3-dihydrobenzofuran) is structurally similar to 1,3-benzodioxole (BDO) but lacks a second oxygen atom in the five-membered ring. The presence of a $CH_2$ group in place of that oxygen decreases the symmetry, affects the planarity, and has implications for the anomeric effect which has an important influence on the conformation of BDO. This chapter explores these differences by comparing and contrasting the rotationally resolved electronic spectra of coumaran and 1,3-benzodioxole.

JAT and LAV performed the experimental measurements; JAT analyzed the spectra and wrote the paper.

## 3.2 INTRODUCTION

Coumaran (COU) and 1,3-benzodioxole (BDO) have been studied in tandem by several authors.[1-3] The most intriguing difference is the presence of the anomeric effect in BDO and the possibility that this effect might be modified in COU. The anomeric effect is found in molecules containing linkages such as $–O-CH_2-O-$; the overlap between a lone pair of one of the more electronegative atoms and an antibonding orbital of the neighboring bond stabilizes a puckered rather than planar structure. Thus, as mentioned in the preceding chapter, the five-membered ring of BDO is found to be less planar in the ground state than predicted for a molecule with lone pairs on the atoms adjacent to a π-bonded system. BDO is even less planar in the excited state because the conjugation between the π electrons of the six-membered ring and the lone pairs on the oxygens is reduced on excitation by light. Thus, the anomeric effect dominates, in agreement with the potential energy surfaces proposed by Laane.[4]

Coumaran, on the other hand, lacks this $–O-CH_2-O-$ linkage; the second oxygen atom is replaced by a $–CH_2$ group. Thus, if the anomeric effect is strong in BDO, it should be considerably weaker in COU. We test this hypothesis here by examining the high resolution spectra of several vibronic bands in COU, deducing information from them about the planarity and active vibrational modes of the isolated molecule in both its ground and first excited electronic states.

## 3.3 EXPERIMENTAL

The experimental set-up was the same as used in the previous study of BDO. Coumaran was purchased from Aldrich (99 % purity) and used without further purification. For the vibrationally resolved experiment, the sample was heated to 75 °C and entrained in 810 Torr of argon before being expanded into a vacuum chamber ($10^{-5}$ Torr) through a pulsed nozzle (General Valve, Series 9). The molecular expansion was crossed by the frequency doubled output of a tunable dye laser pumped by the second harmonic of an $Nd^{3+}$:YAG laser. The resulting fluorescence was collected by a PMT and recorded as a function of laser wavelength.

To obtain the rotationally resolved spectra, COU was heated to ~ 40 °C, seeded into approximately 450 Torr helium gas, and expanded from a 200 μm quartz nozzle into a vacuum chamber held at $10^{-5}$ Torr. The molecular beam was skimmed approximately 2 cm downstream from the nozzle and crossed by a 150 μW CW laser beam. The laser beam was the frequency doubled output of an $Ar^+$ ion pumped dye laser which was scanned over approximately three wavenumbers. The spectrum was linearized and calibrated using an interferometer and a visible $I_2$ spectrum.

## 3.4 RESULTS

The vibrationally resolved spectrum of COU is shown in Figure 3.1. The electronic origin is located at 34963.7 $cm^{-1}$, in good agreement with the value determined by Watkins, *et al.*[5] rather than the 34942 $cm^{-1}$ indicated in an earlier LIF study.[6] The most intense bands are

found in the low frequency region within 300 $cm^{-1}$ of the origin. Four of these bands were studied in high resolution (see arrows in Figure 3.1).

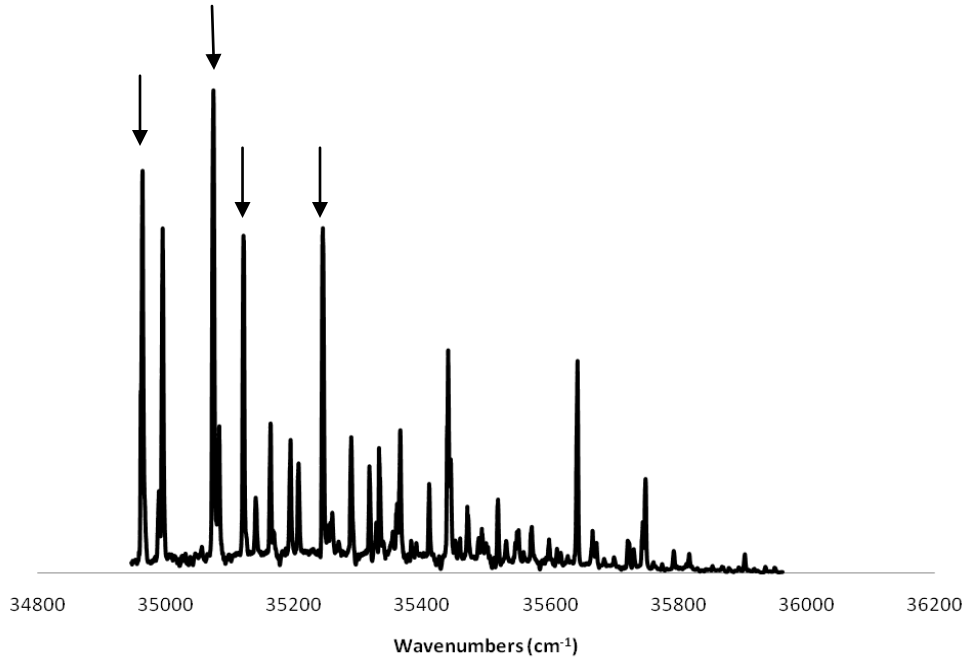


**Figure 3.1. Vibrationally resolved electronic spectrum of coumaran. The electronic origin is located at 34963.7 $cm^{-1}$. The bands marked with arrows were studied in high resolution.**

Figure 3.2 shows the rotationally resolved electronic spectrum of the origin band. The top trace (black) is the experimental spectrum which was fit using an iterative least-squares approach using JB95. The resulting spectrum is the blue trace in Figure 3.2 which is defined by the rotational constants presented in Table 3.1. The spectrum was fit by assigning 184 lines with an uncertainty (observed-minus-calculated) of 4.0 MHz.

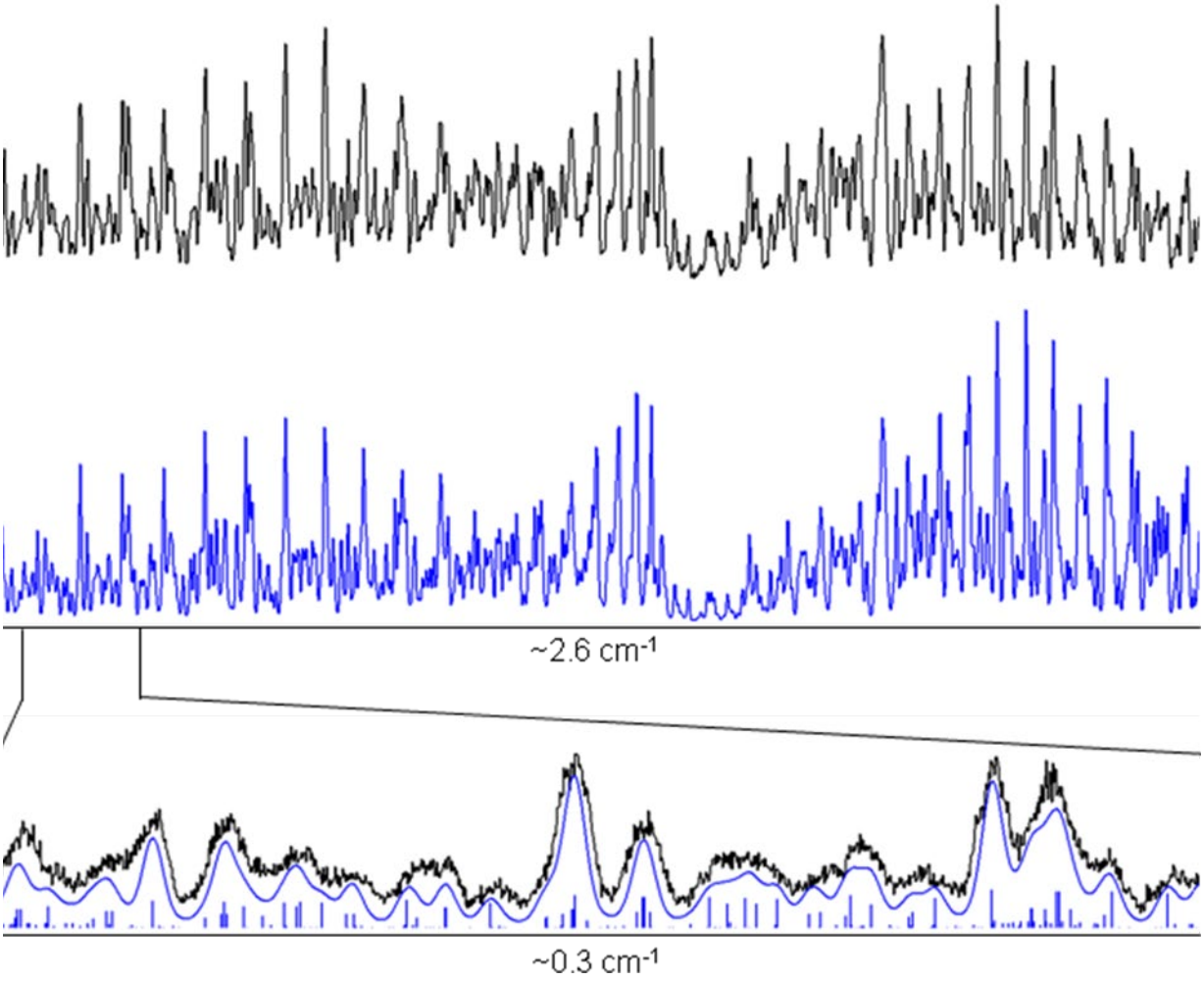


**Figure 3.2. Rotationally resolved spectrum of the electronic origin of coumaran (black) fit to the spectrum simulated in JB95 (blue) in its entirety (top) and zoomed-in to show individual transitions (bottom).**

Rotationally resolved electronic spectra of the three vibronic bands studied are presented in Figure 3.3 which highlights their similarity. The rotational constants for the ground electronic state of each band are the same, within error (Table 3.1), indicating that each transition originates in the same ground state vibrational level, $v = 0$. The ground state constants are also in good agreement with the microwave results of Ottaviani, *et al.*[3] The rotational constants for each excited electronic state, however, are different, indicating that a different vibration and/or

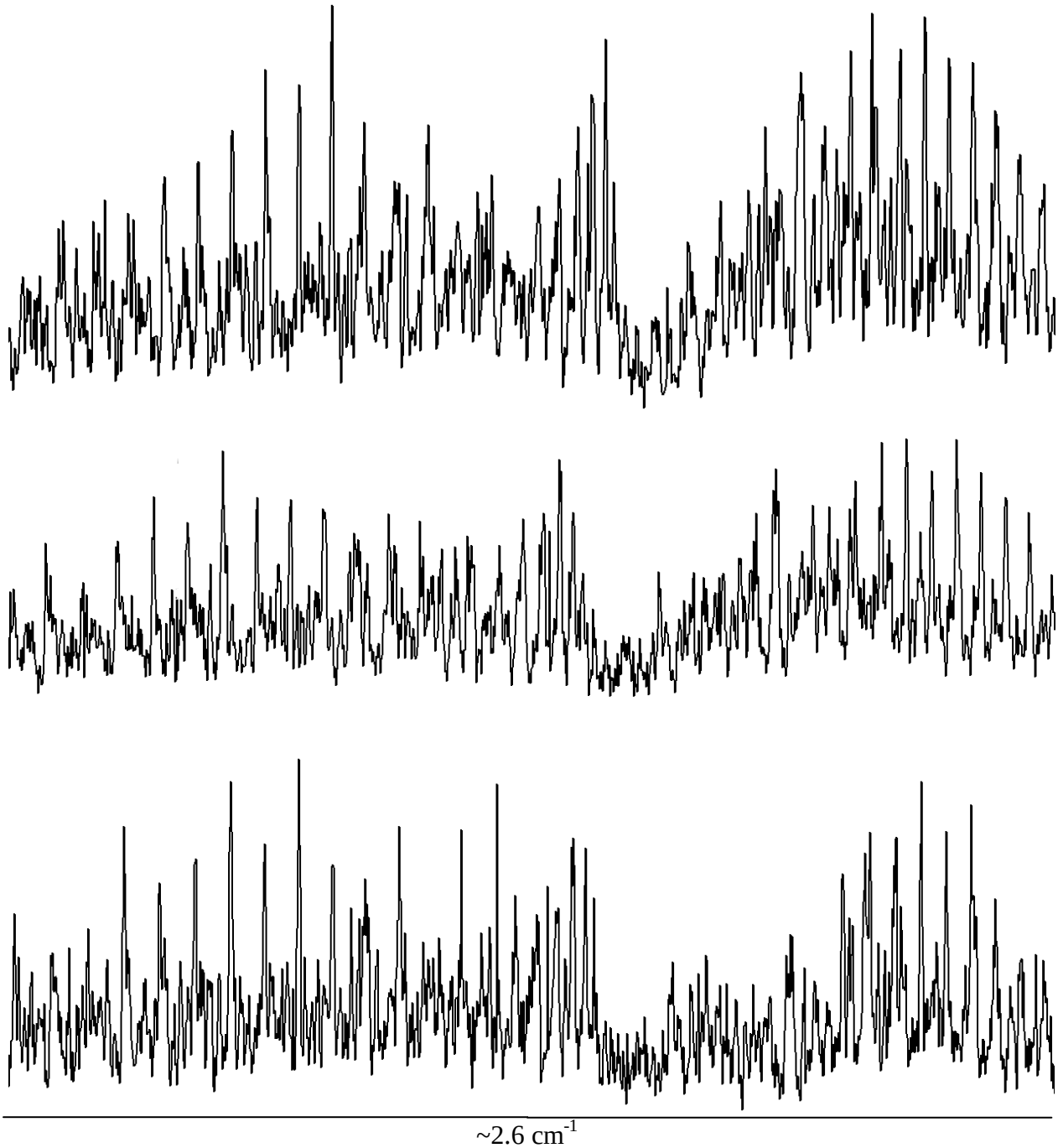


**Figure 3.3. Rotationally resolved vibronic bands of COU occurring at +110.4, +157.7, and +280.4 $cm^{-1}$ above the origin (top to bottom). Each shows a similar contour due to an electronic transition moment with 55 % *a*-type character and 45 % *b*-type character.**

vibrational level is excited for each transition. Each of the bands studied has 55 % *a*- and 45% *b*-type character, in good agreement with the calculated hybrid-band character of *a/b/c* = 50/50/0 (CIS/6-311+G(d,p)) and with the prediction made by Alves, *et al*.[1] This is significantly different from BDO in which all bands exhibit pure *a*-type spectra.

**Table 3.1. Inertial parameters for the electronic origin and selected vibronic bands of coumaran.**

| | Origin = 34963.7 $cm^{-1}$ | +110.4 $cm^{-1}$ | +157.7 $cm^{-1}$ | +280.4 $cm^{-1}$ |
|---|---|---|---|---|
| A″ (MHz) | 3655.9(1) | 3655.8(1) | 3655.9(1) | 3655.7(1) |
| B″ (MHz) | 1558.1(1) | 1558.1(1) | 1558.3(1) | 1558.2(1) |
| C″ (MHz) | 1112.3(1) | 1112.3(1) | 1112.4(1) | 1112.2(1) |
| ΔI″ (amu·$Å^2$) | -8.3(1) | -8.3(1) | -8.2(1) | -8.2(1) |
| A′ (MHz) | 3526.2(1) | 3526.7(1) | 3522.9(1) | 3528.0(1) |
| B′ (MHz) | 1552.4(1) | 1553.6(1) | 1554.0(1) | 1553.9(1) |
| C′ (MHz) | 1094.4(1) | 1096.5(1) | 1097.7(1) | 1097.2(1) |
| ΔI′(amu·$Å^2$) | -7.1(1) | -7.7(1) | -8.3(1) | -7.9(1) |
| OMC (MHz) | 4.0 | 5.0 | 5.1 | 7.1 |
| # lines | 184 | 195 | 169 | 148 |
| a/b/c | 55/45/0 | 55/45/0 | 55/45/0 | 55/45/0 |

**Table 3.2. Comparison of the experimental and theoretical ground state rotational constants of coumaran and 1,3-benzodioxole.**

| Parameter | COU (Experimental) | COU (MP2/6-31G(d,p)) | BDO (Experimental)* | BDO (MP2/6-31G(d,p)) |
|---|---|---|---|---|
| A″ (MHz) | 3655.9(1) | 3653.3 | 3795.2 (1) | 3774.8 |
| B″ (MHz) | 1558.1(1) | 1560.9 | 1621.0 (1) | 1621.1 |
| C″ (MHz) | 1112.3(1) | 1115.6 | 1147.9 (1) | 1148.0 |
| ΔI″ (amu·$Å^2$) | -8.3(1) | -9.10 | -4.68 (0.06) | -5.29 |

*See Chapter 2.

## 3.5 DISCUSSION

Table 3.2 compares the experimental ground state rotational constants of COU with calculated values and with the corresponding values for BDO. All of the calculated rotational constants are underestimated compared to the experimental values, but together they produce an inertial defect that is in good agreement with experiment. Surprisingly, the inertial defect of COU is significantly larger in magnitude (-8.3 amu·Å$^2$) than that of BDO (-4.68 amu·Å$^2$). This cannot be attributed solely to the two sets of out-of-plane hydrogen atoms which would make a contribution of ~ -6.6 amu·Å$^2$ to $\Delta I$ if the attached carbon atoms were in the plane. Thus, COU is either more puckered than BDO or both $CH_2$ groups lie out of the plane of the molecule. The calculated dihedral angles of COU and BDO in the ground state are 26.5 and 23.6 °, respectively. Both O atoms in BDO lie ~ 2 ° above (or below) the plane of the benzene ring; the single O atom in COU is < 1 ° above (or below) this plane. In contrast, the two ring carbon atoms in COU are displaced above and below this plane by ± 4 ° (see Scheme 3.1). Apparently, these displacements are responsible for the larger value of $|\Delta I|$ in ground state COU.

The change in inertial defect of COU from -8.3 to -7.10 amu·Å$^2$ upon excitation of the electronic origin indicates that the molecule becomes more planar in its excited electronic state. For the other transitions measured, however, the change in magnitude of the inertial defect is smaller, and in fact, for the +157.7 cm$^{-1}$ band, the inertial defect of the excited state is the same as the ground state, within error.

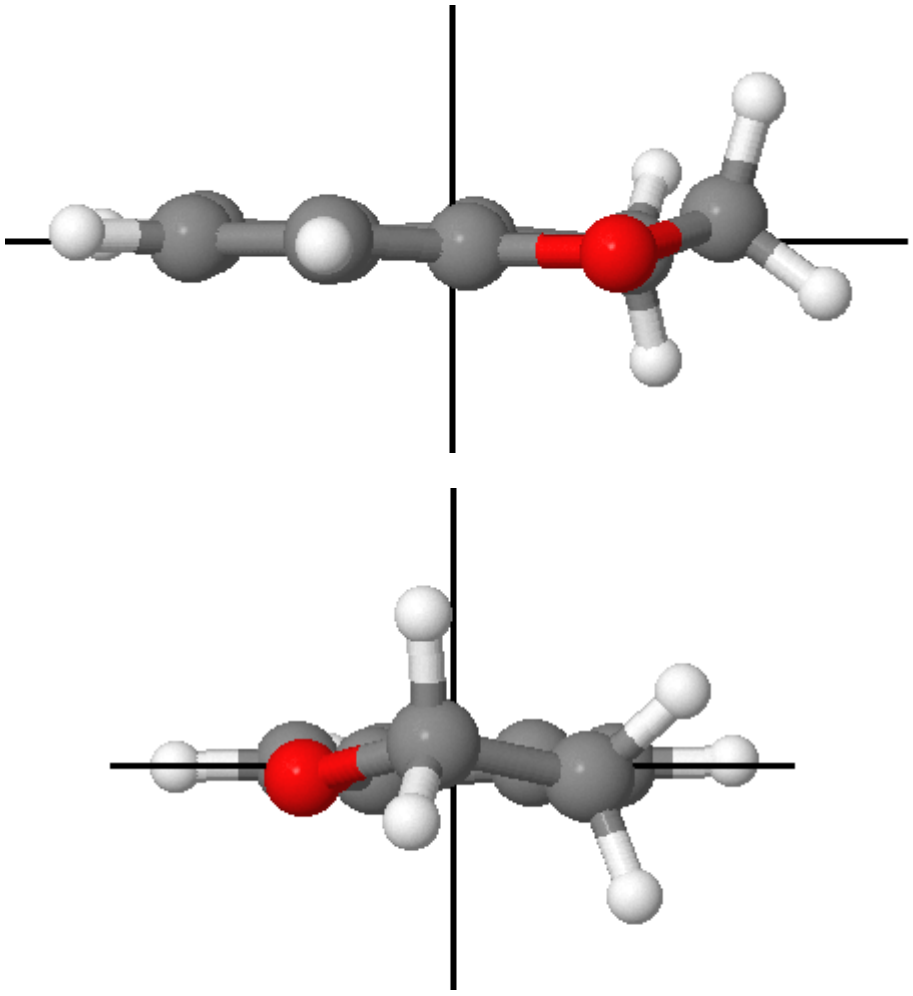

**Scheme 3.1. Two views of the calculated (MP2/6-31G(d,p)) structure of coumaran showing its puckered structure. See description in text.**

The increase in planarity upon excitation of the origin of COU is in agreement with previous work by Yang, *et al*.[2] who determined that the excited state barrier to planarity, 34 $cm^{-1}$, is significantly less than that of the ground state, 154 $cm^{-1}$. Interestingly, as shown in the previous chapter, BDO becomes less planar upon electronic excitation of the origin and all vibronic bands studied due to an increase in barrier height in the two-dimensional PES formed by the puckering and flapping coordinates.

These differences in behavior of COU and BDO may be traced to differences in the electron distributions of the excited states of the two molecules. In BDO, the HOMO and LUMO orbitals that participate in the $S_1$-$S_0$ transition are symmetric with respect to the *a*-axis, leading to a movement of electron density from the five-membered ring to the benzene ring (recall that the transition is a pure *a*-type transition). The resulting decrease in conjugation leads to a less planar molecule. However, in COU, the electron density moves diagonally across the molecule, as illustrated in Figure 3.4. (Both the HOMO → LUMO and HOMO-1 → LUMO+1 transitions contribute to the $S_1$ state of COU). Recall that the $S_0$-$S_1$ transition is an *a/b*-hybrid band. As a result, there is enhanced conjugation between the two rings in the $S_1$ state of COU, leading to a more planar molecule.

The +110.4, +157.7, and +280.4 $cm^{-1}$ bands of COU were assigned by Cockett and coworkers[5] as $45_0^2$, $44_0^1$, and $42_0^1$, respectively, where mode 45 is the puckering of the five-membered ring, mode 44 is a twisting mode involving both rings, and mode 42 is an out-of-plane benzene ring mode. Laane and coworkers[2] later modified these assignments based on a new PES. They assigned the +157.7 $cm^{-1}$ transition to a $44_0^1 45_0^1$ combination mode and the +280.4 $cm^{-1}$ transition to $42_0^1 45_0^1$. Because of the similarity between the assignments of the two authors and the fact that all of the modes in question are out-of-plane modes that do not seem to form long progressions, it is difficult to distinguish between these assignments. However, our observation that these three bands all have $\Delta I$ values that are larger in magnitude than those of the origin band is consistent with their assignment as out-of-plane modes.

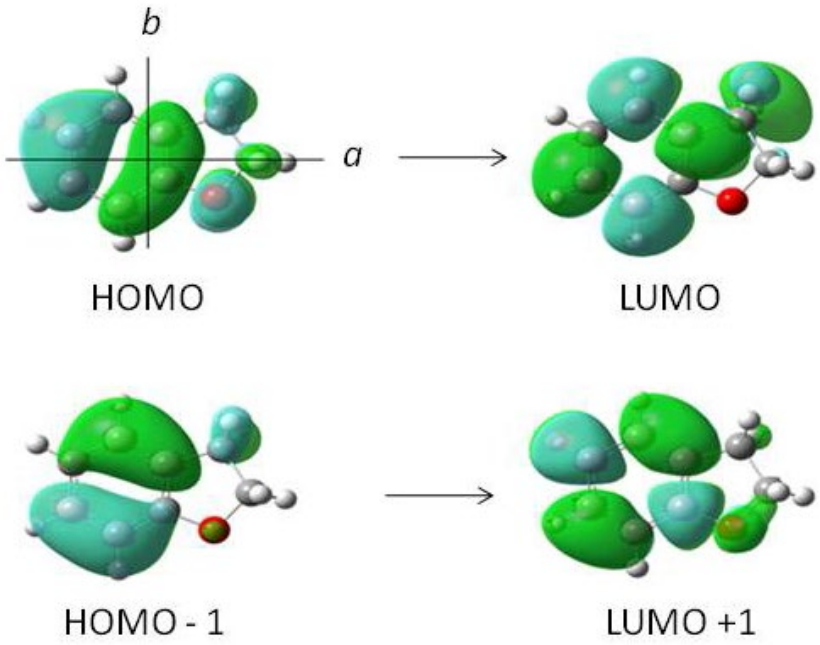


**Figure 3.4. Frontier orbitals for coumaran.**

## 3.6 CONCLUSION

High resolution electronic spectroscopy was used to show that COU has an inertial defect that is larger in magnitude in both the ground and excited electronic states than that of an analogous molecule, BDO. The difference was attributed to the decreased symmetry in COU which results in a/b-hybrid type spectra, a different electron distribution in both the ground and first excited states, and a staggered configuration of the adjacent $CH_2$ groups. Coumaran becomes more planar upon excitation whereas BDO becomes less planar when excited to its first electronically excited state. This indicates that the conjugation of the oxygen lone pairs and the

$\pi$ electrons in COU is not quenched upon excitation as it is in BDO which is dominated by the anomeric effect.

## 3.7 ACKNOWLEDGEMENTS

Justin Young provided assistance in collecting the vibrationally resolved spectrum.

## 3.8 REFERENCES

1. A. C. P. Alves, J. M. Hollas and B. R. Midmore, *J. Molec. Spectros.* **1979**, *77*, 124.
2. J. Yang, M. Wagner, K. Okuyama, K. Morris, Z. Arp, J. Choo, N. Meinander, O. Kwon and J. Laane, *J. Chem. Phys.* **2006**, *125*, 034308.
3. P. Ottaviani and W. Caminati, *Chem. Phys. Lett.* **2005**, *405*, 68.
4. J. Laane, E. Bondoc, S. Sakurai, K. Morris, N. Meinander and J. Choo, *J. Am. Chem. Soc.* **2000**, *122*, 2628.
5. M. J. Watkins, D. E. Belcher and M. C. R. Cockett, *J. Chem. Phys.* **2002**, *116*, 7855.
6. M. Takayanagi and I. Hanazaki, *Chem. Phys. Lett.* **1993**, *208*, 5.

## 4.0 STARK-EFFECT STUDIES OF 1-PHENYLPYRROLE IN THE GAS PHASE. DIPOLE REVERSAL UPON ELECTRONIC EXCITATION.

Jessica A. Thomas,[a] Justin W. Young,[a] Adam J. Fleisher,[a] Leonardo Alvarez-Valtierra,[b] and David W. Pratt[a]

[a]Department of Chemistry, University of Pittsburgh, Pittsburgh, PA 15260, USA
[b]Division de Ciencias e Ingenierias, Universidad de Guanajuato, Leon, Gto. 37150, Mexico

### 4.1 ABSTRACT

High-resolution fluorescence excitation experiments on 1-phenylpyrrole in a molecular beam, both in the absence and presence of an applied electric field, show that the state responsible for the strong features in the gas-phase UV absorption spectrum is the $^1L_b$ state, that this state is significantly more planar than the ground state, and that the direction of the permanent electric dipole moment in the $^1L_b$ state is reversed relative to that of the ground state. Implications of these findings for intramolecular charge transfer in the isolated molecule are discussed.

*J. Chem. Phys. Lett.* **1** (2010) 2017 – 2019.

JAT and LAV collected the vibrationally resolved spectrum; JAT, JWY, and AJF collected the rotationally resolved spectra; JAT analyzed the spectra, with assistance from AJF for the Stark spectra, and wrote the paper.

## 4.2 INTRODUCTION

The molecule 1-phenylpyrrole (1PP) has attracted much attention since it was discovered in 1983 that it exhibits a long wavelength shoulder in its fluorescence spectrum in acetonitrile.[1] Originally, it was thought that electronic excitation led to the formation of a twisted intramolecular charge transfer (TICT) state which might be stabilized in a polar solvent.[2] Later, it was shown in a supersonic jet study of 1PP[3] that the electronically excited $S_1$ state, though twisted, is more planar than the ground electronic state. However, Proppe, *et al.*[4] have argued on the basis of a theoretical study of TICT in 1PP that the transition studied by Okuyama, *et al.*[3] may not correspond "to the electronic transition responsible for the spectroscopic feature with maximum intensity in the lowest energy region of the absorption spectrum," thereby creating some doubt about the relevance of the gas-phase results.

Photoinduced ICT states of organic compounds play a fundamental role in many processes of current interest.[5] For this reason, we report here the results of a high-resolution laser study of 1PP in a molecular beam, both in the absence and presence of a static electric field. These results show that the state responsible for the strong feature in the absorption spectrum is the $^1L_b$ state, that this state is significantly more planar than the ground electronic state, and that the direction of the permanent electric dipole moment in this state is reversed, relative to the ground electronic state. Reversal of the dipole direction may play a previously unappreciated role in the CT process in many molecules.

## 4.3 RESULTS & DISCUSSION

Detailed descriptions of our experimental methods are given in the Supporting Information. There, we also present the results of both vibrationally and rotationally resolved experiments on 1PP in the absence of an electric field. The vibrationally resolved fluorescence excitation spectrum is virtually identical to that presented by Okuyama, *et al.*;[3] the first 1000 $cm^{-1}$ are dominated by a long progression of bands spaced by intervals of ~50 $cm^{-1}$. Rotationally resolved spectra of three of these bands at +269.0, +316.9 and +364.5 $cm^{-1}$ with respect to the weak origin band (originally assigned as $T_0^8$, $T_1^9$, and $T_0^{10}$, where *T* represents a ring-torsional mode[3]) show that all transitions originate in the same ground-state vibrational level, that the upper-state vibrational levels reached in the three transitions all have inertial defects that are substantially lower (in magnitude) than those of the ground state, and that the PES along the torsional coordinate in the excited state most likely has a greatly reduced barrier to planarity and a greatly increased barrier to perpendicularity compared to the ground state.

Also relevant to the issue of CT in the electronically excited state of 1PP is the behavior of the electronic spectrum in the presence of an electric field. Figure 4.1 shows an example, the high resolution spectrum of the $0_0^0$+269 $cm^{-1}$ band at zero field, and selected portions of this spectrum at Stark fields of 211, 423, and 846 V/cm. Like the other bands examined at high resolution, this band is a hybrid band consisting of 87.5 % *b*-type character and 12.5 % *c*-type character. No *a*-type character is observed. This shows that the state accessed in these experiments is a $^1L_b$ state (in the language of Proppe, *et al.*[4] the $1^1B$ state, comprised principally

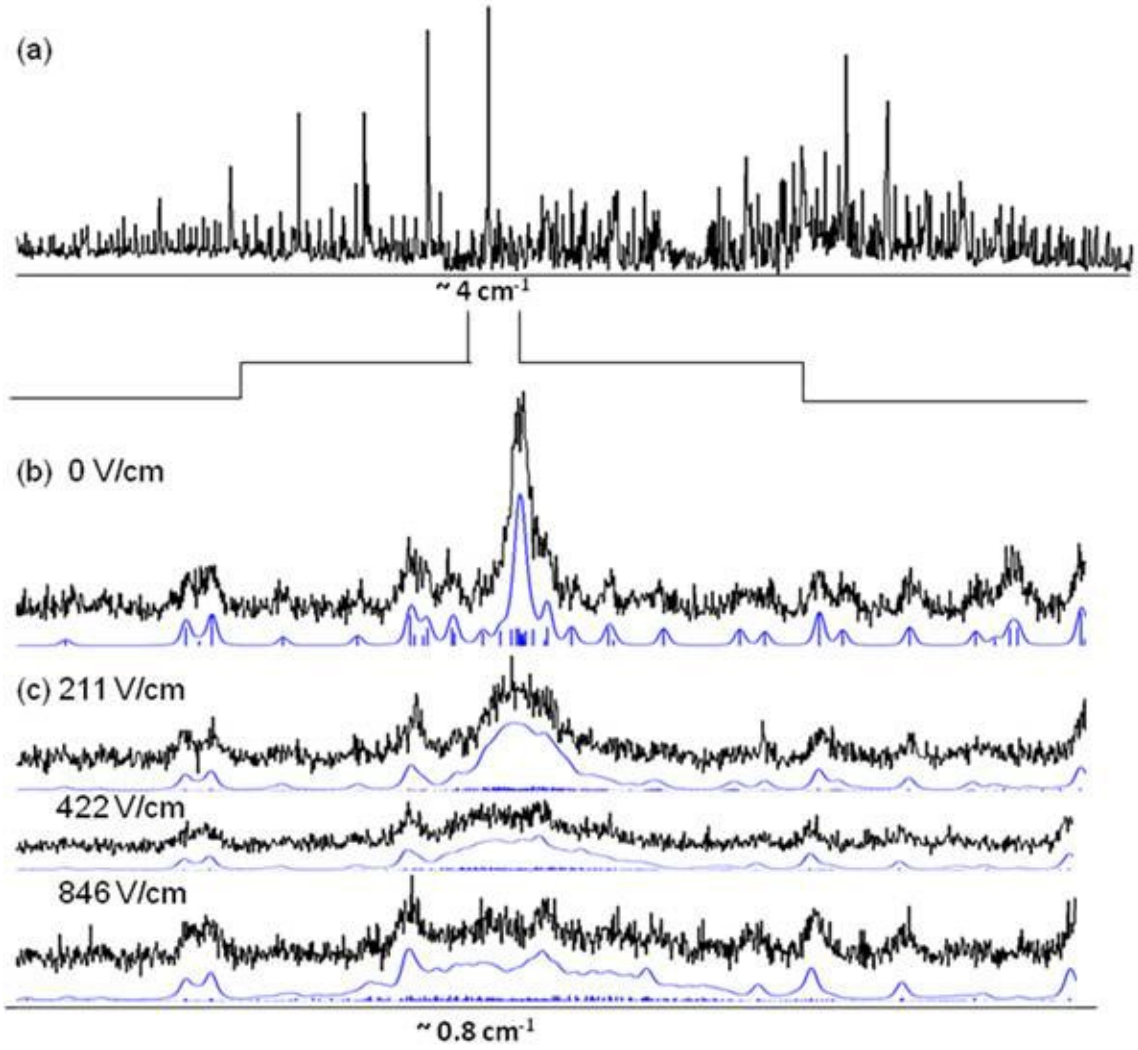


**Figure 4.1. (a) Rotationally resolved spectrum of the origin +269 $cm^{-1}$ band of 1-phenylpyrrole in zero-field. (b) A portion of the Q-branch from the zero field spectrum shown at full resolution. The most intense transitions are (J′, $K_a$′, $K_c$′) ← (J″, $K_a$″, $K_c$″); (10, 3, 8) ← (10, 4, 7), (11, 3, 9) ← (11, 4, 8), and (9, 3, 7) ← (9, 4, 6). The simulated spectrum is shown both as discrete transitions and as a contour comprised of 30 MHz Gaussian and 13 MHz Lorentzian contributions to the observed Voigt line shape profiles. (c) Corresponding portions of the spectrum collected in the presence of the indicated electric fields.**

of two one-electron excitations, 42.6 % HOMO-1 to LUMO+1, and 26.7 % HOMO-2 to LUMO). Excitation of this state utilizes a transition moment that is perpendicular to the long axis of the molecule, lying in the plane of the benzene ring, and rotated by 21° around the *a*-axis of 1PP (see Scheme 4.1).

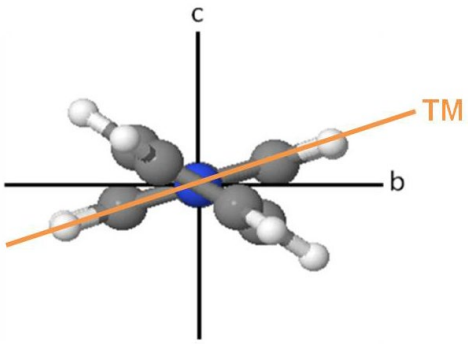


**Scheme 4.1. Electronic transition moment of 1-phenylpyrrole.**

The electric field tuning behavior of a specific transition in an electronic spectrum depends on the values of all three permanent dipole moment components in both electronic states. As in microwave spectroscopy,[6] $\mu_a$ connects states having $\Delta K_a = 0, \pm2, \ldots$ and $\Delta K_c = \pm1, \pm3, \ldots$ and $\mu_b$ connects states having $\Delta K_a = \pm1, \pm3, \ldots$ and $\Delta K_c = \pm1, \pm3, \ldots$; $\mu_c$ connects states having $\Delta K_a = \pm1, \pm3, \ldots$ and $\Delta K_c = 0, \pm2, \ldots$ . The sensitivity of the UV experiment to the different dipole components also depends on the orientation of the transition dipole;[7] for a *b*-type transition, the Stark effect is linear for levels connected by $\mu_a$ and $\mu_c$, and quadratic for levels connected by $\mu_b$. This is apparent from Figure 4.1; the *b*-type Q branch lines with $\Delta K_a$ and $\Delta K_c = \pm1$ are split more than others. A least-squares fit of this behavior yields the values $\mu_a(S_0) = \pm1.56 \pm 0.01$ D and $\mu_a(S_1) = 0.94 \pm 0.01$ D. As expected, both $\mu_b$ and $\mu_c$ were found to be zero, in both electronic states, to within ± 0.01 D. Our fits of the spectra shown in Figure 4.1 included

64 lines and yielded an OMC standard deviation of 4.86 MHz, small compared to the observed linewidth of 40 MHz.

Substantial charge reorganization is revealed by the measured values of $\mu_a$; $|\mu_a| \approx 2.5$ D upon excitation of 1PP by light. More dramatic is the change of sign. As is well-known, the absolute signs (i.e., directions) of dipole moments cannot be determined without interpretation by chemical intuition or theoretical calculations. However, our results show that the pattern of splitting with the dipole moments oriented in different directions in the two states is inherently different from that with the dipole moments pointing in the same direction. This is illustrated in Figure 4.2. Significantly, the spectrum also cannot be fit with an excited state dipole moment that increases in magnitude by ~2.5 D.

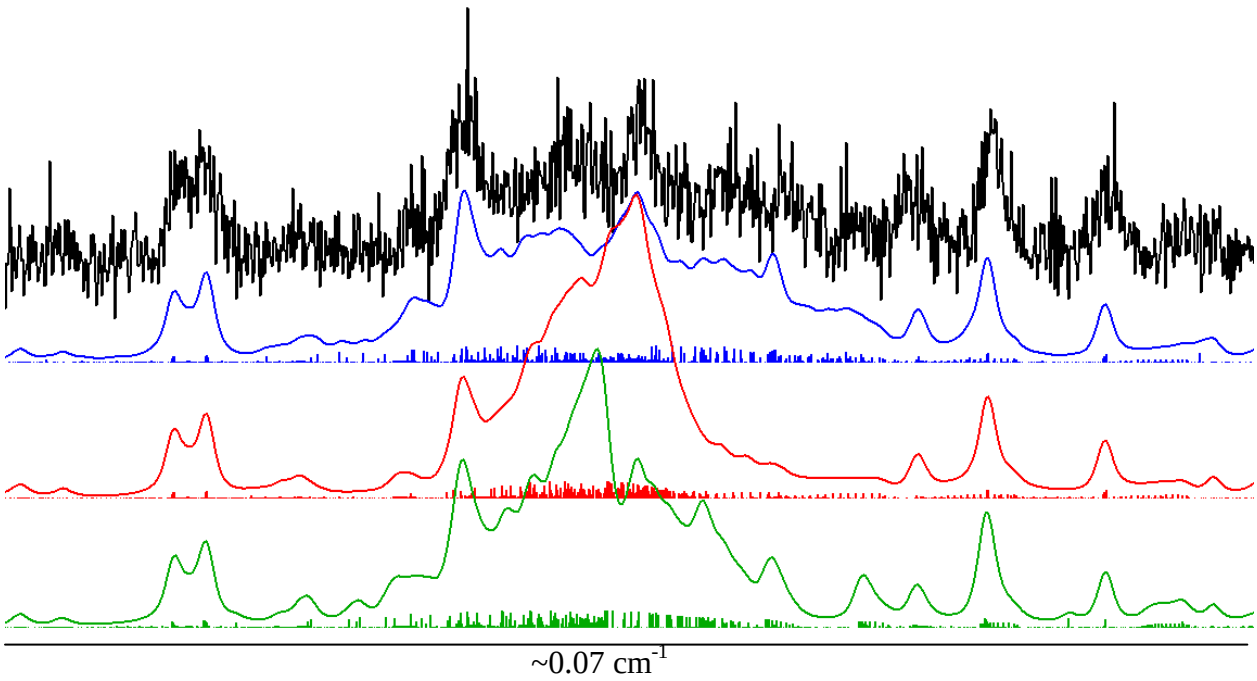


**Figure 4.2. Portions of the 846 V/cm spectrum fit with: $\mu_a'' = -1.56$ D and $\mu_a' = 0.94$ D (top, blue); $\mu_a'' = -1.56$ D and $\mu_a' = -0.94$ D (middle, red); and $\mu_a'' = -1.56$ D and $\mu_a' = -4.06$ D (bottom, green).**

Previous estimates of the ground state dipole moment of 1PP include a measured value of |1.39| D (in benzene solution at 30 °C)[8] and calculated values (for a twisted structure) of -1.51 D,[5] -1.3 D,[9] and -1.9 D.[10] The negative sign of the dipole of ground state 1PP indicates that the center of negative charge is located on the pyrrole ring, which accords with chemical intuition (see Scheme 4.2). Thus, our measured dipole moment for the ground state can be assigned the value -1.56 D, and our measured dipole moment for the excited state can be assigned the value +0.94 D. The center of the negative charge in the excited state is located on the benzene ring. Proppe, *et al.*[4] predict the electronically excited state values of -1.00 D for the twisted $1^1$B state and +3.10 for the twisted $2^1$A state, a conclusion with which Haas and coworkers[9,10] qualitatively concur. Additionally, Yoshihara, *et al.*[11] have determined from a careful solvatochromatic study that the excited-state dipole of 1PP could either be negative or positive, -3.0 or 1.6 D (relative to an assumed value of 10 D for the LE state of DMABN).

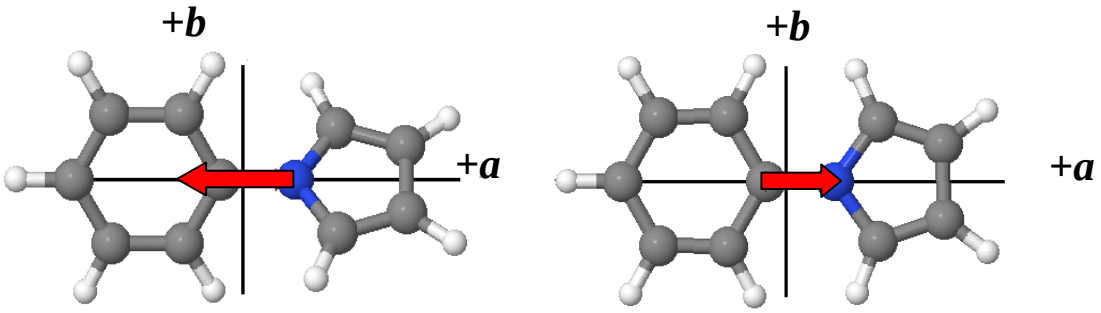


**Scheme 4.2. Ground (left) and excited (right) state permanent electric dipole moments of 1-phenylpyrrole.**

## 4.4 CONCLUSION

A dipole change of $\Delta\mu \approx 2.5$ D is calculated to result from a transfer of charge of ~ 0.15 $e^-$ from the pyrrole ring to the benzene ring, whose centers of mass are separated by 3.6 Å. This amount of charge transfer could easily explain the magnitude of the measured red shift in solution. Notwithstanding the possible effects of solvent, we estimate for the gas phase molecule a shift of 700 $cm^{-1}$. More problematic is the nature of the $S_1$ state accessed in our experiments. According to Proppe, *et al*.,[4] the lower $1^1B$ state has very low oscillator strength and a negative dipole moment, whereas the higher lying $2^1A$, $2^1B$, and $3^1A$ states have both higher oscillator strengths and positive dipole moments. Thus, it may be that the state whose properties are measured here is a mixed state, containing both locally excited as well as charge transfer character. Such mixing may result from efficient vibronic coupling involving the more polar $^1L_a$ state, as in the original PICT model for charge transfer in electronically excited states.[12]

## 4.5 SUPPORTING INFORMATION

### 4.5.1 Methods.

1-Phenylpyrrole (99%) was obtained from Aldrich and used without further purification. The experimental set-up has been described in detail elsewhere[13] and will be summarized here. The vibrationally resolved spectrum was obtained by collecting the fluorescence emitted when a supersonic jet expansion of the molecule in a vacuum chamber was crossed by a UV laser. The

supersonic jet was prepared by heating the molecule to 35 °C in ~2000 Torr of He and passing the resulting mixture through a pulsed nozzle (General Valve, Series 9) into a $10^{-5}$ Torr vacuum chamber. The UV laser was produced by pumping a dye laser with the second harmonic of an $Nd^{3+}$:YAG laser and frequency doubled using a KDP crystal. Presented spectra are power normalized.

The rotationally resolved spectra were collected using a CW set-up.[14] The output of an argon-ion pumped dye laser was frequency doubled. A collimated molecular beam was produced by heating the molecule in a quartz nozzle with a 200 μm orifice producing a supersonic jet expansion which was skimmed approximately 2 cm downstream. Spherical mirrors collected the resulting fluorescence and directed it towards a PMT.

To obtain the Stark spectra, a set of transparent wire mesh plates was positioned approximately 0.5 cm above and below the intersection region of the laser and molecular beams and a voltage was applied across them. The spectra were recorded by collecting the fluorescence in the presence of electric fields of various strengths. The plate separation was calibrated using the known dipole moments of aniline.[7]

Optimization and frequency calculations were performed using Gaussian03[15] with the M05-2X and CIS levels of theory and a 6-31G basis set. The PES's for both the ground and excited electronic states were generated by scanning the torsional angle and optimizing the remainder of the molecule at each step.

### 4.5.2 Spectroscopy Results and Discussion

The vibrationally resolved spectrum of 1PP is shown in Figure 4.3. There are two progressions of bands with spacings of ~50 $cm^{-1}$. These have been studied by Okuyama, *et al.*[3] using both fluorescence excitation and dispersed fluorescence techniques. Based on overlapping 0-0 and 1-1 transitions, they identified the bands of the more intense progression as alternating even-even and odd-odd transitions of the torsional motion. Thus, the bands occurring at +269.0, +316.9, and +364.5 $cm^{-1}$ above the origin were assigned $T_0^8$, $T_1^9$, and $T_0^{10}$, respectively. In this work, we collected and fit the rotationally resolved spectra of these bands and found that the ground state rotational constants of all three bands are the same, within error (see Table 4.1). This indicates that the transitions originate in the same ground state vibrational level. If the transition at +316.9 $cm^{-1}$ originated in $\nu = 1$, then its rotational constants would be different from those of transitions that originate in $\nu = 0$.

The three lowest calculated vibrational frequencies of 1PP (< 200 $cm^{-1}$) are listed in Table 4.2. Since transitions to both even and odd $\nu$ are allowed, the excited state vibrational mode must belong to the A representation. Given its symmetry and calculated frequency, 39.7 $cm^{-1}$, the most likely coordinate for the progression of low energy vibronic bands that are spaced 40 – 50 $cm^{-1}$ apart is the symmetric torsional mode.

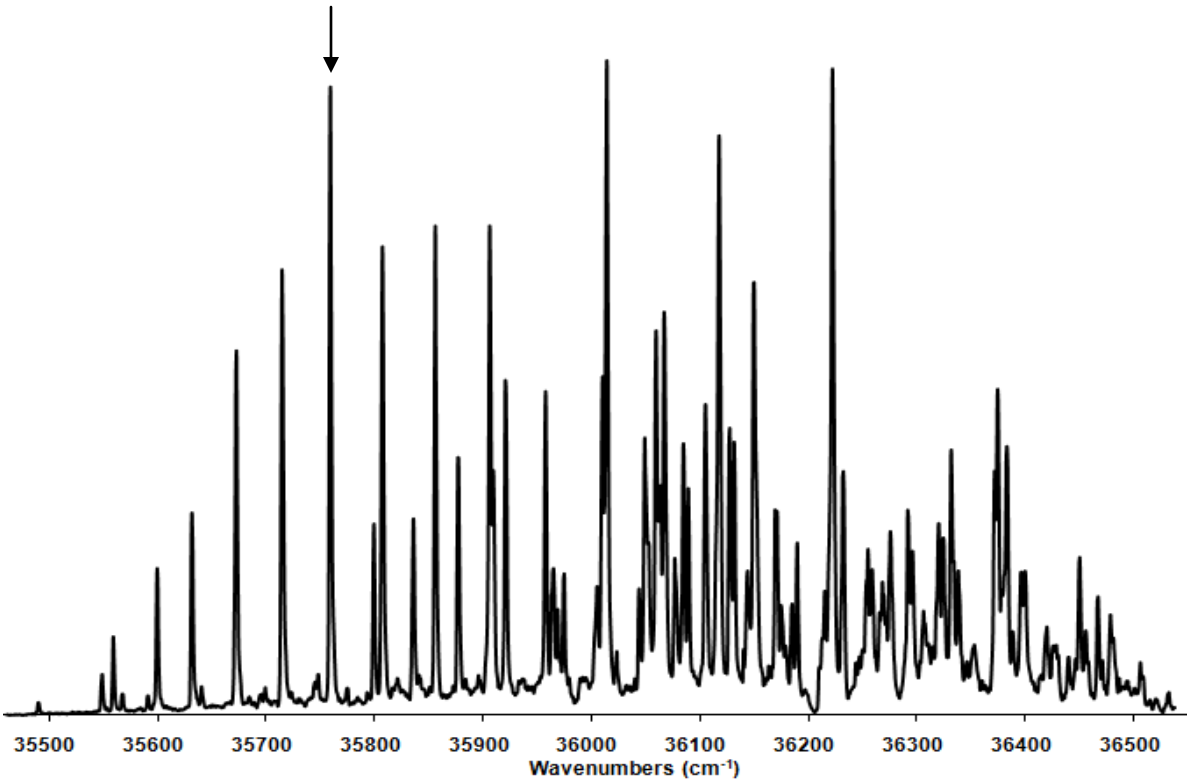


**Figure 4.3. Vibrationally resolved spectrum of 1-phenylpyrrole. The origin is located at 35489.8 $cm^{-1}$. The band marked by an arrow, at +269.0 $cm^{-1}$, was studied in high resolution in the presence of an electric field.**

**Table 4.1. Ground and excited state rotational constants, inertial defects, and dipole moments for 1-phenylpyrrole.**

| | **+269.0 $cm^{-1}$** | **+316.9 $cm^{-1}$** | **+364.5 $cm^{-1}$** |
|---|---|---|---|
| **A" (MHz)** | 3508.3(1) | 3508.4(1) | 3508.9(1) |
| **B" (MHz)** | 703.5(1) | 703.4(1) | 703.4(1) |
| **C" (MHz)** | 604.8(1) | 604.8(1) | 604.8(1) |
| **ΔI" (amu·Å$^2$)** | -26.88(1) | -26.89(1) | -26.87(1) |
| **$\mu_a$" (D)** | -1.56(1) | * | * |
| **A' (MHz)** | 3379.7(1) | 3379.1(1) | 3378.7(1) |
| **B' (MHz)** | 710.6(1) | 710.6(1) | 710.0(1) |
| **C' (MHz)** | 595.4(1) | 596.0(1) | 596.4(1) |
| **ΔI' (amu·Å$^2$)** | -12.00(1) | -12.77(1) | -14.05(1) |
| **$\mu_a$' (D)** | 0.94(1) | * | * |
| **Doppler (MHz)** | 18 | 18 | 18 |
| **Lorentzian (MHz)** | 25 | 25 | 25 |
| ***a/b/c* (%)** | 0/87.5/12.5 | 0/87.5/12.5 | 0/87.5/12.5 |
| **# lines fit** | 264 | 225 | 126 |
| **OMC (MHz)** | 3.88 | 3.46 | 5.03 |
| **OMC (MHz) – Stark** | 4.86 | * | * |

*Not measured

**Table 4.2. Calculated low frequency vibrations of 1-phenylpyrrole (M05-2X/6-31G).**

| $S_0$ | | | $S_1$ | | |
|---|---|---|---|---|---|
| Frequency (MHz) | Description | Symmetry | Frequency (MHz) | Description | Symmetry |
| 74.3 | Torsion | A | 31.2 | Out-of-plane Bend | B |
| 106.0 | Out-of-plane Bend | B | 39.7 | Torsion | A |
| 147.7 | In-plane Bend | B | 176.9 | Complicated motion similar to in-plane bend | B |

If the observed progression is monotonic in this coordinate, an explanation for the appearance of both "even" and "odd" transitions is required. The energies and rotational constants for structures with a range of torsional angles were calculated at the M05-2X level of theory using the 6-31G basis set. The resulting graph, Figure 4.4 (bottom), reveals a 4-fold potential over the 360° torsional space with barriers to planarity of 634 $cm^{-1}$ and barriers to perpendicularity of 824 $cm^{-1}$. The molecule is most stable at one of four equivalent torsion angles with the pyrrole group oriented ±37.3° with respect to the phenyl group.

The PES along the torsion coordinate of the excited electronic state was also calculated (Figure 4.4, top). The barrier to planarity of 164 $cm^{-1}$ is greatly reduced with respect to the ground state. The barrier to perpendicularity, on the other hand, is about an order of magnitude larger than in the ground state. The difference in PES's indicates a significant change in the equilibrium structure in the excited state. This change is confirmed by the appearance of a progression of bands in the vibrationally resolved spectrum. Large overlap of the ground and excited state wavefunctions leads to intense bands. When there is no shift of the excited state wavefunction with respect to the ground state, the origin is the most intense band. That is not the case here. The origin has very low intensity and the +269.0 $cm^{-1}$ band is among the most intense

of the spectrum. The significant change in equilibrium structure upon excitation results in a change in the selection rules and the appearance of both “even” and “odd” transitions in the spectrum.

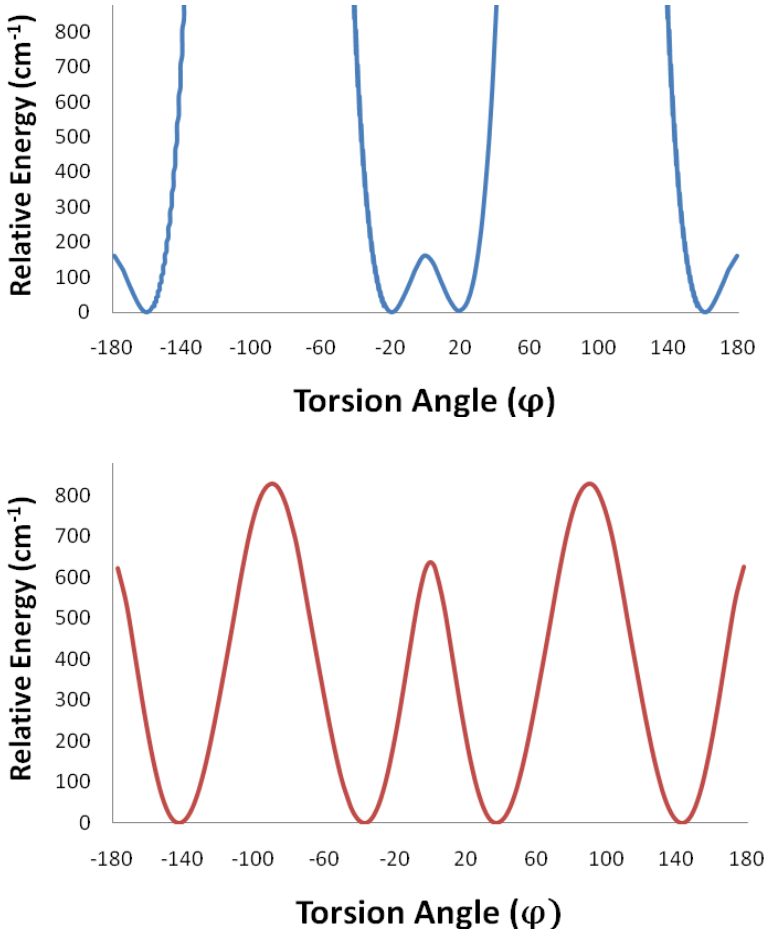


**Figure 4.4. PES’s for the torsional coordinate in the ground (bottom) and excited (top) states calculated at M05-2X/6-31g and CIS/6-31g, respectively.**

## 4.6 REFERENCES


1. W. Rettig and F. Marschner, *Nouv. J. Chim.* **1983**, *7*, 425.
2. K. Rotkiewicz, K. H. Grellmann and Z. R. Grabowski, *Chem. Phys. Lett.* **1973**, *19*, 315. See also *Chem. Phys. Lett*. **1973**, 321, 212(E).
3. K. Okuyama, Y. Numata, S. Odawara and I. Suzuka, *J. Chem. Phys.* **1998**, *109*, 7185.
4. B. Proppe, M. Merchán and L. Serrano-Andrés, *J. Phys. Chem. A* **2000**, *104*, 1608.
5. M. Klessinger and J. Michl, *Excited States and Photochemistry of Organic Molecules*, John Wiley & Sons, **1995**.
6. S. Golden and E. B. Wilson, *J. Chem. Phys.* **1948**, *16*, 669.
7. T. M. Korter, D. R. Borst, C. J. Butler and D. W. Pratt, *J. Am. Chem. Soc.* **2001**, *123*, 96.
8. H. Lumbroso, D. M. Bertin and M. Freimut, *J. Molec. Struct.* **1988**, *178*, 187.
9. S. Zilberg and Y. Haas, *J. Phys. Chem. A* **2002**, *106*, 1.
10. S. Cogan, S. Zilberg and Y. Haas, *J. Am. Chem. Soc.* **2006**, *128*, 3335.
11. T. Yoshihara, S. I. Druzhinin, A. Demeter, N. Kocher, D. Stalke and K. A. Zachariasse, *J. Phys. Chem. A* **2005**, *109*, 1497.
12. K. A. Zachariasse, *Chem. Phys. Lett.* **2000**, *320*, 8.
13. J. R. Johnson, K. D. Jordan, D. F. Plusquellic and D. W. Pratt, *J. Chem. Phys.* **1990**, *93*, 2258.
14. W. A. Majewski, J. F. Pfanstiel, D. F. Plusquellic and D. W. Pratt in *High resolution optical spectroscopy in the ultraviolet, Vol. XXIII* Eds.: A. B. Myers and T. R. Rizzo), John Wiley & Sons, Inc., **1995**, p. 101.
15. M. J. Frisch, *et al.*, *Gaussian03*, Revision C.02, Gaussian, Inc., Wallingford, CT, **2004**.

# 5.0 A LASER ABLATION SOURCE FOR THE VIBRATIONALLY RESOLVED ELECTRONIC SPECTROSCOPY EXPERIMENT

Jessica A. Thomas and David W. Pratt

Department of Chemistry, University of Pittsburgh, Pittsburgh, PA 15260, USA

## 5.1 ABSTRACT

The vibrationally resolved electronic spectroscopy experiment used by the Pratt Group at the University of Pittsburgh is a laser induced fluorescence (LIF) experiment. Typically, a solid or liquid sample is heated to increase its vapor pressure and the vaporized molecules are then entrained in an inert gas that is expanded into a vacuum chamber through a pulsed nozzle to create a supersonic expansion. Some molecules, particularly those the size of amino acids and larger, decompose before enough heat is added to achieve a sufficient vapor pressure. Thus, a laser ablation source, based on the one used by Piuzzi, *et al.*[1] was added to the LIF experiment for use with molecules that tend to decompose with intense heating. The new source was tested first on 2-methoxynaphthalene and tryptophol, samples that were previously studied in our lab using the thermal vaporization source, then on acetyl-tryptophan-amide and acetyl-tryptophan-methylamide which are protected amino acids that also decompose when heated.

## 5.2 THEORY

While the terms ablation and desorption are commonly used interchangeably, they actually describe two different processes. Desorption is the removal of a layer of sample from the surface of a substrate; the opposite of adsorption. Ablation, on the other hand, occurs when a sample is mixed homogeneously with a matrix and a volume of the mixture is ejected by the laser pulse.[2]

Figure 5.1 illustrates the difference between the two processes where (a) shows a substrate supporting a layer of sample and (b) shows a pellet made from a mixture of sample and matrix molecules as is used in the experiment described below. However, the distinction between desorption and ablation is not absolute. One can imagine a laser pulse that is powerful enough to ablate part of the substrate along with a sample prepared for desorption as well as a laser weak enough to merely desorb sample molecules from a matrix rather than ablate them. In addition to the power of the laser, its wavelength and the identity of the substrate or matrix also play a role in determining the depth to which the laser can penetrate the sample pellet.

Samples that are desorbed or ablated rather than heated are less likely to decompose because of the time scale of the processes. When a sample container is heated the molecules are constantly exposed to the heat source, even after vaporization, until they are entrained in the inert gas and escape through the nozzle. The heating time can be shortened by placing the heated sample container after the nozzle as was done by Simons and coworkers;[3] however, this technique reduces decomposition only in small biomolecules. Both desorption and ablation

occur on a shorter time scale than thermal vaporization as described in the following paragraphs, though the mechanism of ablation is not as well understood as that of desorption.

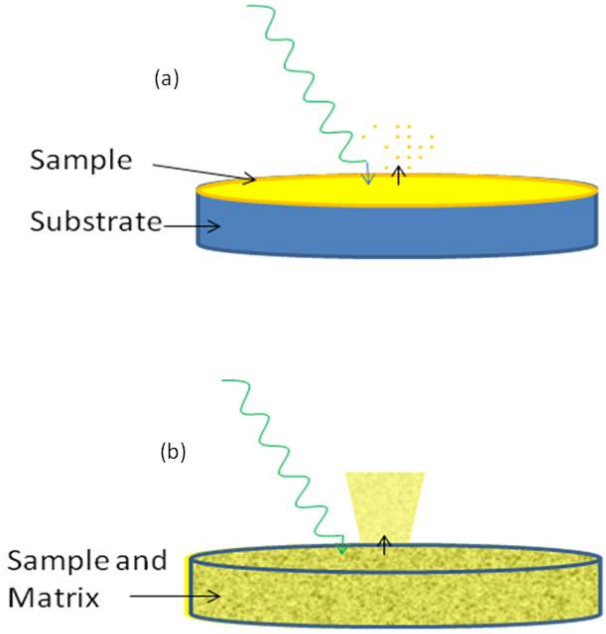


**Figure 5.1. Schematic of (a) thermal laser desorption and (b) non-thermal laser ablation or ejection. Adapted from Ref. 2.**

Although the activation energy required for decomposition is often lower than that needed for desorption, fast heating kinetically favors the desorption pathway over decomposition. In the equations below from Levis,[2] $E_{des}$ and $E_{react}$ are the barriers to desorption and decomposition, respectively where $E_{des} > E_{react}$. However, if the frequency factor for desorption, $\upsilon_{des}$, is significantly larger than $\upsilon_{react}$, then the rate of desorption, $\frac{d[\theta]_{des}}{dt}$, will be faster than the rate of decomposition, $\frac{d[\theta]_{react}}{dt}$, and intact gas phase molecules will be produced.

$$\frac{d[\theta]_{des}}{dt} = [\theta]_{ads}^{n} \cdot \nu_{des} \cdot e^{\frac{-E_{des}}{RT}} \tag{5.1}$$

$$\frac{d[\theta]_{react}}{dt} = [\theta]_{ads}^{n} \cdot \nu_{react} \cdot e^{\frac{-E_{react}}{RT}} \tag{5.2}$$

In addition to the kinetic model described in the preceding paragraph, desorption (and ablation) can also be explained by energy transfer. The incident energy from the laser is absorbed by the substrate (or matrix). Because the vibrations of the sample molecules occur at different frequencies than those of the substrate (matrix), the intermolecular interactions between the sample and substrate (matrix) are broken by the absorbed energy before it can be transferred to the sample molecules causing excitation and fragmentation. This also explains why ablated molecules have lower vibrational temperatures than the molecules that remain in the solid sample.[2]

The remainder of this chapter will focus on laser ablation rather than desorption as it is the method implemented at the University of Pittsburgh. The matrix used in a sample pellet must be chemically inert to the sample, able to homogeneously mix with the sample, and able to absorb the incident laser light. Common matrices used in matrix-assisted laser desorption ionization (MALDI) of biomolecules are 2,5-dihydroxybenzoic acid[4,5] and α-cyano-4-hydroxycinnamic acid.[6,7] Good results have been obtained using fluorescent dyes as a matrix,[8,9] but care needs to be taken that such a matrix does not interfere with a fluorescence experiment. Alonso and coworkers[10] have used a variety of matrices, including cellulose derivatives and starch, to study small, biologically relevant molecules. In this work, powered graphite was used to prepare most of the pellets, as in the work by Piuzzi, *et al.*[1]

Various wavelengths of light from IR to UV have been used for ablation. Infrared light tends to ablate more sample per pulse than UV light. Conversely, UV light can be used to probe the same spot on a pellet hundreds of times, releasing a moderate amount of sample each time, whereas an IR laser pulse exhausts a spot on the pellet after only a few shots.[2]

## 5.3 IMPLEMENTATION

The vibrationally resolved LIF experiment has been described in previous chapters. For the addition of laser ablation a mount was designed to attach to the face of the General Valve nozzle to position the sample pellet and optical fiber near the opening of the nozzle (see Figure 5.2). A collar holds the mount in place and is easily detachable for switching back to a thermal vaporization set-up.

The sample pellets consist of the sample and a matrix. Successful matrices used in this experiment include graphite and diatomaceous earth. A small amount of sample is mixed with the matrix, usually in a 1:4 molar ratio which was determined to be optimal by Piuzzi, *et al.*[1] The mixing is achieved by hand in a mortar and pestle which grinds the matrix into fine particles for homogeneous mixing. The mixture is then pressed into a pellet of approximately 1 cm diameter and 3 mm width using a die and a hydraulic press. The edge of the pellet is filed to create a flat surface for interaction with the laser beam. The flat edge of the pellet is mounted approximately 1 mm from the aperture of the nozzle. To conserve sample when working with expensive and/or custom-made biomolecules, a pellet can also be made using a 6 mm rather than 1 cm diameter die.

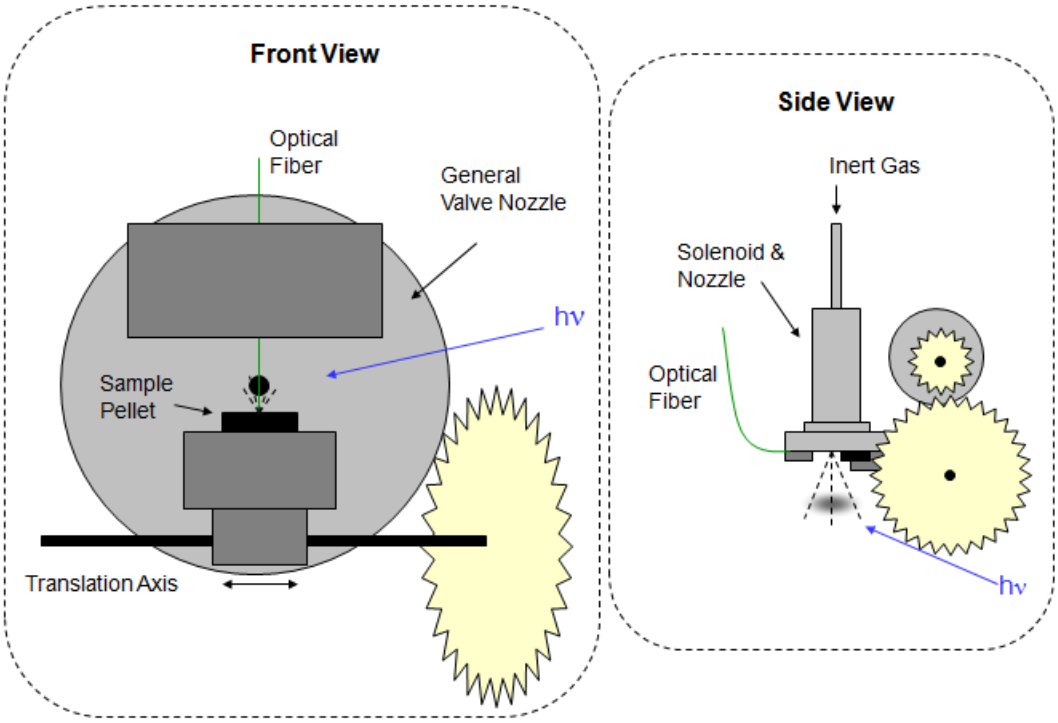


**Figure 5.2. Front and side views of laser ablation mount with motor.**

The radiation used for ablation is the second harmonic of an Nd:YAG laser (Continuum Minilite I). Approximately 5 mJ/pulse is required for sufficient ablation to occur. The radiation is directed to the pellet *via* an optical fiber. As the radiation leaves the laser, it is focused by a lens into a 1 mm diameter optical fiber that is coated for total internal reflection in the UV/vis region of the spectrum. The fiber passes through one of the flanges of the vacuum chamber through a modified Swagelok connection where a 1 mm diameter hole is bored through a Teflon fitting.[11] The output end of the fiber is mounted on the face of the nozzle approximately 1 mm from the aperture and directly across from the mounted sample pellet.

The pre-existing configuration of the vacuum chamber had the nozzle directed down towards the diffusion pump. In order to align the pellet and optical fiber on the nozzle mount, a

camera is temporarily mounted above the diffusion pump and aimed at the nozzle as needed. The image is displayed on a television screen mounted next to the vacuum chamber and can be seen by the researcher while fine adjustments are made. A handheld mirror is also used to check the size and location of the laser beam spot on the edge of the pellet.

In order to increase the amount of time a pellet can be used before opening the chamber and refiling its surface, the nozzle mount was modified by adding a motor to move the pellet and expose fresh sample. The motor moves the stage holding the pellet back and forth across the face of the nozzle. Adjustable magnets are used to indicate the turn-around positions and confine the motion to the unique width of the filed surface of the pellet. A control box located outside the vacuum chamber is used to turn the motor off and on and to control the speed of the translation. Fast translation counteracts slight heterogeneities in the pellet by averaging them out. Because the 532 nm light does not deplete all of the sample molecules from a spot with a single shot, the pellet can be scanned back and forth many times before it needs to be refiled.

## 5.4 RESULTS

### 5.4.1 2-Methoxynaphthalene (2MN)

Scheme 5.1 shows the species studied in this work. The sample used to perform the first test of the laser ablation device was 2-methoxynaphthalene because the frequency of its electronic origin is well known,[12] it has a high fluorescence intensity, it is structurally similar to tryptophan (the target molecule), and it is relatively inexpensive.

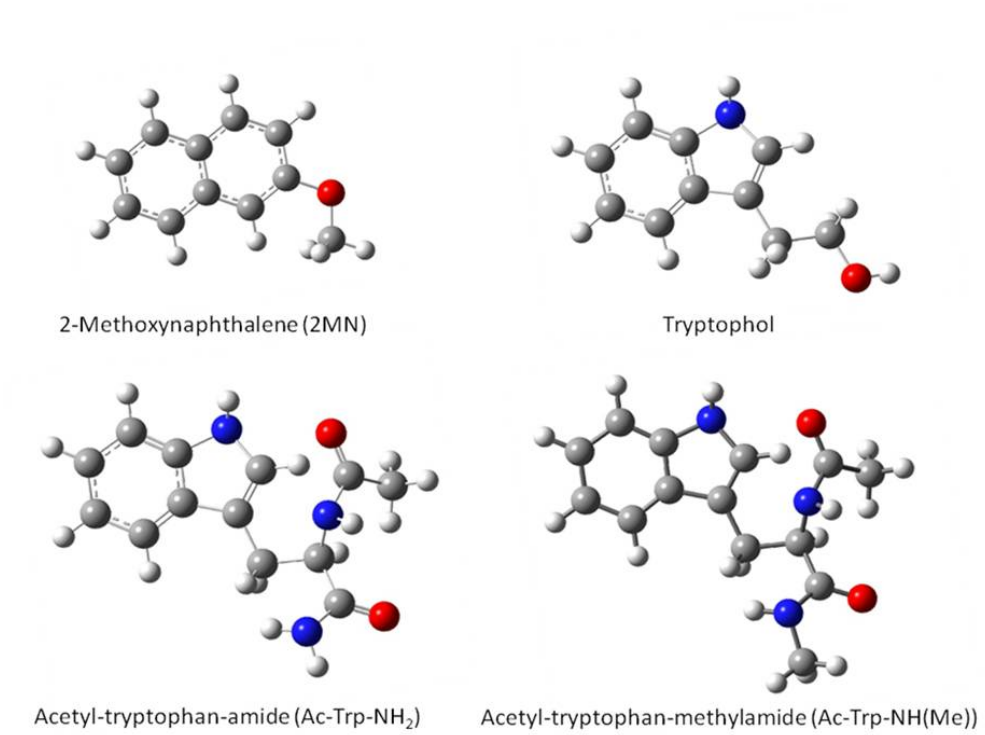


**Scheme 5.1. Molecular structures of molecules studied via laser ablation.**

Figure 5.3 compares the spectra obtained by (a) heating the sample and (b) laser ablation. The intensity of the *cis* origin was approximately the same in both cases, depending on the power of the ablation laser. Thus, the laser ablation set-up was successful at producing enough gas phase molecules to collect a spectrum. However, the noise in the laser ablation spectrum suggests that the sample molecules were not cooled as much as they were in the thermal vaporization experiment. This is apparent from the increase in spectral noise with increasing ablation laser power represented by the two traces in Figure 5.3 (b). At the higher ablation power, the molecules were hotter, resulting in populated vibrational levels above the ground state and a greater proportion of molecules in the less-favored *trans* configuration. The populated

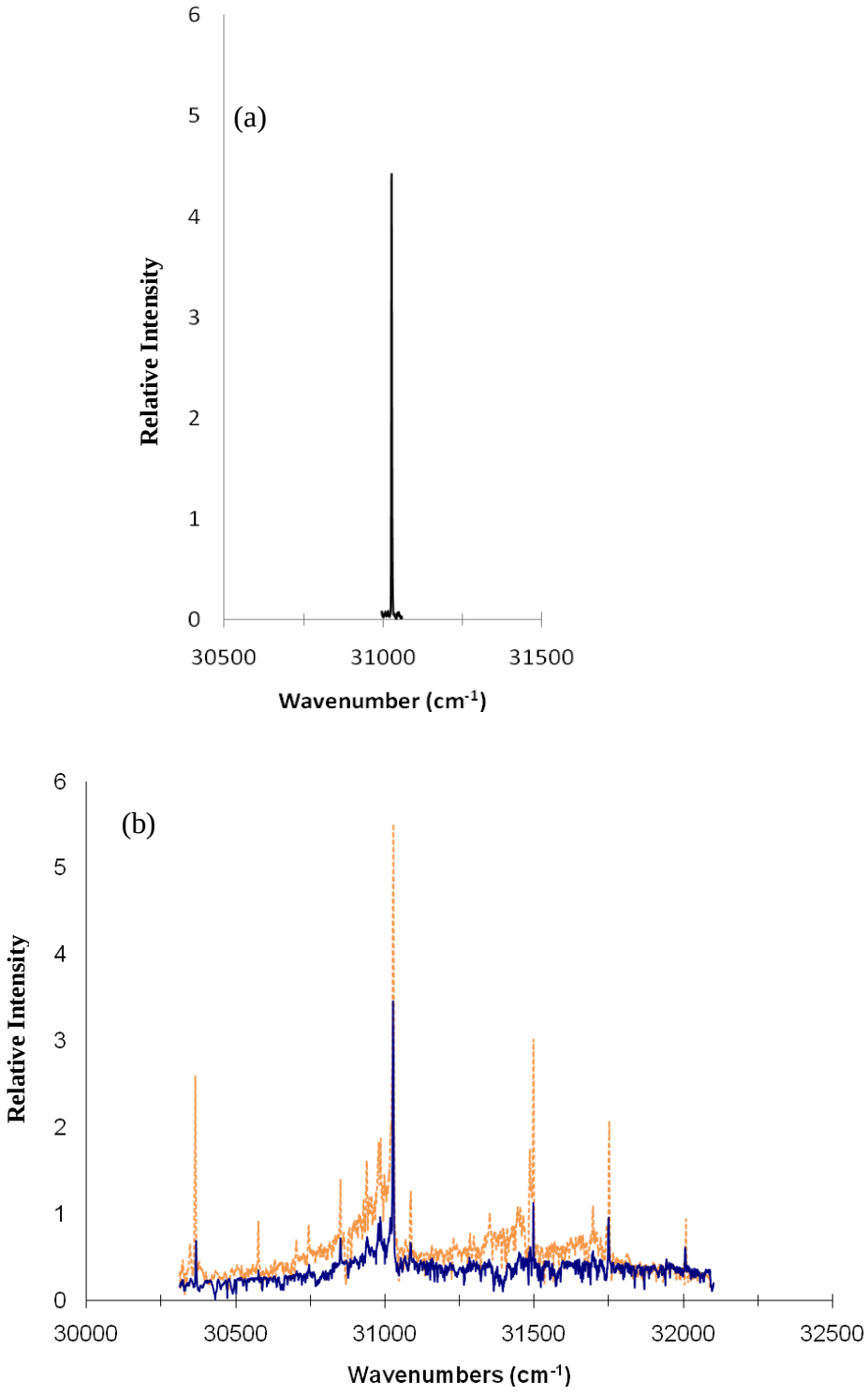


**Figure 5.3. (a) Electronic origin of the *cis* conformer of 2-methoxynaphthalene obtained by heating the sample. (b) Vibrationally resolved electronic spectrum of 2-methoxynaphthalene obtained by laser ablation. The orange, dashed spectrum was collected with higher ablation laser power.**

vibrational levels lead to hot bands to the red of the electronic transitions originating from the ground state. The increased population of the *trans* conformer can be seen in the relative increase of the transition at 30367 $cm^{-1}$ with respect to the transition at 31028 $cm^{-1}$.

### 5.4.2 Tryptophol

Tryptophol was used for a pressure study to determine the effects of backing pressure on linewidth. In Figure 5.4 it is apparent that raising the pressure of the backing gas lowers the linewidth of each band. It also becomes clear that this changes the relative abundance of the conformers in the expansion. The peaks labeled A, B, and C correspond to different conformers. The remaining band, A′ is a vibronic band of the A conformer which was previously identified as the most stable.[13] While the intensity of conformer A is affected very little by the increase in backing pressure, the intensities of conformers B and C are affected significantly. Both the decrease in relative intensity of the B and C bands and the decrease in the linewidth of all the transitions when pressure is increased provide evidence that the sample molecules entrained in the higher pressure inert gas are cooled more efficiently. This is because cooler sample molecules result in fewer populated vibrational levels and the observation of only low energy conformers. When the backing pressure is high, there are more collisions between the sample molecules and the backing gas, resulting in more occurrences of excess energy transfer from the sample to the inert gas and effective sample cooling.

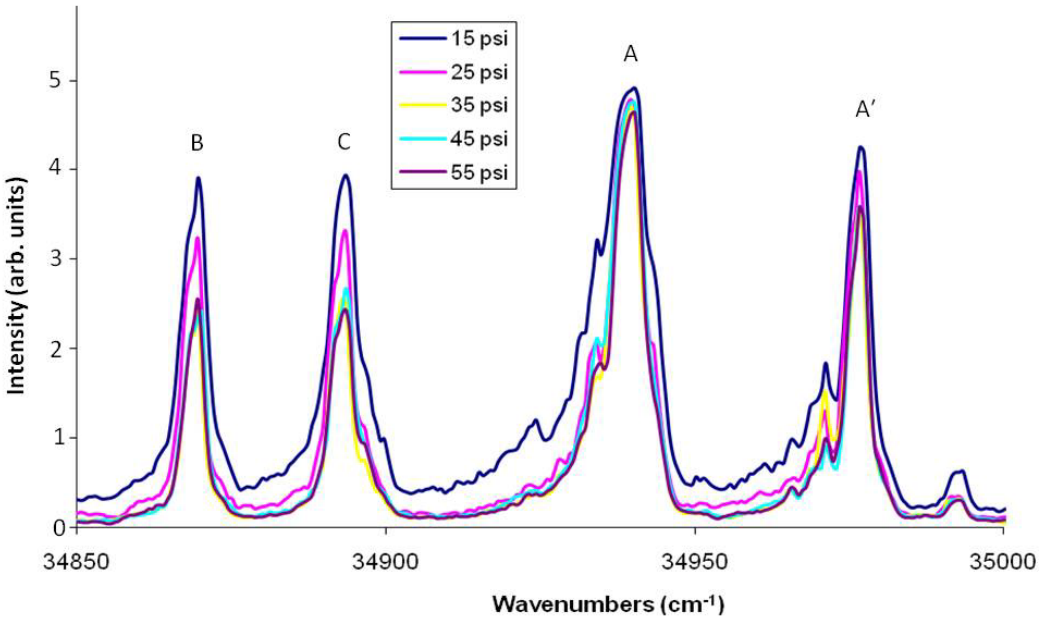


**Figure 5.4. Vibrationally resolved spectrum of tryptophol collected using laser ablation. Each trace was collected with a different inert gas backing pressure.**

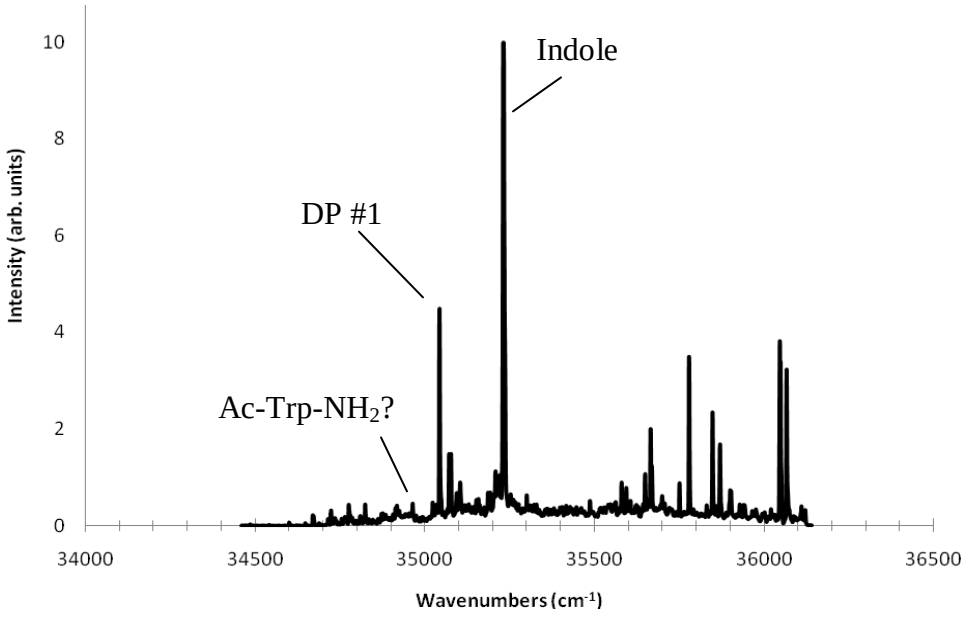


**Figure 5.5. Vibrationally resolved electronic spectrum of Ac-Trp-$NH_2$ obtained using the thermal vaporization source. The largest peaks correspond to indole and another decomposition product labeled DP#1 by Dian *et al.*[14]**

### 5.4.3 Acetyl-tryptophan-amide (Ac-Trp-$NH_2$)

Acetyl-tryptophan-amide (Scheme 5.1) is the amino acid tryptophan with an N-terminal acetyl group and a C-terminal amide group. These caps are analogous to a short segment of a neighboring amino acid within a peptide. According to Dian, *et al.*,[14] Ac-Trp-$NH_2$ forms two conformers in the gas phase. One conformer produces narrow vibronic transitions with an electronic origin at 34961 $cm^{-1}$. The other conformer produces a broad fluorescence spectrum.

In this work, when Ac-Trp-$NH_2$ was heated, only a small fluorescence signal was detected near the electronic origin (see Figure 5.5) and the sample turned from white to brown in color. Intense fluorescence was detected at 35231 $cm^{-1}$ which corresponds to the electronic origin of indole[15] confirming the decomposition. Use of an external oven, similar to that used by Simons and coworkers,[3] resulted in the spectrum in Figure 5.6. Here, the intensity of the desired peak is significantly stronger than the peak due to the indole decomposition product. However, the signal-to-noise is low indicating that the sample molecules are not as cool as in the thermal vaporization spectrum of Figure 5.5.

Figure 5.7 shows the spectrum obtained from the ablation of Ac-Trp-$NH_2$. As with the other molecules studied *via* ablation, Ac-Trp-$NH_2$ produced a broad spectrum that seems to indicate radiationless decay. However, the pathway is unknown. According to Piuzzi,[16] this is typical for the fluorescence of tryptophan compounds. Perhaps this is also the case for related molecules such as 2MN.

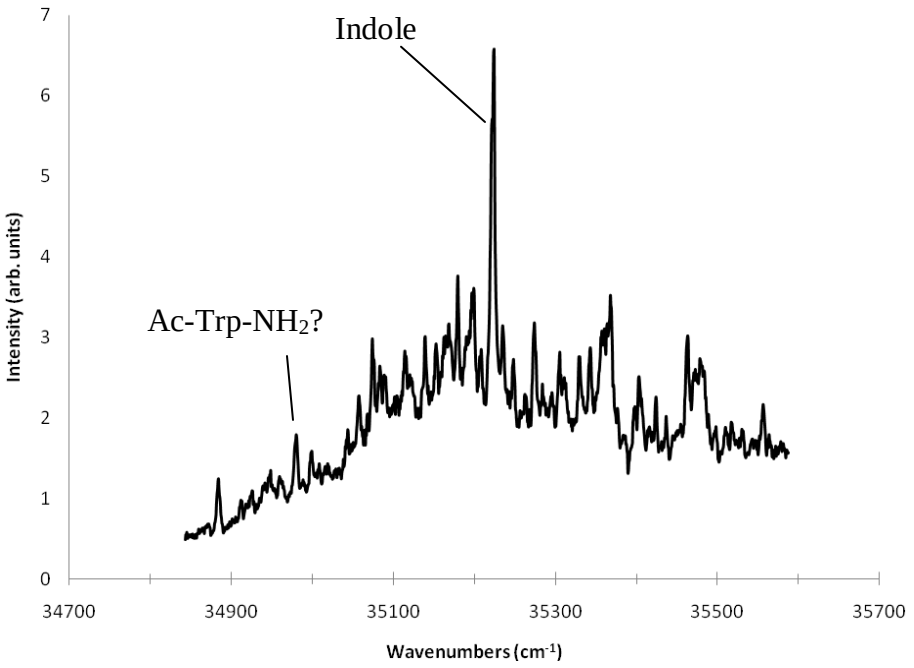


**Figure 5.6. Vibrationally resolved electronic spectrum of Ac-Trp-$NH_2$ obtained by heating the sample using an external oven.**

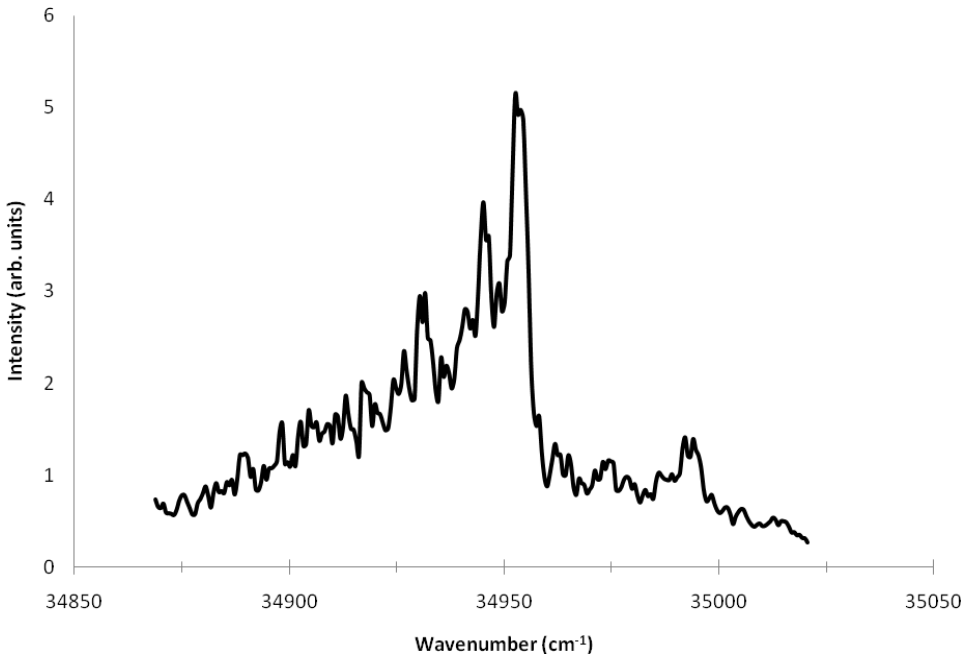


**Figure 5.7. Vibrationally resolved spectrum of Ac-Trp-$NH_2$ collected using laser ablation.**

The spectra in Figure 5.8 were collected before the addition of the translation motor to the laser ablation mount and show how the sample is depleted as it is ablated by the laser pulse. Scan "a" was collected by positioning an unused portion of the pellet in front of the optical fiber. The subsequent scans, b-e, were collected one after another without repositioning the pellet. The intensity of each scan is lower than the previous one demonstrating the need for the motorized mount to move the pellet and expose fresh sample without opening the chamber.

An attempt was made to collect rotationally resolved electronic spectra of Ac-Trp-$NH_2$ using thermal vaporization, but sticky brown decomposition products repeatedly clogged the 200 μm nozzle. The addition of a laser ablation source to the high resolution experiment has been discussed, but the implementation would be quite different than the experiment described here. The rotationally resolved experiment has a CW laser and continuous nozzle, thus the 10 Hz Nd:YAG used for ablation here would not be appropriate. A kHz YAG laser has been proposed. Also, the fragile quartz nozzle has a unique shape that could not support the collar mounted device designed for the low resolution experiment. A new mount, perhaps supported by the walls of the chamber, would be necessary.

### 5.4.4 Acetyl-tryptophan-methylamide (Ac-Trp-NH(Me))

Finally, the spectrum of a related molecule was collected. Acetyl-tryptophan-methylamide differs from Ac-Trp-$NH_2$ by a methyl group on the terminal nitrogen which further approximates a peptide structure. Ac-Trp-NH(Me) was synthesized by a colleague, Matthew Kofke, using the method described by Dian, *et al.*[14] and its identity was confirmed *via* NMR.

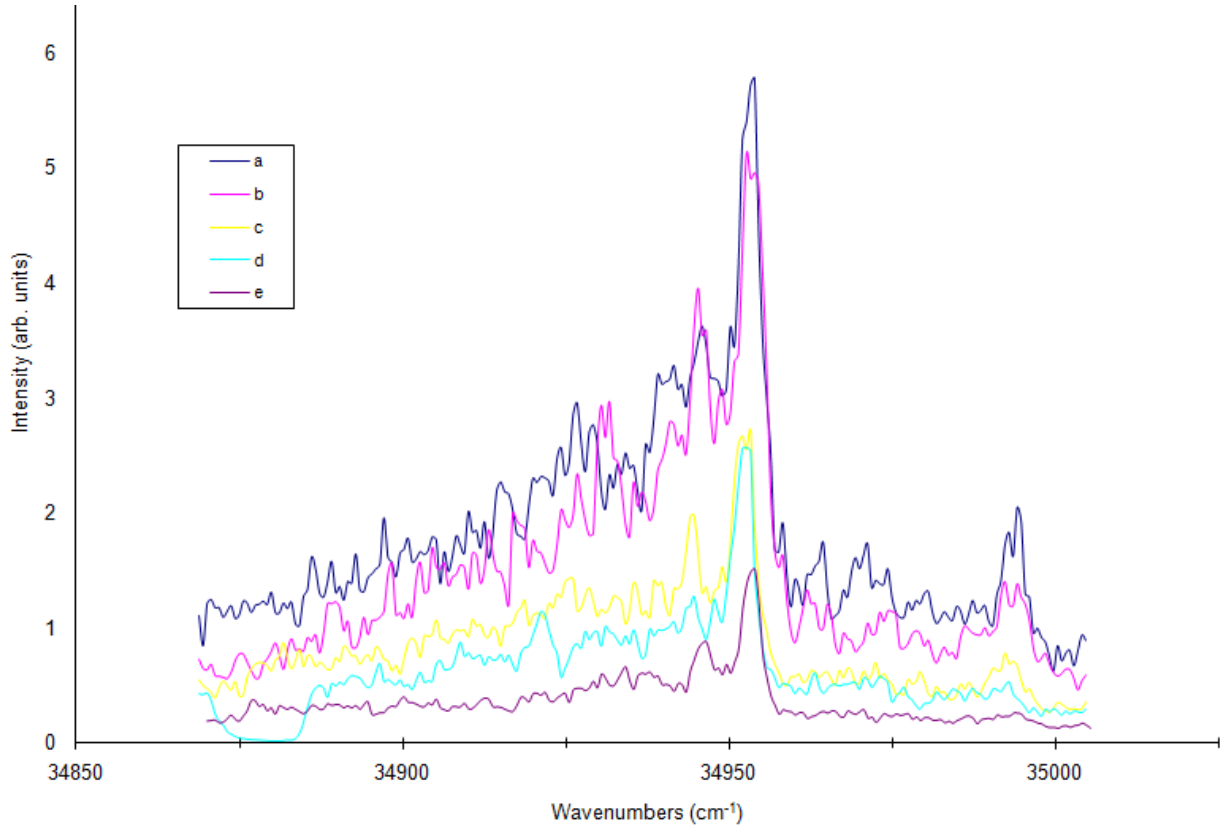


**Figure 5.8. Vibrationally resolved electronic spectrum of Ac-Trp-$NH_2$ collected using laser ablation. All traces were collected with the ablation laser focused on the same spot on the sample pellet. The decrease in intensity with each scan after scan "a" indicates that the sample is being used up.**

Despite the relatively small difference in chemical formula, the vibrationally resolved electronic spectra of Ac-Trp-$NH_2$ and Ac-Trp-NH(Me) are significantly different (compare Figures 5.7 and 5.9). Using UV-UV hole burning, Dian, *et al.*[17] distinguished three conformers of Ac-Trp-NH(Me), one of which produced a broad fluorescence of low intensity. The electronic origins of all three conformers of Ac-Trp-NH(Me) are red-shifted with respect to those of Ac-Trp-$NH_2$. The two conformers with narrow transitions can be identified in the vibrationally resolved spectrum produced using laser ablation.

Dian, *et al*.[17] subsequently performed IR/UV double resonance spectroscopy experiments on this molecule to collect the IR spectra of each conformer, similar to the experiments detailed in the next chapter. The IR spectra were used to identify intramolecular interactions in the molecule for comparison with the lowest calculated structures resulting in conformational assignments.

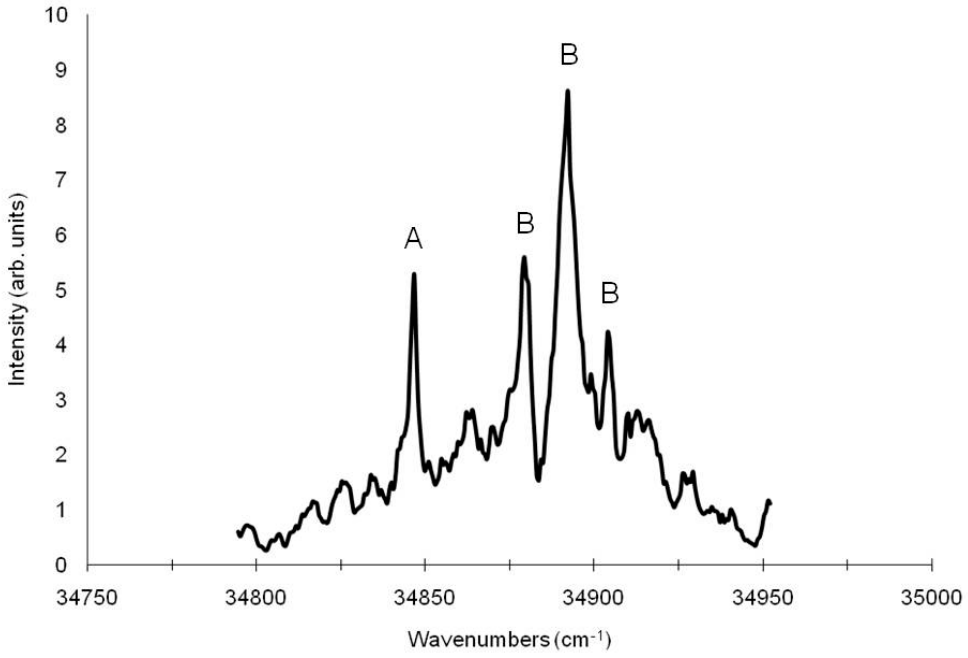


**Figure 5.9. Vibrationally resolved spectrum of Ac-Trp-NH(Me) obtained using laser ablation. Bands corresponding to two different conformers identified by Dian, et al.[17] are labeled A and B.**

## 5.5 CONCLUSION

Laser ablation was successfully implemented in the vibrationally resolved laser induced fluorescence experiment at the University of Pittsburgh. While the spectrum of a molecule that

is facile to obtain in the gas phase by heating such as 2MN will have a lower signal-to-noise ratio when vaporized by laser ablation, the results of the Ac-Trp-$NH_2$ experiment shows that decomposition of more sensitive molecules is reduced leading to fluorescence spectra that would not otherwise be obtained. In addition, it is possible to attain spectra of multiple conformers such as in the case of Ac-Trp-NH(Me). However, the relative intensities of these conformers can be affected by the temperature of the sample so the pressure of the inert backing gas and the power of the ablation laser must be adjusted to optimize the linewidth and signal-to-noise ratio.

The primary matrix used was powdered graphite, as used in the Mons group, although experiments with diatomaceous earth also were successful. The laser ablation apparatus is removable so that it can be added to the nozzle for the study of molecules that tend to decompose and removed to make room for the sample container used for thermal vaporization. The stage that holds the pellet is moveable and can be translated back-and-forth by a motor exposing more sample molecules without opening the chamber to atmospheric pressure.

## 5.6 ACKNOWLEDGEMENTS

Several members of the Department of Chemistry at the University of Pittsburgh provided assistance for this project. Dennis Sicher of the machine shop built and modified the laser ablation mount. Bob Muha of the electronics shop added the translation motor and external control box. Matthew Kofke, a fellow graduate student, synthesized the Ac-Trp-NH(Me) sample and Damodaran Krishnan, director of the NMR facility, took the NMR spectrum. Casey

Clements, another fellow graduate student, assisted in the collection of some of the ablation spectra.

François Piuzzi and Michel Mons answered countless questions *via* email regarding their laser ablation device leading up to my visit to CEA/Saclay. There I was able to use their equipment in person and benefit from their experience as well as that of Eric Gloaguen and Benjamin Tardivel. The experiments performed at CEA/Saclay are detailed in the next chapter.

## 5.7 REFERENCES

1. F. Piuzzi, I. Dimicoli, M. Mons, B. Tardivel and Q. Zhao, *Chem. Phys. Lett.* **2000**, *320*, 282.
2. R. J. Levis, *Annu. Rev. Phys. Chem.* **1994**, *45*, 483.
3. J. P. Simons, R. A. Jockusch, P. Carçabal, I. Hunig, R. T. Kroemer, N. A. Macleod and L. C. Snoek, *Int. Rev. Phys. Chem.* **2005**, *24*, 489.
4. I. Fournier, A. Brunot, J. C. Tabet and G. Bolbach, *Int. J. Mass Spectrom.* **2002**, *213*, 203.
5. M. E. Bier in *The Basics of MALDI and ESI Mass Spectrometers for Polymer Analysis*, New Orleans, LA, **2003**.
6. R. C. Beavis, T. Chaudhary and B. T. Chait, *Org. Mass Spectrom.* **1992**, *27*, 156.
7. I. Fournier, A. Brunot, J. C. Tabet and G. Bolbach, *J. Mass Spectrom.* **2005**, *40*, 50.
8. J. R. Cable, M. J. Tubergen and D. H. Levy, *J. Am. Chem. Soc.* **1987**, *109*, 6198.
9. K. Tang, S. L. Allman, R. B. Jones and C. H. Chen, *Org. Mass Spectrom.* **1992**, *27*, 1389.
10. A. Lessari, S. Mata, J. C. Lopez and J. L. Alonso, *Rev. Sci. Instrum.* **2003**, *74*, 4799.
11. E. R. I. Abraham and E. A. Cornell, *Applied Optics* **1998**, *37*, 1762.
12. L. Alvarez-Valtierra in *Molecular Excited State Dynamics via High Resolution Electronic Spectroscopy in the Gas Phase.*, Ph.D. Thesis, University of Pittsburgh, Pittsburgh, **2007**.
13. J. T. Yi and D. W. Pratt, *Phys. Chem. Chem. Phys.* **2005**, *7*, 3680.
14. B. C. Dian, A. Longarte, S. Mercier, D. A. Evans, D. J. Wales and T. S. Zwier, *J. Chem. Phys.* **2002**, *117*, 10688.
15. C. Kang, T. M. Korter and D. W. Pratt, *J. Chem. Phys.* **2005**, *122*, 174301.
16. F. Piuzzi, CEA/Saclay, Gif-sur-Yvette, France. Personal Communication, **2008**.
17. B. C. Dian, A. Longarte, P. R. Winter and T. S. Zwier, *J. Chem. Phys.* **2004**, *120*, 133.

# 6.0 STRUCTURAL DETERMINATION OF A FOLDING NUCLEUS IN THE GAS PHASE

Jessica A. Thomas,[a] Eric Gloaguen,[b] David W. Pratt,[a] Benjamin Tardivel,[b] François Piuzzi,[b] and Michel Mons[b]

[a]Department of Chemistry, University of Pittsburgh, Pittsburgh, PA, 15260, USA
[b]Laboratoire Francis Perrin, CEA/DSM/IRAMIS/SPAM – CRNS URA 2453, CEA/Saclay, 91191 Gif-sur-Yvette, France

## 6.1 ABSTRACT

Two peptides representing segments of the folding nucleus of β-lactoglobulin were studied using IR/UV double resonance spectroscopy. The gas phase structures of the peptides are determined by intramolecular interactions which provide insight as to why this region of the molecule folds first. The peptides, Ac-Trp-Tyr-$NH_2$ and Ac-Trp-Tyr-Ser-$NH_2$, were compared to Ac-Trp-$NH_2$ to determine the effect of each amino acid on the shape of the peptide. While chain length accounts for some of the differences, the identity of the side chains play an important role in the overall shapes of these molecules.

JAT, EG, BT, FP, and MM performed the experimental measurements; EG performed the calculations on Ac-Trp-Tyr-$NH_2$; JAT performed the calculations on Ac-Trp-Tyr-Ser-$NH_2$ and wrote the paper.

## 6.2 INTRODUCTION

The proper or improper function of a protein, an abundant and essential component of living things, is determined by its three-dimensional structure. The study of the structure of proteins is therefore necessary to develop an understanding of how naturally occurring proteins function and how they may malfunction, and also to lay the foundation for the development of drugs that can serve specific therapeutic purposes in the body. While certain sequences of amino acids have been associated with particular secondary structures, such as the helix that tends to form from a chain of alanine residues, it is not yet possible to predict an overall three-dimensional structure given only the primary structure, or amino acid composition, of a protein.

Many approaches towards reaching this goal have been suggested. One such approach makes use of the concept of a "foldon". Luthey-Schulten[1] and co-workers have identified short strands of certain proteins called folding nuclei (foldons) which seem to fold first as a protein finds its native conformation and perhaps induce the rest of the molecule to fold correctly. This would help to explain Levinthal's paradox which states that, given the estimated age of the universe, few proteins would yet be folded correctly if all the possible structures were randomly sampled in an attempt to find the most stable configuration. If, instead, a region or several regions in the molecule, once folded, arranged their neighbors into a favorable position, this would dramatically increase the possibility of the protein finding its native conformation on the time scale observed experimentally. Experiments have shown that proteins fold on rapid time scales, milliseconds to seconds,[2] indicating that the majority of possible configurations are not sampled.

In this work, a short peptide identified as a neutral folding nucleus of bovine β-lactoglobulin,[3] a protein found in bovine milk, was selected to be studied *via* gas phase IR/UV double resonance spectroscopy. This technique identifies intramolecular interactions and, when combined with theoretical calculations, can be used to determine the three-dimensional structure of the molecule. This folding nucleus of β-lactoglobulin consists of five amino acids, Trp-Tyr-Ser-Leu-Ala, and was selected because it contains UV chromophores that can be used to probe the electronic transitions of the peptide. Additionally, the tryptophan residue seems to play a large role in the structure and stability of the protein as a whole.[4] The UV and IR spectra of two segments of this sequence are presented here. Spectroscopic studies of a longer sequence were inhibited by the fragmentation of the molecule. The sample was studied in the gas phase to obtain spectra with a resolution that is comparable to *ab initio* calculations. In order to better simulate the environment of the peptides as segments of a larger protein, the ends of the molecules were capped with an acetyl group on the N-terminus and an amine group on the C-terminus. Thus, in addition to the peptide bonds linking the individual amino acids together, there also is a complete peptide bond at each end of the chain.

The structure of the backbone of each molecule was determined from the analysis of the amide A spectroscopy (NH stretch bands), known to be exquisitely sensitive to H-bonding. Hydrogen bonds within the molecule were assigned by comparison with *ab initio* calculations and experimental results for other peptides. The notation $C_5$, $C_7$, $C_{10}$ is used to denote backbone configurations where a ring containing 5, 7, or 10 atoms is formed by a hydrogen bond. The $C_7$ and $C_{10}$ configurations correspond to the γ-turn and β-turn secondary structures,[5] respectively. In addition to interactions within the backbone, the NH groups can interact with the side chains and

the side chains can interact with one another. These interactions are revealed by shifts due to NH-π interactions or red-shifting of the OH stretch vibrations of the tyrosine and serine residues.

## 6.3 EXPERIMENT

The experimental methods have been described previously[6,7] and will be summarized here. Laser ablation was used to produce gas phase samples. The sample molecule was thoroughly mixed with graphite powder in a 1:4 molar ratio and pressed into a pellet with a 6 mm diameter and 1 - 2 mm thickness under approximately 2 tons of pressure. The edge of the pellet was filed down to expose a flat surface before it was mounted on the face of a General Valve 0.35 mm pulsed nozzle with its flat edge approximately 0.25 to 0.5 mm from the nozzle orifice. A motor was used to move the pellet back and forth during the experiment to expose more sample than if the pellet were stationary. A 600 μm optical fiber directed the second harmonic of an Nd:YAG laser (Continuum Minilite I) at the pellet creating a ablated plume directly in front of the nozzle orifice. Ablated molecules were then picked up and cooled by a supersonic expansion of argon in a vacuum chamber.

The gas phase sample was detected using time-of-flight mass spectroscopy. Ablated molecules were ionized by a UV laser produced by a frequency doubled dye laser (Lambda Physik LPD 3000) pumped by an excimer laser (Lambda Physik EMG 102 MSC) and directed towards the detector by charged plates. The presence of the parent molecule was confirmed and the presence of fragments was detected.

There are two possible sources of fragmentation. If the intensity of the fragment peaks varies in relation to the intensity of the parent peak when the intensity of the ablation laser is changed, then the fragmentation is occurring during the irradiation process. Fragmentation due to excited or ionic state dynamics, however, is intrinsic to the molecule rather than due to the power of the ablation laser and cannot be avoided.

Electronic spectra were collected *via* resonant two-photon ionization (R2PI), where the resulting ions were detected by mass spectrometry so that, as the laser was scanned, a spectrum of the number of ions detected versus UV frequency was produced. When the UV frequency corresponded to an electronic transition in the molecule, the pair of photons then provided enough energy to ionize the molecule and cause a peak in the UV spectrum.

IR spectra are used to determine the conformations of the molecule by determining the presence and location of hydrogen bonds and interactions between hydrogens and π electrons. Gas phase IR spectra were collected *via* a IR/UV double resonance technique similar to that developed by Page, *et al*.[8] Some more recent applications are described by Zwier.[9] A UV laser beam is passed through the vacuum chamber twice. On the first pass it is overlapped with the beam from an IR laser produced by an Nd:YAG (Quantel Brilliant) pumped $LiNbO_3$ OPO (Euroscan Co.). The IR frequency is scanned and, when it is resonant with a vibrational mode in the molecule, the molecule is promoted from the ground state and is unavailable for an electronic transition. Thus, two spectra were recorded simultaneously; a reference spectrum and a spectrum containing depletions. When the results are analyzed using the equation $1-\frac{signal}{reference}$, a vibrational spectrum for the molecule results where the y-axis indicates the fraction of depletion.

Further information can be obtained from fluorescence and lifetime measurements. A photomultiplier tube (PMT) is used to detect a molecule's fluorescence after interacting with a UV laser. The UV laser is scanned to produce a laser induced fluorescence (LIF) spectrum. When the molecule is excited and the resulting fluorescence is detected by the PMT, the oscilloscope displays the intensity versus time. This curve can be fit by an exponential decay to obtain the associated lifetime of the molecule.

## 6.4 THEORY

Molecular dynamics calculations were used to identify low energy conformations of Ac-Trp-Tyr-$NH_2$ and Ac-Trp-Tyr-Ser-$NH_2$ which were then optimized using *ab initio* methods. Calculations for the former were done by the group in France; a similar procedure was performed in Pittsburgh for the latter. Both approaches are described in the following paragraphs.

### 6.4.1 Ac-Trp-Tyr-$NH_2$

Molecular dynamics simulations were performed using the HyperChem™ Professional 7.51 package. The force fields used were AMBER 99[10] and CHARMM 27.[11] Conformations that could potentially match the experimental results were selected for quantum mechanics calculations. TURBOMOLE 5.10[12] was used to optimize these conformations at the

RI-B97-D/TZVPP level. Harmonic frequency calculations were performed on the optimized structures using the same level of theory and basis set.

Mode dependent scaling factors have been shown to more accurately predict experimental spectra than scaling all frequencies by the same value.[13,14] The procedure used to scale the calculated frequencies for Ac-Trp-Tyr-$NH_2$ is the same as that described in the supplementary information contained in Ref. 15. A plot of assigned experimental frequencies versus those calculated at the RI-B97-D/TZVPP level produces four different linear trends corresponding to NH, $NH_2^{sym}$, $NH_2^{anti}$, and OH stretches. Each trend was fit with different values of $a$ and $b$ in the equation $freq^{scaled} = a \cdot freq^{harm} + b$ where $b$ is in $cm^{-1}$ and $a$ is a dimensionless scaling factor.

**Table 6.1. Calculated structures of Ac-Trp-Tyr-$NH_2$ that best match the experimental data. Each structure is described according to the intramolecular interactions of its NH and OH bonds. This, however, does not uniquely identify the structures. Thus, a .xyz file for each structure mentioned is included in Appendix A. The identifying labels are defined in Scheme 6.1.**

| | | Backbone | | | Side Chains | | |
|---|---|---|---|---|---|---|---|
| **Structure** | **Relative energy (kJ/mol)** | **A** | **B** | **C/D** | **F** | **G** | **Aromatic Ring Interaction** |
| A1 | 2.4 | V ($C_5$) | W & Y | V ($C_7$) | Y | W | Parallel displaced |
| B1 | 0 | W | Y | U ($C_{10}$) | free | free | T-shaped |
| B2 | 0.6 | W | Y | U ($C_{10}$) | free | free | T-shaped |
| B3 | 0.7 | W | Y | U ($C_{10}$) | free | free | T-shaped |
| B4 | 2.6 | W | Y | U ($C_{10}$) | free | free | T-shaped |
| B5 | 5.5 | W | Y | U ($C_{10}$) | G | F | Parallel displaced |
| B6 | 7.2 | W | free | U ($C_{10}$) | G | F | Parallel displaced |

The conformers that best match the experimental results are listed in Table 6.1 along with their relative energies. For brevity, structures are described by their backbone structures and aromatic ring configurations, though that does not completely describe the structure of a molecule of this size.

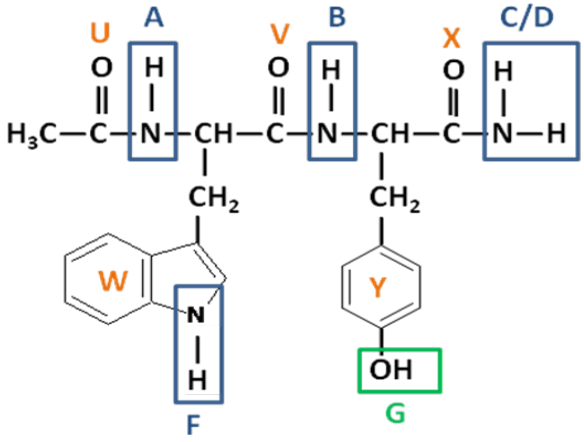


**Scheme 6.1. Structure of Ac-Trp-Tyr-$NH_2$ indicating the labelling scheme used in Table 6.1. NH and OH stretches are labelled A – D, F & G. The potential sites for hydrogen bonding and π-electron interactions are labelled U – Y.**

### 6.4.2 Ac-Trp-Tyr-Ser-$NH_2$

Amber10 and AmberTools were used to perform the molecular dynamics calculations. Three starting conformations of Ac-Trp-Tyr-Ser-$NH_2$ were minimized, then the dynamics were simulated for 50 ns using the 99SB force field. From the results, 88 structures were selected and optimized using *ab initio* calculations.

The *ab initio* calculations were performed using Orca 2.8. First, each structure was optimized using the Perdew-Burke-Ernzerhof generalized gradient approximation (pbe GGA) functional[16] with Dunning's correlation-consistent polarized valence double-zeta (cc-pvdz) basis

set and the van der Waals correction[17,18] to account for dispersion interactions between the conjugated rings. The resulting structures were ranked by relative energy and a visual inspection of key features such as hydrogen bonding was used to group the results into 21 unique structures. Vibrational frequencies for these representative structures were calculated at the same level of theory and with the same basis set and the calculated frequencies were compared to the experimental results. Because a different method was used to calculate the vibrational frequencies of Ac-Trp-Tyr-Ser-$NH_2$, the scaling equation used for the Ac-Trp-Tyr-$NH_2$ frequencies is not appropriate. Instead, calculated frequencies were scaled by 0.987 to put certain motifs in the ranges tabulated by Chin, *et al*. in Fig. 4 of Reference 19. This scaling factor also produced a reasonable match between the experimental spectrum and the spectra of the four lowest energy calculated conformers.

Table 6.2 and Scheme 6.2 identify the principal conformers and interactions identified in this search.

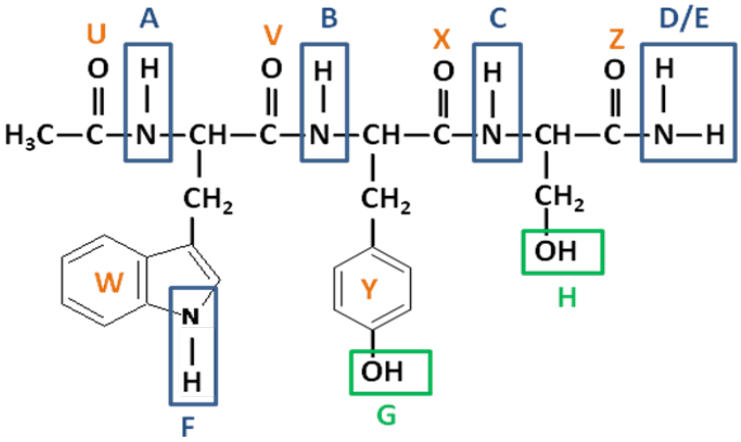


**Scheme 6.2. Structure of Ac-Trp-Tyr-Ser-$NH_2$ indicating the labeling scheme used in Table 6.2. NH and OH stretches are labeled A – H. The potential sites for hydrogen bonding and π-electron interactions are labeled U – Z.**

**Table 6.2. Calculated structures of Ac-Trp-Tyr-Ser-$NH_2$ that best match the experimental data. Each structure is described according to the intramolecular interactions of its NH and OH bonds. This, however, does not uniquely identify the structures. Thus, a .xyz file for each structure mentioned is included in Appendix A. The identifying labels are defined in Scheme 6.2.**

| | | Backbone | | | | Side Chains | | | |
|---|---|---|---|---|---|---|---|---|---|
| **Structure** | **Relative Energy (kJ/mol)** | **A** | **B** | **C** | **D/E** | **F** | **G** | **H** | **Aromatic Ring Interaction** |
| Conformer 1 | 0 | W | Y | Z ($C_5$) & W | free | Z | U | V | None* |
| Conformer 2 | 1.2 | W | Y | U ($C_{10}$) | X ($C_7$) | free | free | U | T-shaped |
| Conformer 3 | 1.7 | W | Y | W | X ($C_7$) | Z | U | V | None |
| Conformer 4 | 2.4 | W | Y | Z ($C_5$) & W | free | Z | free | V | None |

* A notation of "none" for the aromatic ring interaction indicates that the rings are located on opposite sides of the backbone.

## 6.5 RESULTS

### 6.5.1 Acetyl-Tryptophan-Tyrosinamide (Ac-Trp-Tyr-$NH_2$)

When acetyl-tryptophan-tyrosinamide (Ac-Trp-Tyr-$NH_2$) was ablated, little fragmentation was detected by TOF-MS. An electronic spectrum was recorded for the tryptophan chromophore and is shown in Fig. 6.1. As in other tryptophan-containing peptides,[20] the electronic spectrum of Ac-Trp-Tyr-$NH_2$ includes both narrow and broad transitions. The IR/UV double resonance experiment resulted in two different IR spectra when they were

detected using the narrow and broad UV transitions. This indicates that there are two gas phase conformers of Ac-Trp-Tyr-$NH_2$. In this work these conformers will be referred to as A and B and calculated structures will be numbered (see Table 6.1).

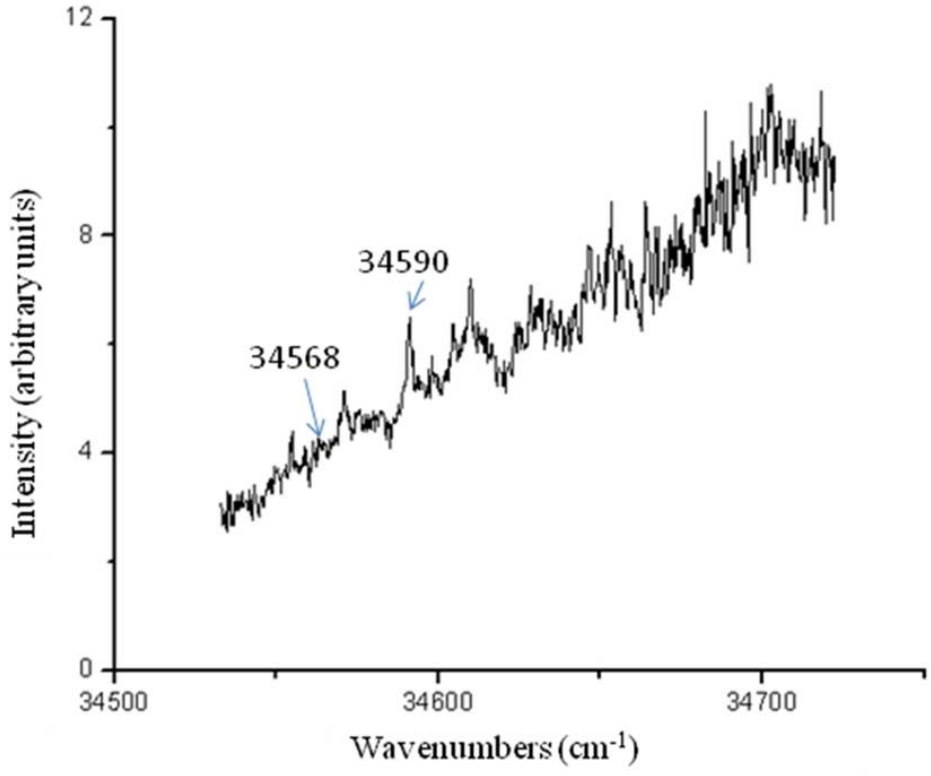


**Figure 6.1. Electronic spectrum of Ac-Trp-Tyr-$NH_2$ obtained using R2PI.**

For the first double resonance experiment, one of the narrow electronic transitions, at 34590 $cm^{-1}$ (289.1 nm), was used as the UV probe frequency. When the IR laser was scanned, depletions in the spectrum corresponded to IR transitions of the conformer designated A. The resulting IR spectrum is shown in Figure 6.2, where the black trace is the experimental spectrum

and the red bars indicate the frequencies of the calculated transitions for Conformer A1, with the typical uncertainty of ± 15 $cm^{-1}$ for such isolated systems.

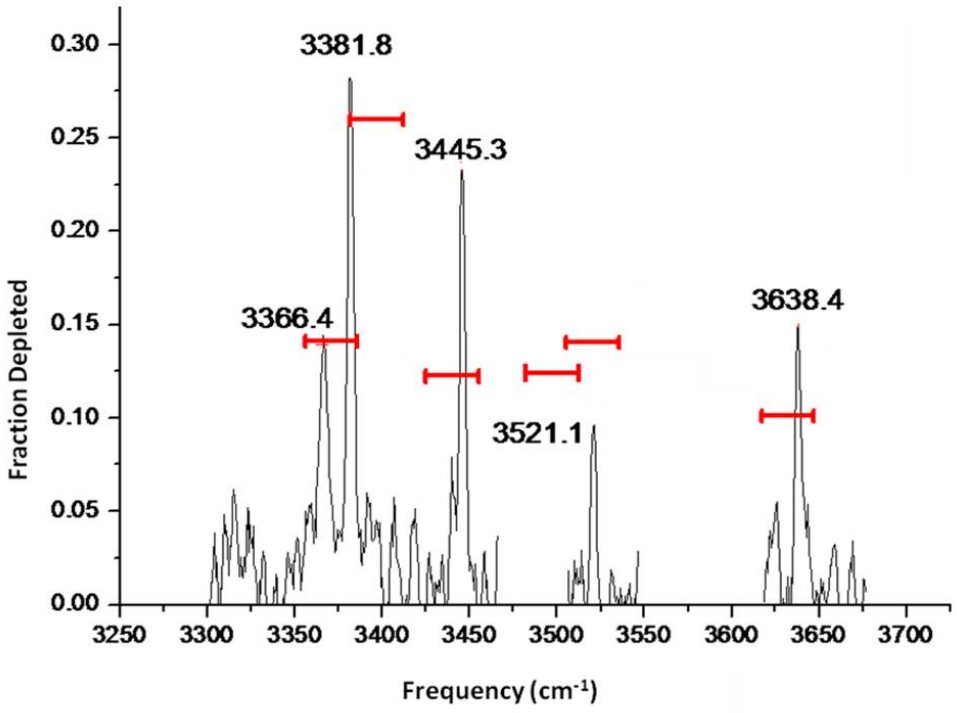


**Figure 6.2. Experimental IR spectrum of Conformer A of Ac-Trp-Tyr-$NH_2$ and predicted regions of vibrational transitions based on calculations and previous experiments on similar molecules (red bars).**

Ac-Trp-Tyr-$NH_2$ contains two NH bonds and an $NH_2$ group in the backbone, as well as an NH bond on the Trp residue and an OH bond on the Tyr residue (see Scheme 6.1) for a total of six possible bands in the NH and OH stretch region. Five transitions were observed. It is likely that the remaining transition is located in a region of the spectrum not covered by the OPO crystal, approximately 3460 – 3510 $cm^{-1}$.

The assignment of the experimental results to a particular structure begins with a qualitative assessment. Remarkable intramolecular interactions present in the molecule can be

revealed by their typical IR signature, in particular H-bonds, through the red shift they are known to induce (from previously studied molecules) and a first qualitative assignment can be given. The IR spectrum of Ac-Trp-Tyr-$NH_2$ has several transitions that are shifted from the free amide A NH and phenol OH stretch regions of the spectrum, typically at 3470 and 3660 $cm^{-1}$, respectively.[21,22] For example, the band of highest energy, 3638.4 $cm^{-1}$, is red-shifted with respect to the free OH stretch indicating that the OH bond is involved in an intramolecular interaction. The two bands below 3400 $cm^{-1}$ also indicate two strong interactions involving NH bonds.

**Table 6.3. Comparison of experimental and calculated values for high frequency vibrational transitions of Conformer A of Ac-Trp-Tyr-$NH_2$.**

| Exptl. Conformer A ($cm^{-1}$) | Calculated Spectrum* A1 ($cm^{-1}$) | Assignment |
|---|---|---|
| 3366.4 | 3371.1 | $C_7$ |
| 3381.8 | 3396.8 | $C_5$ |
| 3445.6 | 3440.0 | $NH_{backbone}$-$\pi$ |
| Inaccessible region | 3497.6 | $NH_{indole}$-$\pi$ |
| 3521.1 | 3520.4 | $NH_2^{anti}$ |
| 3638.4 | 3631.9 | OH-$\pi$ |

*Calculated frequencies are scaled as described in the theory section, 6.4.1.

A refined assignment is then obtained by a close comparison with calculated low energy structures. Conformations selected to provide two strong NH interactions were obtained from the force field exploration and eventually led to 68 different optimized structures (DFT-D level),

ensuring the exploration regarding Conformer A was exhaustive. Scaled harmonic frequencies compared to experiment led us unambiguously to assign Conformer A to a $C_5$-$C_7$ backbone configuration described as Conformer A1 in Tables 6.1 and 6.3.

One can comment on two interesting features of this spectrum, compared to previously observed $C_5$-$C_7$ structures.[23] The transition occurring at 3366 $cm^{-1}$, assigned to the $C_7$ band, is unusually blue indicating a distorted gamma turn, presumably due to strong side-chain/side-chain interactions such as in Ac-Phe-Phe-$NH_2$.[24] The transition occurring at 3381.8 $cm^{-1}$ corresponds to an unusually strong interaction between a backbone NH bond and the π electrons of the tryptophan residue. Such transitions typically occur between 3430 and 3470 $cm^{-1}$.[19] In this case however, the NH bond is located between the two aromatic rings and possibly experiences some additional stabilization from the tyrosine residue.

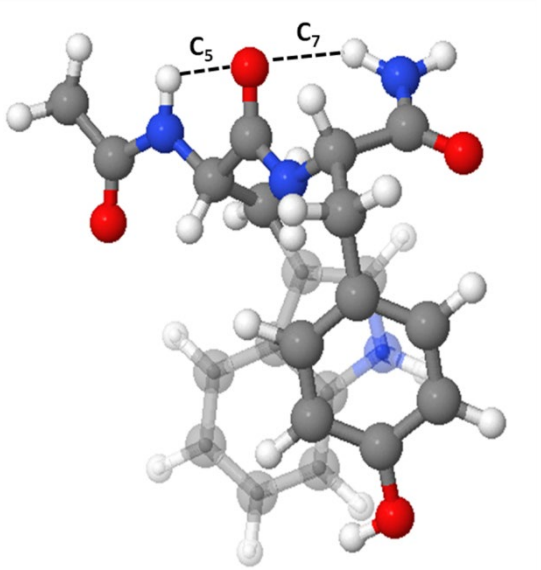


**Figure 6.3. Calculated structure of Conformer A1 of Ac-Trp-Tyr-$NH_2$ showing the hydrogen bonds that dominate the backbone structure and the parallel displaced configuration of the aromatic side chains. The indole ring of Trp was made translucent for clarity.**

The aromatic side chains have a parallel displaced configuration with an interaction between the NH of Trp and the π-electrons of Tyr as well as one between the OH of Tyr and the π-electrons of Trp. The parallel displaced arrangement of the side chains in Conformer A is quite different from the T-shaped arrangement observed in Ac-Phe-Phe-$NH_2$.[24] The interaction of each polar bond with its neighboring aromatic ring stabilizes the otherwise higher energy parallel displaced structure.

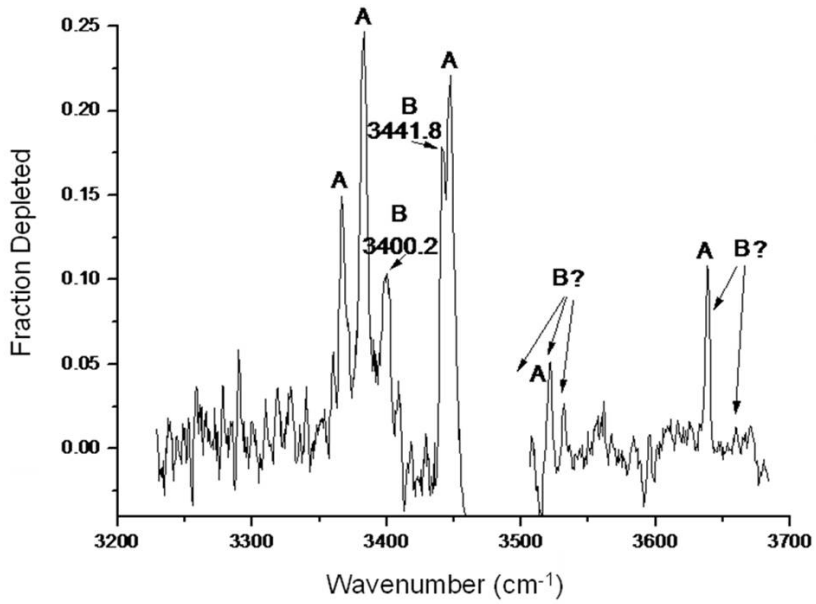


**Figure 6.4. IR spectra of the A and B conformers of Ac-Trp-Tyr-$NH_2$.**

A second IR spectrum (Figure 6.4) was collected using a probe frequency, 34568 $cm^{-1}$, that corresponds to the broad background in the electronic spectrum. The fact that a different probe frequency resulted in a different IR spectrum indicates that there is a second conformer present, Conformer B. Because this conformer did not have any narrow transitions in the UV spectrum, it was not possible to completely isolate Conformer B so the corresponding IR

spectrum contains residual bands produced by Conformer A. Transitions at 3400.2 and 3441.8 $cm^{-1}$ clearly belong to Conformer B, but the presence of the Conformer A bands and the poor signal-to-noise in the high frequency region makes it difficult to conclusively identify other transitions.

The lowest energy structures (within 10 kJ/mol of the minimum) that contained transitions within ± 20 $cm^{-1}$ of the experimental frequencies are listed as Conformers B1 - B6 in Table 6.1. Fortuitously, all of these structures have the same backbone configuration, $C_{10}$. Thus, we can confidently identify the backbone structure of Conformer B despite the lack of experimental transitions. This is the case because the $NH_2^{sym}$ transition occurs at a significantly higher frequency when involved in a $C_{10}$ interaction than it does in a $C_7$ interaction,[19] as in Conformer A. Additional experimental data, in the 3450 – 3700 $cm^{-1}$ region would be needed to unambiguously identify the relative orientation of the aromatic rings.

### 6.5.2 Acetyl-Tryptophan-Tyrosine-Serinyl-amide (Ac-Trp-Tyr-Ser-$NH_2$)

The addition of a serine residue to the C-terminus (Scheme 6.2) had a marked effect on the ablation of the sample. Unlike Ac-Trp-Tyr-$NH_2$, Ac-Trp-Tyr-Ser-$NH_2$ formed many fragments upon ablation. The TOF-MS spectrum indicated that one of these fragments resulted from the loss of 30 amu and is likely the loss of formaldehyde from the serine side chain. In addition, it was noted that more laser power was needed to ablate Ac-Trp-Tyr-Ser-$NH_2$ than was required for Ac-Trp-Tyr-$NH_2$ and, perhaps as a result, the sample pellet had to be refilled more frequently.

The ultraviolet spectrum of Ac-Trp-Tyr-Ser-$NH_2$ was broad and more red-shifted than Ac-Trp-Tyr-$NH_2$ or NATA. A pump frequency of 34432 $cm^{-1}$ was used to collect the IR spectrum, Fig. 6.5. Five bands were observed out of a possible eight due to the presence of six NH and two OH bonds in the molecule. All of the bands observed belonged to the same conformer.

The most interesting feature of the calculated structures (see section 6.4) is that, among the 21 unique structures within 13 kJ/mol of the global minimum, none displayed a free Ser OH group. Within these calculated structures the Ser side chain formed a variety of hydrogen bonds (with each of the different backbone C=O groups, with the NH of the Trp 5-membered ring, with the phenyl OH of Tyr, and with the terminal $NH_2$ group). In most cases the Ser OH acted as the hydrogen donor, but in a few cases it was the acceptor or participated simultaneously as both the donor and acceptor.

Figure 6.6 shows the four calculated IR spectra that best match the experimental results in the region 3300 – 3450 $cm^{-1}$. These also happen to be the four lowest energy structures. The experimental results above 3500 $cm^{-1}$ had a poor signal-to-noise ratio, but the presence of a band at 3510 $cm^{-1}$ narrows the identity of Ac-Trp-Tyr-Ser-$NH_2$ to calculated Conformers 2 and 3. These have energies 1.2 and 1.7 kJ/mol above the minimum energy structure, respectively.

Conformer 2 is a $C_{10}/C_7$ structure where the backbone forms an "S" shape due to hydrogen bonds between the backbone NH of the Ser residue and the C=O of the acetyl cap ($C_{10}$) and between the C=O of the Tyr backbone with the terminal $NH_2$ group ($C_7$, see Scheme 6.3). In addition, the Ser OH group participates as a second proton donor in a hydrogen bond with the C=O of the acetyl group. This strong interaction shifts the OH band all the way down to

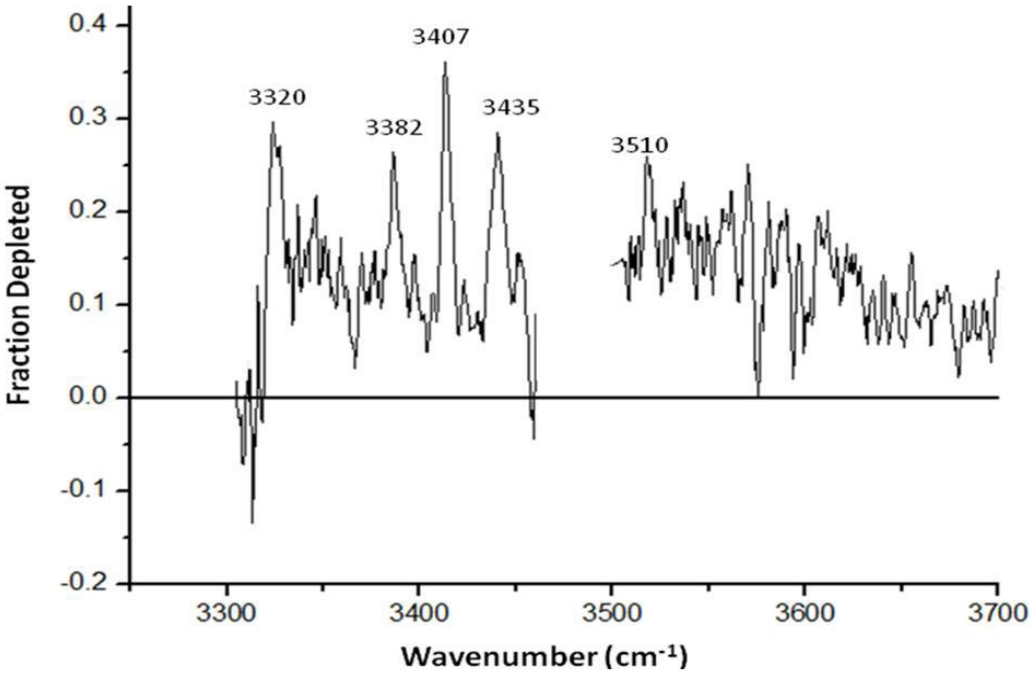


**Figure 6.5. Experimental IR/UV double resonance spectrum of Ac-Trp-Tyr-Ser-$NH_2$.**

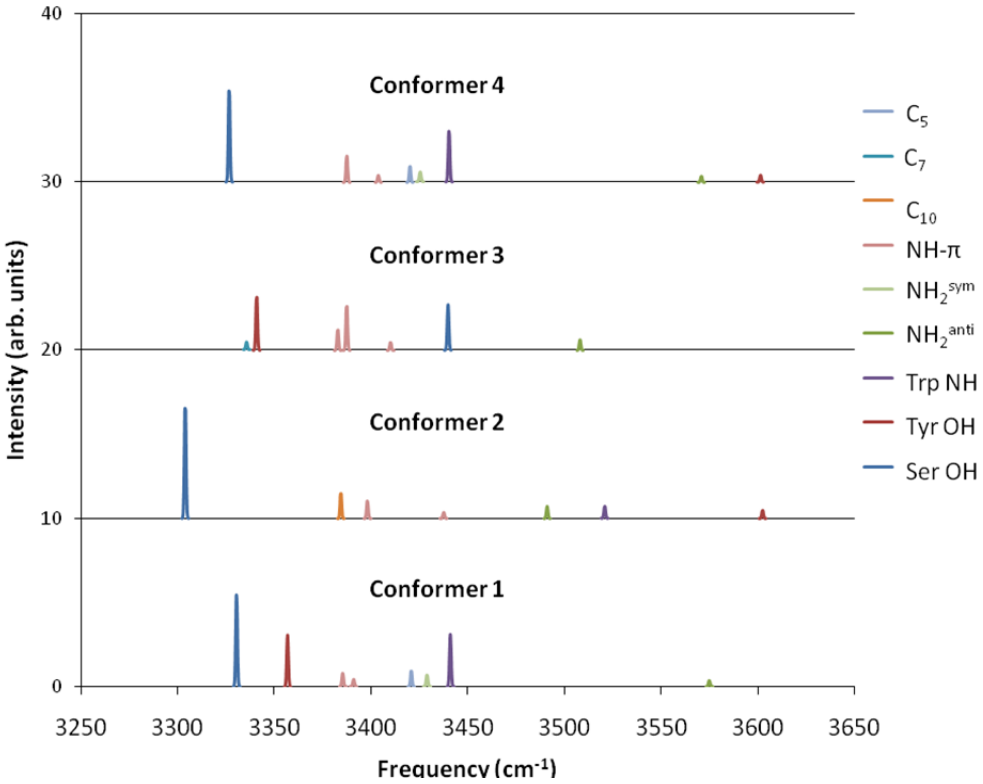


**Figure 6.6. Selected calculated IR spectra of Ac-Trp-Tyr-Ser-$NH_2$. All frequencies are scaled by 0.987.**

3304 $cm^{-1}$. Finally, the two aromatic rings are oriented in a T-shaped configuration with a free OH stretching mode on the tyrosine residue.

Conformer 3 has the same $C_7$ structure involving the $NH_2$ group which accounts for the presence of the $NH_2$ antisymmetric stretching mode near 3500 $cm^{-1}$. The rest of the structure is quite different (see Scheme 6.3). The IR spectrum clearly shows that there is not a free O-H stretch. In fact, the O-H stretching mode of the tyrosine is strongly red-shifted due to an interaction with the C=O of the acetyl cap. The serine O-H is not shifted as strongly (3440 $cm^{-1}$) when it interacts with the C=O of the Trp residue. In Conformer 3 the relative position of the aromatic rings is also different with each located on opposite sides of the backbone.

The incomplete data set, together with the number of possible conformations in the flexible side chains, makes it difficult to disentangle the contributions of the NH and OH stretches in the IR spectrum of Ac-Trp-Tyr-Ser-$NH_2$.

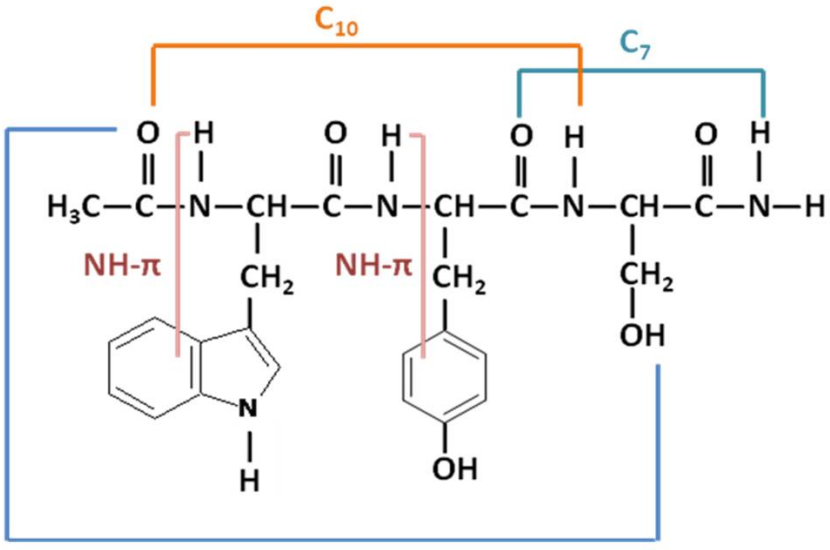


**Scheme 6.3. Map of intramolecular interactions in Conformer 2 of Ac-Trp-Tyr-Ser-$NH_2$.**

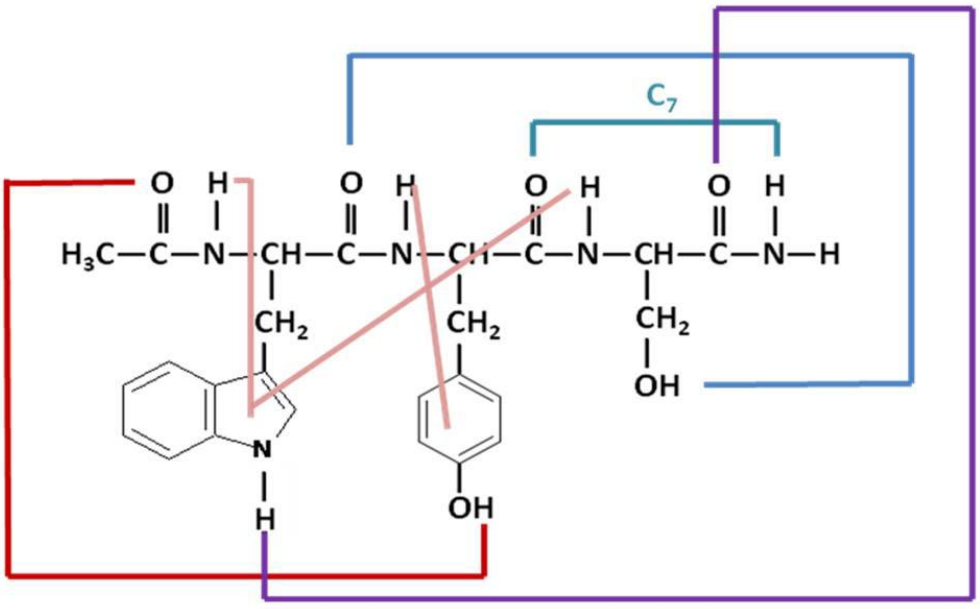


**Scheme 6.4. Map of intramolecular interactions in Conformer 3 of Ac-Trp-Tyr-Ser-$NH_2$.**

### 6.5.3 Acetyl-Tryptophan-Tyrosine-Serine-Leucinamide (Ac-Trp-Tyr-Ser-Leu-$NH_2$)

Lastly, a sample of Ac-Trp-Tyr-Ser-Leu-$NH_2$ was ablated. However, due to significant fragmentation, there was not enough signal to collect UV and IR spectra. As in Ac-Trp-Tyr-Ser-$NH_2$, a significant portion of the fragmentation can be attributed to the loss of a formaldehyde fragment. Interestingly, for Ac-Trp-Tyr-Ser-Leu-$NH_2$, it was also possible to detect the presence of hydrated clusters containing the parent and one or two water molecules in the TOF-MS spectrum.

## 6.6 DISCUSSION

Ac-Trp-$NH_2$ (NATA) was studied by Zwier and co-workers[20] using IR/UV double resonance. Two conformations of NATA were observed: one with a $C_5$, or straight chain, backbone configuration and the other with a $C_7$ configuration. One conformation, the $C_5$, lead to narrow vibronic transitions while the other led to a broad UV spectrum. As noted above, spectra for Ac-Trp-Tyr-$NH_2$ also revealed two conformers; one with narrow and one with broad transitions.

The longer backbone of Ac-Trp-Tyr-$NH_2$ relative to NATA accounts for its ability to form a $C_5/C_7$ configuration or a $C_{10}$ configuration. Neither the $C_5/C_7$ combination nor the $C_{10}$ (β-turn) are possible for NATA which contains only 8 atoms in its backbone. An analogous structure, Ac-Phe-Phe-$NH_2$, also forms a $C_{10}$ backbone and in both Ac-Phe-Phe-$NH_2$ and Ac-Trp-Tyr-$NH_2$ this is calculated to be the lowest energy structure.[24] However, despite the similarity of these two molecules, the arrangement of the side chains is different. Whereas the two aromatic rings of Ac-Phe-Phe-$NH_2$ are oriented with a T-shaped position, those of Conformer A of Ac-Trp-Tyr-$NH_2$ are parallel displaced. Not enough information was available to determine the arrangement of the rings in Conformer B, the $C_{10}$ structure. However, it is likely that Conformer B is the C10 β-turn with a T-shaped arrangement of the Trp and Tyr side chains.

Although chain length can account for the differences in backbone structure between NATA and Ac-Trp-Tyr-$NH_2$, the calculations showed that the presence of the serine group had a significant effect on the structure of the next largest structure, Ac-Trp-Tyr-Ser-$NH_2$. None of the calculated structures had a free OH on the serine side chain. Thus, the addition of this residue

necessarily made a significant change to the structure of the peptide. In addition, the presence of the serine residue seems to be the primary cause of fragmentation of the Ac-Trp-Tyr-Ser-$NH_2$ sample as the mass of the major fragment corresponds to the loss of formaldehyde, a likely decomposition product.

**Table 6.4. Summary of assignments.**

| Peptide | Number of Conformers | Backbone Configurations | Aromatic Ring Interactions |
|---|---|---|---|
| NATA (Ref. 18) | 2 | $C_5$ | *Not applicable* |
| | | $C_7$ | |
| NATMA (Ref. 18) | 3 | $C_5$ | *Not applicable* |
| | | $C_5$ | |
| | | $C_7$ | |
| Ac-Phe-Phe-$NH_2$ (Ref. 24) | 1 | $C_{10}$ | T-shaped |
| Ac-Trp-Tyr-$NH_2$ | 2 | $C_5/C_7$ | Parallel displaced |
| | | $C_{10}$ | *Not determined* |
| Ac-Trp-Tyr-Ser-$NH_2$ | 1 | $C_7$ (& probable $C_{10}$) | T-shaped |

The assignments for the conformation of the peptides discussed in this work are summarized in Table 6.4. This table also highlights another trend in the flexibility of peptides. As noted by Rizzo,[25] as a peptide chain increases in length, the number of conformers initially increases as would be expected due to the increased flexibility of the backbone. However, the number of observed conformers then tends to decrease as intramolecular interactions stabilize a few conformations significantly more than others.

A comparison between the Ac-Trp-Tyr-$NH_2$ and Ac-Trp-Tyr-Ser-$NH_2$ structures shows a great deal of similarity between one of the candidates for Conformer B of Ac-Trp-Tyr-$NH_2$ and the best match for the sole conformer of Ac-Trp-Tyr-Ser-$NH_2$. Both have a $C_{10}$ backbone on the N-terminal side of the peptide and a T-shaped interaction between the aromatic rings. Thus, an important effect of the addition of the third amino acid is the stabilization of the $C_{10}$, T-shaped configuration over the $C_5/C_7$, parallel displaced configuration.

## 6.7 CONCLUSION

The identity of the amino acids in the folding nucleus have a significant effect on the conformation of a peptide due to side chain – side chain and side chain – backbone interactions. A pair of aromatic side chains on neighboring amino acids tend to interact in either a parallel displaced configuration, as in Ac-Trp-Tyr-$NH_2$, or a T-shaped configuration, as in Ac-Phe-Phe-$NH_2$ or Ac-Trp-Tyr-Ser-$NH_2$, rather than being found on opposite sides of the backbone as in some of the calculated structures. The third amino acid, serine, has a polar OH group that has the ability to form a variety of hydrogen bonds and is not calculated to be free in any of the conformations within 13 kJ/mol of the global minimum. It would be interesting to determine the significance of the serine hydrogen bond by replacing its –OH with a nonpolar group.

The stabilization provided by the intramolecular interactions enumerated above results in the observation of only one of the two backbone structures of Ac-Trp-Tyr-$NH_2$ being observed experimentally in Ac-Trp-Tyr-Ser-$NH_2$.

## 6.8 FUTURE WORK

It would be interesting to examine the effect of the remaining two amino acids in this folding nucleus. The leucine and alanine amino acids do not have side chains that can participate in hydrogen bonds or NH-π interactions; thus, it is likely that the serine residue will continue to have the dominating effect. However, it is possible that an interaction between the serine side chain and the portion of the backbone corresponding to the leucine and alanine residues could be significant.

If additional experimental results are not achievable due to decomposition of the longer chains, computational results could provide further insights. The current results for Ac-Trp-Tyr-Ser-$NH_2$ could be compared to Ac-Trp-Tyr-Ala-$NH_2$ to confirm the significance of the OH group on the serine residue. It would also be interesting to determine the lowest energy structure for the entire folding nucleus even if experimental results were not available for comparison.

## 6.9 ACKNOWLEDGEMENTS

Glen Jenness, a fellow graduate student at the University of Pittsburgh helped me learn how to use Orca. The Center for Molecular and Materials Simulation, also at the University of Pittsburgh, provided computational resources. I was able to travel to the Laboratoire Francis Perrin to do the experimental work thanks to support from both CEA-CNRS and the University of Pittsburgh.

## 6.10 REFERENCES


1. A. Panchenko, Z. Luthey-Schulten, R. Cole and P. G. Wolynes, *J. Mol. Bio.* **1997**, *272*.
2. B. Nolting, Protein Folding Kinetics: Biophysical Methods, 2nd ed., Springer, New York, **2006**.
3. L. Ragona, M. Catalano, L. Zetta, R. Longhi, F. Fogolari and H. Molinari, *Biochem.* **2002**, *41*, 2786.
4. Z. Bao, S. Wang, W. Shi, S. Dong and H. Ma, *J. Proteome Res.* **2007**, *6*, 3835.
5. G. N. Ramachandran and V. Sasisekharan, "*Conformation of Polypeptides and Proteins*" in Advances in Protein Chemistry, Vol. 23, ed. C. B. Anfinsen, Jr., Academic Press Inc., New York, **1968**.
6. D. Uridat, V. Brenner, I. Dimicoli, J. Le Calve, P. Millie, M. Mons and F. Piuzzi, *Chem. Phys.* **1998**, *239*, 151.
7. F. Piuzzi, I. Dimicoli, M. Mons, B. Tardivel and Q. Zhao, *Chem. Phys. Lett.* **2000**, *320*, 282.
8. R. H. Page, Y. R. Shen, and Y. T. Lee, *J. Chem. Phys*., **1988**, 88, 4621.
9. T. S. Zwier, *J. Phys. Chem. A*, **2006**, 110, 4133.
10. D.A. Case et al. **2006**, AMBER 9, University of California, San Francisco.
11. MacKerell, A. D.; Banavali, N.; Foloppe, N. *Biopolymers* **2000**, 56, 257.
12. Ahlrichs, R.; Bar, M.; Haser, M.; Horn, H.; Kolmel, C. *Chem. Phys. Lett*. **1989**, 162, 165.
13. E. Gloaguen, H. Valdes, F. Pagliarulo, R. Pollet, B. Tardivel, P. Hobza, F. Piuzzi, M. Mons, *J. Phys. Chem. A* **2010**, 114, 2973.
14. Bouteiller, Y.; Poully, J. C.; Desfrancois, C.; Gregoire, G. *J. Phys. Chem. A* **2009**, 113, 6301.
15. H. S. Biswal, Y. Loquais, B. Tardivel, E. Gloaguen, M. Mons, *J. Am. Chem. Soc*., accepted Jan. **2011**.
16. J. P. Perdew, K. Burke and M. Ernzerhof, *Phys. Rev. Lett.* **1996**, *77*, 3865.
17. Grimme, S. *J. Comput. Chem.*, **2004,** 25, 1463.
18. Grimme, S. *J. Comput. Chem.*, **2006,** 27, 1787.
19. W. Chin, F. Piuzzi, I. Dimicoli, and M. Mons, *Phys. Chem. Chem. Phys.* **2006**, 8, 1033.
20. B. C. Dian, A. Longarte, S. Mercier, D. A. Evans, D. J. Wales and T. S. Zwier, *J. Chem. Phys.* **2002**, *117*, 10688.
21. W. Chin, J.-P. Dognon, F. Piuzzi, I. Dimicoli, and M. Mons, *Mol. Phys.*, **2005**, 103, 1579.
22. Y. Inokuchi, Y. Kobayashi, T. Ito, and T. Ebata, *J. Phys. Chem. A*, **2007**, 111, 3209.
23. E. Gloaguen, F. Pagliarulo, V. Brenner, W. Chin, F. Piuzzi, B. Tardivel, and M. Mons, *Phys. Chem. Chem. Phys.*, **2007**, 9, 4491.
24. E. Gloaguen, H. Valdes, F. Pagliarulo, R. Pollet, B. Tardivel, P. Hobza, F. Piuzzi and M. Mons, *J. Phys. Chem. A* **2010**, *114*, 2973.
25. T. R. Rizzo, O. V. Boyarkin, J. A. Stearns, A. Svendson, M. Guidi, C. Seaiby, G. Papadopoulos, N. Nagornova, U. Lorenz, **2010**, "Probing conformational landscapes of large, gas-phase biomolecular ions." *239th ACS National Meeting.* San Francisco, CA.

# APPENDIX A: .xyz Files of Selected Structures of Ac-Trp-Tyr-$NH_2$ and Ac-Trp-Tyr-Ser-$NH_2$.

## A.1 Introduction

Included in this section are the .xyz files for Ac-Trp-Tyr-$NH_2$ and Ac-Trp-Tyr-Ser-$NH_2$ that resulted from the *ab initio* calculations described in Chapter 6. Those in Section 7.2 were calculated by E. Gloaguen and those in Section 7.3 were calculated by J. Thomas. These files can be viewed in a molecular viewer such as JMol (which is an open-source, free program available for download from the internet). While dozens of structures were calculated for each molecule, only those that best match the experimental results are included here.

## A.2 Ac-Trp-Tyr-$NH_2$

### A.2.1 CONFORMER A1

54
Coordinates from A99-0111
H -0.065516 1.330282 -6.633422
C 0.734497 0.769375 -6.136442
H 0.68835 -0.279166 -6.451637
H 1.688482 1.204225 -6.453135

| | | | |
|---|---|---|---|
| C | 0.592922 | 0.95632 | -4.631138 |
| O | 0.699388 | 2.058765 | -4.098538 |
| N | 0.332924 | -0.180902 | -3.925563 |
| H | 0.27191 | -1.07886 | -4.387053 |
| C | 0.169747 | -0.177752 | -2.486241 |
| H | 0.926439 | 0.483069 | -2.048034 |
| C | 0.341771 | -1.612617 | -1.973085 |
| O | 0.230102 | -2.59491 | -2.719389 |
| C | -1.238789 | 0.36855 | -2.061626 |
| H | -1.44414 | 1.207407 | -2.735647 |
| H | -1.988819 | -0.408504 | -2.251792 |
| C | -1.297831 | 0.849014 | -0.646728 |
| C | -1.855957 | 0.221871 | 0.446448 |
| H | -2.335033 | -0.745911 | 0.517588 |
| C | -0.773716 | 2.103366 | -0.172252 |
| N | -1.74763 | 1.033047 | 1.559488 |
| H | -1.908418 | 0.724384 | 2.505075 |
| C | -1.077833 | 2.188472 | 1.215563 |
| C | -0.079579 | 3.157173 | -0.795114 |
| H | 0.168817 | 3.102643 | -1.852607 |
| C | -0.73682 | 3.306726 | 1.984193 |
| H | -1.016666 | 3.373866 | 3.032149 |
| C | 0.287313 | 4.257242 | -0.024487 |
| H | 0.827733 | 5.079626 | -0.486627 |
| C | -0.044164 | 4.334993 | 1.34671 |
| H | 0.232806 | 5.221818 | 1.912427 |
| N | 0.555412 | -1.707583 | -0.642533 |
| H | 0.467366 | -0.862022 | -0.090163 |
| C | 0.619956 | -2.966606 | 0.096568 |
| H | 1.071533 | -3.700235 | -0.583221 |
| C | -0.796108 | -3.521279 | 0.443543 |
| O | -1.147529 | -3.803939 | 1.580664 |
| C | 1.527696 | -2.8215 | 1.339924 |
| H | 1.414397 | -3.736728 | 1.928106 |
| H | 2.560983 | -2.775579 | 0.975818 |
| C | 1.251592 | -1.610835 | 2.206166 |
| C | 1.858227 | -0.379583 | 1.914256 |
| H | 2.544342 | -0.308128 | 1.072354 |
| C | 0.389427 | -1.674527 | 3.310909 |
| H | -0.096954 | -2.615984 | 3.544398 |
| C | 1.603283 | 0.758899 | 2.678379 |
| H | 2.063149 | 1.710421 | 2.421138 |
| C | 0.135389 | -0.548992 | 4.094383 |
| H | -0.524348 | -0.605399 | 4.956737 |
| C | 0.737166 | 0.674433 | 3.773644 |

| | | | |
|---|---|---|---|
| O | 0.439526 | 1.758377 | 4.560615 |
| H | 0.808339 | 2.548891 | 4.143699 |
| N | -1.597039 | -3.683067 | -0.64633 |
| H | -1.222579 | -3.571988 | -1.582714 |
| H | -2.496139 | -4.121429 | -0.510621 |

### A.2.2 CONFORMER B1

54

Coordinates from A99-0009

| | | | |
|---|---|---|---|
| H | 0.687265 | -2.4087 | -2.44048 |
| C | 0.104192 | -3.19037 | -1.93645 |
| H | -0.18208 | -3.93601 | -2.68351 |
| H | 0.736524 | -3.65227 | -1.16978 |
| C | -1.15449 | -2.55247 | -1.36846 |
| O | -2.12028 | -2.2614 | -2.07244 |
| N | -1.11816 | -2.28246 | -0.02928 |
| H | -0.25616 | -2.43804 | 0.478166 |
| C | -2.17378 | -1.55205 | 0.662162 |
| H | -3.13548 | -2.00023 | 0.392942 |
| C | -2.31229 | -0.0638 | 0.251576 |
| O | -3.30943 | 0.568331 | 0.583015 |
| C | -1.97941 | -1.67082 | 2.198336 |
| H | -2.76394 | -1.06223 | 2.660541 |
| H | -2.15385 | -2.71602 | 2.479973 |
| C | -0.62161 | -1.23749 | 2.666607 |
| C | 0.4472 | -2.0657 | 2.935901 |
| H | 0.495557 | -3.14758 | 2.940077 |
| C | -0.14956 | 0.109712 | 2.855993 |
| N | 1.555993 | -1.30967 | 3.272364 |
| H | 2.444271 | -1.67955 | 3.567149 |
| C | 1.219774 | 0.027824 | 3.24108 |
| C | -0.75283 | 1.376444 | 2.745308 |
| H | -1.79336 | 1.467919 | 2.447141 |
| C | 1.99601 | 1.163677 | 3.498617 |
| H | 3.043048 | 1.08462 | 3.781661 |
| C | 0.014277 | 2.506676 | 3.005493 |
| H | -0.43776 | 3.491647 | 2.920923 |
| C | 1.374374 | 2.40291 | 3.373516 |

| | | | |
|---|---|---|---|
| H | 1.946292 | 3.307321 | 3.563896 |
| N | -1.27025 | 0.444292 | -0.44691 |
| H | -0.48182 | -0.16101 | -0.62246 |
| C | -1.1939 | 1.778785 | -1.00761 |
| H | -1.91842 | 2.403161 | -0.47418 |
| C | -1.59979 | 1.855787 | -2.50608 |
| O | -1.47262 | 2.911121 | -3.11827 |
| C | 0.232284 | 2.361474 | -0.80383 |
| H | 0.274446 | 3.298352 | -1.36679 |
| H | 0.357235 | 2.576357 | 0.261648 |
| C | 1.30286 | 1.397562 | -1.25995 |
| C | 1.953428 | 0.569643 | -0.33132 |
| H | 1.741161 | 0.694018 | 0.727167 |
| C | 1.595926 | 1.222545 | -2.62036 |
| H | 1.101408 | 1.851666 | -3.35633 |
| C | 2.860381 | -0.41024 | -0.73719 |
| H | 3.363055 | -1.04545 | -0.01233 |
| C | 2.502164 | 0.24744 | -3.04081 |
| H | 2.721054 | 0.123061 | -4.10096 |
| C | 3.132779 | -0.57751 | -2.09959 |
| O | 4.020105 | -1.56488 | -2.45585 |
| H | 4.138228 | -1.54883 | -3.41405 |
| N | -2.0874 | 0.721839 | -3.06517 |
| H | -2.20814 | -0.14828 | -2.5616 |
| H | -2.40153 | 0.77245 | -4.0225 |

### A.2.3 CONFORMER B2

54

Coordinates from A99-0003

| | | | |
|---|---|---|---|
| H | 0.60991 | 3.150685 | 1.086294 |
| C | -0.46803 | 3.187154 | 0.893122 |
| H | -0.97517 | 2.568205 | 1.644649 |
| H | -0.83276 | 4.213067 | 0.998234 |
| C | -0.84254 | 2.669247 | -0.48666 |
| O | -1.93523 | 2.895483 | -1.00349 |
| N | 0.10695 | 1.893373 | -1.09364 |

| | | | |
|---|---|---|---|
| H | 0.934972 | 1.650449 | -0.56701 |
| C | -0.12144 | 1.212879 | -2.36531 |
| H | -0.58176 | 1.929981 | -3.05323 |
| C | -1.11981 | 0.024392 | -2.2959 |
| O | -1.50507 | -0.51763 | -3.32555 |
| C | 1.218443 | 0.719927 | -2.96327 |
| H | 0.980061 | 0.283858 | -3.93785 |
| H | 1.864331 | 1.59059 | -3.13005 |
| C | 1.916018 | -0.28934 | -2.09784 |
| C | 1.744278 | -1.65385 | -2.14297 |
| H | 1.130481 | -2.24245 | -2.81178 |
| C | 2.817915 | -0.02916 | -1.00718 |
| N | 2.488673 | -2.25504 | -1.14449 |
| H | 2.555715 | -3.24727 | -0.98868 |
| C | 3.158467 | -1.28773 | -0.4274 |
| C | 3.372357 | 1.14171 | -0.45344 |
| H | 3.153154 | 2.115068 | -0.88793 |
| C | 4.006003 | -1.39847 | 0.678873 |
| H | 4.248519 | -2.36583 | 1.112303 |
| C | 4.214397 | 1.03664 | 0.650357 |
| H | 4.650424 | 1.934378 | 1.081522 |
| C | 4.526553 | -0.22074 | 1.212156 |
| H | 5.190285 | -0.27256 | 2.071268 |
| N | -1.48075 | -0.33767 | -1.04278 |
| H | -1.03396 | 0.14381 | -0.27671 |
| C | -2.44388 | -1.35263 | -0.6719 |
| H | -2.66581 | -1.94231 | -1.56796 |
| C | -3.80546 | -0.77145 | -0.19558 |
| O | -4.65073 | -1.51386 | 0.292404 |
| C | -1.84056 | -2.27957 | 0.423742 |
| H | -2.65354 | -2.90547 | 0.803614 |
| H | -1.09493 | -2.92275 | -0.05789 |
| C | -1.18805 | -1.47795 | 1.526717 |
| C | 0.188893 | -1.21799 | 1.486177 |
| H | 0.793416 | -1.68092 | 0.711845 |
| C | -1.94855 | -0.84894 | 2.525979 |
| H | -3.01998 | -1.02953 | 2.570242 |
| C | 0.798033 | -0.35315 | 2.397308 |
| H | 1.86788 | -0.15909 | 2.332234 |
| C | -1.35622 | 0.013451 | 3.448864 |
| H | -1.94708 | 0.497578 | 4.221673 |

| | | | |
|---|---|---|---|
| C | 0.020293 | 0.269557 | 3.381103 |
| O | 0.551679 | 1.146142 | 4.295111 |
| H | 1.504103 | 1.208203 | 4.148422 |
| N | -3.98775 | 0.561043 | -0.36415 |
| H | -3.29427 | 1.178199 | -0.76838 |
| H | -4.87984 | 0.947483 | -0.09474 |

### A.2.4 CONFORMER B3

54

Coordinates from A99-0001

| | | | |
|---|---|---|---|
| H | -2.612 | -1.00936 | 1.596003 |
| C | -3.20981 | -0.46112 | 0.856713 |
| H | -4.24455 | -0.80842 | 0.933512 |
| H | -3.15367 | 0.607054 | 1.092518 |
| C | -2.67917 | -0.79943 | -0.5277 |
| O | -2.88214 | -1.88756 | -1.06421 |
| N | -1.92141 | 0.175538 | -1.11493 |
| H | -1.70418 | 1.002995 | -0.57633 |
| C | -1.2392 | -0.01457 | -2.39232 |
| H | -1.95484 | -0.44995 | -3.09786 |
| C | -0.05342 | -1.01617 | -2.35011 |
| O | 0.475637 | -1.38871 | -3.39104 |
| C | -0.73592 | 1.341765 | -2.94421 |
| H | -0.30933 | 1.134748 | -3.93011 |
| H | -1.60066 | 2.002576 | -3.0812 |
| C | 0.287304 | 1.993231 | -2.05942 |
| C | 1.647946 | 1.794985 | -2.11196 |
| H | 2.223741 | 1.19427 | -2.80334 |
| C | 0.044763 | 2.856199 | -0.93371 |
| N | 2.263427 | 2.485385 | -1.0841 |
| H | 3.256877 | 2.529397 | -0.92823 |
| C | 1.309342 | 3.147449 | -0.34148 |
| C | -1.11527 | 3.40889 | -0.35558 |
| H | -2.09305 | 3.227538 | -0.79799 |
| C | 1.436166 | 3.943134 | 0.801055 |
| H | 2.407715 | 4.144747 | 1.245913 |
| C | -0.994 | 4.198612 | 0.784181 |

| | | | |
|---|---|---|---|
| H | -1.88325 | 4.626739 | 1.239562 |
| C | 0.268846 | 4.460619 | 1.358329 |
| H | 0.331931 | 5.078346 | 2.250123 |
| N | 0.329249 | -1.38965 | -1.10632 |
| H | -0.14604 | -0.95944 | -0.32676 |
| C | 1.360822 | -2.34742 | -0.76942 |
| H | 1.955483 | -2.525 | -1.6722 |
| C | 0.807102 | -3.73622 | -0.34361 |
| O | 1.567226 | -4.58646 | 0.107926 |
| C | 2.274202 | -1.76679 | 0.348127 |
| H | 2.942999 | -2.5701 | 0.670617 |
| H | 2.87292 | -0.96315 | -0.09577 |
| C | 1.461139 | -1.22116 | 1.499616 |
| C | 0.912568 | -2.06805 | 2.473051 |
| H | 1.154845 | -3.1277 | 2.455379 |
| C | 1.118502 | 0.139948 | 1.540045 |
| H | 1.524974 | 0.809202 | 0.787525 |
| C | 0.045812 | -1.56968 | 3.447753 |
| H | -0.37501 | -2.23809 | 4.198598 |
| C | 0.249511 | 0.653721 | 2.502237 |
| H | -0.01101 | 1.708412 | 2.509881 |
| C | -0.29473 | -0.20937 | 3.460425 |
| O | -1.16078 | 0.326289 | 4.382313 |
| H | -1.43807 | -0.36891 | 4.99223 |
| N | -0.52305 | -3.93499 | -0.51073 |
| H | -1.15406 | -3.23707 | -0.88529 |
| H | -0.89159 | -4.84469 | -0.27776 |

### A.2.5 CONFORMER B4

54

Coordinates from A99-0017

| | | | |
|---|---|---|---|
| H | -0.83237 | -3.64572 | 1.099726 |
| C | -0.22067 | -3.20163 | 1.893646 |
| H | -0.80876 | -2.41841 | 2.389458 |
| H | 0.029632 | -3.96086 | 2.639699 |
| C | 1.065495 | -2.57727 | 1.374258 |
| O | 2.01335 | -2.3125 | 2.111851 |
| N | 1.076199 | -2.28726 | 0.038381 |

| | | | |
|---|---|---|---|
| H | 0.230555 | -2.42523 | -0.50048 |
| C | 2.16591 | -1.56704 | -0.60884 |
| H | 3.110682 | -2.03306 | -0.31127 |
| C | 2.315552 | -0.08556 | -0.17842 |
| O | 3.328993 | 0.535079 | -0.48154 |
| C | 2.024463 | -1.66806 | -2.1518 |
| H | 2.828779 | -1.06025 | -2.57989 |
| H | 2.201383 | -2.71131 | -2.43905 |
| C | 0.686553 | -1.22109 | -2.6626 |
| C | -0.37029 | -2.04219 | -2.99237 |
| H | -0.41752 | -3.1237 | -3.02204 |
| C | 0.223068 | 0.130691 | -2.84294 |
| N | -1.46594 | -1.27801 | -3.35531 |
| H | -2.33134 | -1.64021 | -3.71953 |
| C | -1.12923 | 0.05832 | -3.28554 |
| C | 0.821733 | 1.394207 | -2.68217 |
| H | 1.84913 | 1.478148 | -2.33974 |
| C | -1.89299 | 1.199868 | -3.55462 |
| H | -2.92695 | 1.128066 | -3.884 |
| C | 0.067024 | 2.530411 | -2.95271 |
| H | 0.51564 | 3.51294 | -2.83058 |
| C | -1.27622 | 2.435805 | -3.38 |
| H | -1.83882 | 3.344529 | -3.57744 |
| N | 1.267796 | 0.429838 | 0.505187 |
| H | 0.463922 | -0.16209 | 0.65418 |
| C | 1.20214 | 1.758501 | 1.081704 |
| H | 1.951133 | 2.375785 | 0.574581 |
| C | 1.57344 | 1.808983 | 2.590587 |
| O | 1.452986 | 2.85961 | 3.211778 |
| C | -0.20756 | 2.369501 | 0.849617 |
| H | -0.25349 | 3.291809 | 1.436098 |
| H | -0.29543 | 2.615318 | -0.2128 |
| C | -1.30751 | 1.410834 | 1.242945 |
| C | -1.96672 | 0.651618 | 0.266535 |
| H | -1.73883 | 0.820712 | -0.78256 |
| C | -1.61983 | 1.170097 | 2.591465 |
| H | -1.1167 | 1.748066 | 3.362696 |
| C | -2.90568 | -0.32207 | 0.618524 |
| H | -3.4108 | -0.90197 | -0.15415 |
| C | -2.55369 | 0.202039 | 2.95761 |
| H | -2.79424 | 0.021675 | 4.001705 |

| | | | |
|---|---|---|---|
| C | -3.19842 | -0.55205 | 1.968259 |
| O | -4.10024 | -1.50384 | 2.380815 |
| H | -4.50031 | -1.91332 | 1.603644 |
| N | 2.026038 | 0.659145 | 3.14633 |
| H | 2.134421 | -0.20888 | 2.636559 |
| H | 2.312148 | 0.689815 | 4.113255 |

### A.2.6 CONFORMER B5

54

Coordinates from A99-0011

| | | | |
|---|---|---|---|
| H | 0.287565 | 2.762632 | -2.84118 |
| C | -0.77796 | 2.695869 | -3.08961 |
| H | -1.33634 | 3.446247 | -2.51901 |
| H | -0.91384 | 2.925745 | -4.15253 |
| C | -1.38012 | 1.324691 | -2.81503 |
| O | -2.57778 | 1.093995 | -2.97367 |
| N | -0.50108 | 0.377024 | -2.3725 |
| H | 0.462104 | 0.636421 | -2.20891 |
| C | -0.88321 | -1.01366 | -2.14351 |
| H | -1.57405 | -1.30099 | -2.94497 |
| C | -1.68459 | -1.27038 | -0.84245 |
| O | -2.09192 | -2.39843 | -0.58992 |
| C | 0.355692 | -1.93657 | -2.1929 |
| H | -0.01353 | -2.95483 | -2.04039 |
| H | 0.784855 | -1.88205 | -3.20094 |
| C | 1.398081 | -1.59668 | -1.16872 |
| C | 1.468224 | -2.06784 | 0.123211 |
| H | 0.809868 | -2.75565 | 0.636605 |
| C | 2.497798 | -0.68386 | -1.32731 |
| N | 2.565482 | -1.52646 | 0.762444 |
| H | 2.767458 | -1.61163 | 1.745877 |
| C | 3.208506 | -0.66043 | -0.08912 |
| C | 2.959072 | 0.116418 | -2.39055 |
| H | 2.454177 | 0.098982 | -3.35489 |
| C | 4.348398 | 0.128915 | 0.099526 |
| H | 4.90934 | 0.095501 | 1.030937 |
| C | 4.080349 | 0.920632 | -2.19744 |
| H | 4.444849 | 1.541279 | -3.0121 |

| | | | |
|---|---|---|---|
| C | 4.768986 | 0.925775 | -0.96507 |
| H | 5.653047 | 1.547609 | -0.85044 |
| N | -1.91995 | -0.18603 | -0.06245 |
| H | -1.48949 | 0.687275 | -0.32297 |
| C | -2.7827 | -0.20566 | 1.104014 |
| H | -2.65904 | -1.17113 | 1.604199 |
| C | -4.29462 | -0.08174 | 0.786526 |
| O | -5.11467 | -0.27821 | 1.673747 |
| C | -2.38653 | 0.936418 | 2.073684 |
| H | -2.61286 | 1.89818 | 1.592569 |
| H | -3.03363 | 0.845926 | 2.951015 |
| C | -0.92713 | 0.874198 | 2.443708 |
| C | -0.46201 | -0.05185 | 3.387812 |
| H | -1.17704 | -0.68029 | 3.915023 |
| C | 0.015424 | 1.673136 | 1.785482 |
| H | -0.32214 | 2.411908 | 1.059794 |
| C | 0.89833 | -0.19045 | 3.658715 |
| H | 1.253862 | -0.90743 | 4.394438 |
| C | 1.381958 | 1.545216 | 2.037672 |
| H | 2.104415 | 2.157335 | 1.500897 |
| C | 1.823428 | 0.602415 | 2.970234 |
| O | 3.159856 | 0.39223 | 3.228153 |
| H | 3.676607 | 0.965764 | 2.64643 |
| N | -4.61739 | 0.308184 | -0.47422 |
| H | -3.93557 | 0.394419 | -1.21705 |
| H | -5.59722 | 0.37054 | -0.7063 |

### A.2.7 CONFORMER B6

54

Coordinates from A99-0005

| | | | |
|---|---|---|---|
| H | 2.402546 | -3.3964 | 0.219682 |
| C | 2.246387 | -3.6192 | -0.84186 |
| H | 3.056838 | -3.17826 | -1.43303 |
| H | 2.285008 | -4.70412 | -0.99272 |
| C | 0.915822 | -3.109 | -1.37693 |
| O | 0.595348 | -3.23894 | -2.55877 |
| N | 0.113871 | -2.49153 | -0.46125 |

| | | | |
|---|---|---|---|
| H | 0.451158 | -2.37124 | 0.484391 |
| C | -1.24063 | -2.0369 | -0.76404 |
| H | -1.68321 | -2.76944 | -1.45029 |
| C | -1.32979 | -0.69972 | -1.54211 |
| O | -2.42653 | -0.25099 | -1.85451 |
| C | -2.09908 | -1.97546 | 0.521042 |
| H | -3.09649 | -1.65255 | 0.20986 |
| H | -2.18276 | -2.99345 | 0.920739 |
| C | -1.54925 | -1.05205 | 1.567346 |
| C | -1.83478 | 0.287382 | 1.715771 |
| H | -2.50073 | 0.911515 | 1.135104 |
| C | -0.57442 | -1.3728 | 2.575245 |
| N | -1.11361 | 0.808129 | 2.77011 |
| H | -1.06577 | 1.784223 | 3.018785 |
| C | -0.31037 | -0.17285 | 3.301832 |
| C | 0.107738 | -2.55038 | 2.942016 |
| H | -0.09609 | -3.49002 | 2.43138 |
| C | 0.623861 | -0.11762 | 4.340989 |
| H | 0.816439 | 0.809069 | 4.876438 |
| C | 1.039404 | -2.49894 | 3.976114 |
| H | 1.571811 | -3.40133 | 4.266374 |
| C | 1.298731 | -1.29355 | 4.664296 |
| H | 2.033187 | -1.28431 | 5.465515 |
| N | -0.14699 | -0.12142 | -1.87845 |
| H | 0.701178 | -0.55591 | -1.5493 |
| C | -0.02457 | 0.990316 | -2.80296 |
| H | -0.96457 | 1.548928 | -2.76654 |
| C | 0.164586 | 0.575139 | -4.28629 |
| O | 0.188956 | 1.439313 | -5.15417 |
| C | 1.139863 | 1.916778 | -2.37873 |
| H | 2.076184 | 1.341425 | -2.40187 |
| H | 1.217547 | 2.700757 | -3.13848 |
| C | 0.919288 | 2.496923 | -1.00537 |
| C | -0.00456 | 3.531575 | -0.81131 |
| H | -0.51895 | 3.958658 | -1.6696 |
| C | 1.56531 | 1.967264 | 0.119101 |
| H | 2.29061 | 1.166362 | -0.01123 |
| C | -0.29062 | 4.010484 | 0.46781 |
| H | -1.02188 | 4.805627 | 0.608025 |
| C | 1.297959 | 2.436622 | 1.404385 |
| H | 1.788799 | 2.006805 | 2.27231 |

| | | | |
|---|---|---|---|
| C | 0.355773 | 3.452582 | 1.57576 |
| O | 0.057237 | 3.830691 | 2.873915 |
| H | -0.52263 | 4.602671 | 2.849411 |
| N | 0.330245 | -0.74947 | -4.53271 |
| H | 0.243614 | -1.46694 | -3.82296 |
| H | 0.424872 | -1.03417 | -5.4961 |

## A.3 Ac-Trp-Tyr-Ser-$NH_2$

### A.3.1 CONFORMER 1

65

Coordinates from ORCA-job str10

| | | | |
|---|---|---|---|
| H | 0.199856 | 0.853644 | -0.012131 |
| C | 1.159992 | 0.846610 | -0.565196 |
| H | 1.916567 | 1.339605 | 0.080883 |
| H | 1.047606 | 1.402654 | -1.515932 |
| C | 1.597998 | -0.590869 | -0.752075 |
| O | 1.677888 | -1.383712 | 0.202165 |
| N | 1.959165 | -0.932148 | -2.035383 |
| H | 1.587109 | -0.339602 | -2.787251 |
| C | 2.293450 | -2.298243 | -2.424050 |
| H | 2.475503 | -2.853183 | -1.480981 |
| C | 1.131231 | -2.959964 | -3.215076 |
| H | 1.464437 | -3.975590 | -3.503272 |
| H | 0.265559 | -3.061013 | -2.528719 |
| C | 0.788020 | -2.139342 | -4.423202 |
| C | 1.373534 | -2.252284 | -5.677409 |
| H | 2.079028 | -3.002524 | -6.058224 |
| N | 0.935862 | -1.227725 | -6.493280 |
| H | 1.345933 | -1.067763 | -7.417005 |
| C | 0.080063 | -0.408195 | -5.789905 |
| C | -0.584570 | 0.771461 | -6.172243 |
| H | -0.470211 | 1.185334 | -7.184943 |

| | | | |
|---|---|---|---|
| C | -1.390707 | 1.401940 | -5.217595 |
| H | -1.917020 | 2.329551 | -5.484648 |
| C | -1.542440 | 0.866631 | -3.912308 |
| H | -2.193017 | 1.383119 | -3.191112 |
| C | -0.882707 | -0.306266 | -3.531211 |
| H | -1.009479 | -0.716616 | -2.518189 |
| C | -0.049016 | -0.962717 | -4.470106 |
| C | 3.594224 | -2.394735 | -3.248336 |
| O | 3.996075 | -3.501219 | -3.650779 |
| N | 4.231870 | -1.219931 | -3.531061 |
| H | 3.931027 | -0.439732 | -2.935226 |
| C | 5.639936 | -1.171664 | -3.950799 |
| H | 5.833526 | -0.100109 | -4.168211 |
| C | 6.632831 | -1.631479 | -2.835636 |
| H | 6.736582 | -2.731235 | -2.894750 |
| H | 7.622415 | -1.194461 | -3.072088 |
| C | 6.102107 | -1.212025 | -1.491318 |
| C | 6.079384 | 0.140335 | -1.094081 |
| H | 6.656242 | 0.883484 | -1.668312 |
| C | 5.279154 | 0.569862 | -0.024202 |
| H | 5.219578 | 1.632096 | 0.255260 |
| C | 4.478640 | -0.360403 | 0.667689 |
| O | 3.575698 | 0.097512 | 1.590886 |
| H | 2.802356 | -0.521797 | 1.525670 |
| C | 4.590379 | -1.731886 | 0.359519 |
| H | 3.989022 | -2.456826 | 0.925455 |
| C | 5.381177 | -2.142552 | -0.717774 |
| H | 5.396250 | -3.204256 | -1.009433 |
| C | 5.916909 | -1.945270 | -5.253866 |
| O | 7.008033 | -2.494424 | -5.443646 |
| N | 4.922222 | -1.943177 | -6.189500 |
| H | 3.999488 | -1.547071 | -5.984167 |
| C | 5.034300 | -2.816666 | -7.341427 |
| H | 6.059579 | -2.710075 | -7.760613 |
| C | 4.872194 | -4.305645 | -6.908424 |
| H | 4.861981 | -4.952469 | -7.813170 |
| H | 5.772433 | -4.558543 | -6.305857 |
| O | 3.673238 | -4.535717 | -6.198174 |
| H | 3.830046 | -4.220496 | -5.269644 |
| C | 4.010790 | -2.400294 | -8.400228 |
| O | 3.129592 | -1.554604 | -8.194134 |
| N | 4.141841 | -3.039394 | -9.595635 |
| H | 4.848528 | -3.758178 | -9.747817 |
| H | 3.445732 | -2.863838 | -10.321013 |

### A.3.2 CONFORMER 2

65

Coordinates from ORCA-job str33

| | | | |
|---|---|---|---|
| H | 0.386817 | 0.224444 | -0.039477 |
| C | 1.322481 | 0.225400 | -0.629443 |
| H | 2.113733 | 0.791497 | -0.098285 |
| H | 1.154176 | 0.740458 | -1.599346 |
| C | 1.848971 | -1.153919 | -0.953699 |
| O | 2.891416 | -1.327820 | -1.623935 |
| N | 1.102865 | -2.215310 | -0.526645 |
| H | 0.184078 | -2.033472 | -0.107264 |
| C | 1.414420 | -3.588783 | -0.917297 |
| H | 2.520690 | -3.673042 | -0.940862 |
| C | 0.821138 | -4.602330 | 0.081353 |
| H | 1.118298 | -5.604194 | -0.282917 |
| H | 1.283536 | -4.442770 | 1.076688 |
| C | -0.675075 | -4.500398 | 0.161746 |
| C | -1.584852 | -5.189443 | -0.625140 |
| H | -1.393327 | -5.944660 | -1.394433 |
| N | -2.873104 | -4.770097 | -0.327703 |
| H | -3.722152 | -5.134124 | -0.754918 |
| C | -2.827322 | -3.792030 | 0.648641 |
| C | -3.858223 | -3.048602 | 1.247514 |
| H | -4.911955 | -3.204281 | 0.972319 |
| C | -3.493139 | -2.089660 | 2.200546 |
| H | -4.274336 | -1.486072 | 2.683569 |
| C | -2.135005 | -1.881292 | 2.552256 |
| H | -1.885577 | -1.122453 | 3.308051 |
| C | -1.111464 | -2.626711 | 1.957907 |
| H | -0.060601 | -2.462463 | 2.240333 |
| C | -1.446937 | -3.597616 | 0.982862 |
| C | 0.943624 | -3.952637 | -2.355173 |
| O | 1.002380 | -5.110591 | -2.776622 |
| N | 0.521800 | -2.878449 | -3.082372 |
| H | 0.316991 | -2.026134 | -2.555501 |
| C | -0.038110 | -2.912704 | -4.417508 |
| H | 0.176314 | -3.918832 | -4.836267 |
| C | -1.574624 | -2.660060 | -4.378737 |
| H | -1.899757 | -2.454913 | -5.416791 |
| H | -2.068566 | -3.581865 | -4.013875 |
| C | -1.871175 | -1.506131 | -3.447859 |

| | | | |
|---|---|---|---|
| C | -2.216841 | -1.754500 | -2.101955 |
| H | -2.418445 | -2.786999 | -1.783161 |
| C | -2.274257 | -0.726771 | -1.150864 |
| H | -2.536624 | -0.933887 | -0.102984 |
| C | -1.971657 | 0.590975 | -1.544514 |
| O | -1.969455 | 1.558119 | -0.572515 |
| H | -1.711179 | 2.401420 | -0.996417 |
| C | -1.655259 | 0.865021 | -2.889559 |
| H | -1.424806 | 1.898577 | -3.196918 |
| C | -1.604520 | -0.174862 | -3.829190 |
| H | -1.321781 | 0.039022 | -4.870358 |
| C | 0.639560 | -1.849106 | -5.313594 |
| O | 0.077388 | -1.464603 | -6.361116 |
| N | 1.833364 | -1.373587 | -4.884727 |
| H | 2.181331 | -1.697957 | -3.974163 |
| C | 2.521000 | -0.244791 | -5.521554 |
| H | 1.737448 | 0.498292 | -5.786416 |
| C | 3.534863 | 0.372345 | -4.545412 |
| H | 4.354716 | -0.363970 | -4.389397 |
| H | 3.990249 | 1.245660 | -5.058018 |
| O | 2.941282 | 0.794257 | -3.329095 |
| H | 3.101574 | 0.072415 | -2.666336 |
| C | 3.244994 | -0.683588 | -6.826819 |
| O | 4.473598 | -0.758382 | -6.901768 |
| N | 2.389696 | -0.928304 | -7.861948 |
| H | 1.389430 | -1.063357 | -7.634324 |
| H | 2.792703 | -1.356160 | -8.698694 |

### A.3.3 CONFORMER 3

65

Coordinates from ORCA-job str12

| | | | |
|---|---|---|---|
| H | -0.677606 | 0.722412 | -0.856758 |
| C | 0.182805 | 0.555015 | -0.179383 |
| H | -0.183497 | 0.283327 | 0.830337 |
| H | 0.771167 | 1.490178 | -0.073094 |
| C | 1.137315 | -0.518835 | -0.658421 |
| O | 2.135610 | -0.852642 | 0.002765 |
| N | 0.853087 | -1.053205 | -1.893094 |
| H | -0.089031 | -0.905839 | -2.272994 |
| C | 1.653585 | -2.103254 | -2.513484 |

| | | | |
|---|---|---|---|
| H | 2.536285 | -2.244211 | -1.857391 |
| C | 0.860907 | -3.436071 | -2.634299 |
| H | 1.581552 | -4.216338 | -2.945568 |
| H | 0.478178 | -3.699064 | -1.626772 |
| C | -0.230746 | -3.316065 | -3.657403 |
| C | -0.107520 | -3.712534 | -4.983012 |
| H | 0.712116 | -4.277521 | -5.442715 |
| N | -1.199322 | -3.280398 | -5.719796 |
| H | -1.271060 | -3.298834 | -6.754895 |
| C | -2.045993 | -2.579914 | -4.885438 |
| C | -3.258284 | -1.927539 | -5.173488 |
| H | -3.661536 | -1.918022 | -6.196783 |
| C | -3.923431 | -1.298473 | -4.115488 |
| H | -4.876325 | -0.784892 | -4.306702 |
| C | -3.400308 | -1.326071 | -2.796960 |
| H | -3.963179 | -0.843657 | -1.984799 |
| C | -2.191964 | -1.971337 | -2.511406 |
| H | -1.810355 | -2.009339 | -1.478730 |
| C | -1.480346 | -2.600194 | -3.564742 |
| C | 2.183166 | -1.718005 | -3.915293 |
| O | 2.896104 | -2.509177 | -4.550636 |
| N | 1.726255 | -0.521896 | -4.407882 |
| H | 1.337119 | 0.085940 | -3.679895 |
| C | 2.311749 | 0.198776 | -5.545157 |
| H | 1.809050 | 1.186030 | -5.551395 |
| C | 3.845080 | 0.469869 | -5.379374 |
| H | 4.398108 | -0.467618 | -5.582188 |
| H | 4.119944 | 1.217175 | -6.149085 |
| C | 4.073089 | 0.927316 | -3.962101 |
| C | 3.577772 | 2.169234 | -3.512762 |
| H | 3.258867 | 2.924865 | -4.249165 |
| C | 3.403212 | 2.429610 | -2.145703 |
| H | 2.963427 | 3.374558 | -1.794604 |
| C | 3.718067 | 1.433913 | -1.198835 |
| O | 3.360611 | 1.625470 | 0.109000 |
| H | 3.126223 | 0.721285 | 0.448358 |
| C | 4.345810 | 0.246801 | -1.629514 |
| H | 4.628834 | -0.509078 | -0.883965 |
| C | 4.504293 | -0.003328 | -2.996592 |
| H | 4.902031 | -0.973401 | -3.330448 |
| C | 2.033127 | -0.414383 | -6.920026 |
| O | 2.413670 | 0.164576 | -7.951160 |
| N | 1.395555 | -1.617619 | -6.933592 |
| H | 0.959719 | -1.972450 | -6.075595 |
| C | 1.262086 | -2.381910 | -8.169634 |

| | | | |
|---|---|---|---|
| H | 2.073182 | -2.017375 | -8.831567 |
| C | 1.428895 | -3.884824 | -7.898769 |
| H | 0.464948 | -4.291076 | -7.512045 |
| H | 1.608144 | -4.395426 | -8.867625 |
| O | 2.522154 | -4.184157 | -7.050094 |
| H | 2.582661 | -3.498656 | -6.341779 |
| C | -0.104195 | -2.018097 | -8.778001 |
| O | -1.147544 | -2.649462 | -8.535362 |
| N | -0.054886 | -0.904106 | -9.555395 |
| H | 0.786046 | -0.315268 | -9.491649 |
| H | -0.941408 | -0.482090 | -9.841907 |

### A.3.4 CONFORMER 4

65

Coordinates from ORCA-job str6

| | | | |
|---|---|---|---|
| H | 0.123403 | 0.460645 | 0.070788 |
| C | 1.169887 | 0.107715 | 0.132445 |
| H | 1.357911 | -0.216895 | 1.178853 |
| H | 1.868539 | 0.934134 | -0.111377 |
| C | 1.336832 | -1.094505 | -0.779768 |
| O | 0.436115 | -1.914039 | -0.984542 |
| N | 2.607760 | -1.235503 | -1.307959 |
| H | 3.234619 | -0.422908 | -1.284670 |
| C | 2.925117 | -2.267512 | -2.286342 |
| H | 1.982039 | -2.827545 | -2.465879 |
| C | 3.441914 | -1.656020 | -3.615631 |
| H | 3.678589 | -2.499760 | -4.292221 |
| H | 2.618599 | -1.067269 | -4.069599 |
| C | 4.654914 | -0.808880 | -3.366871 |
| C | 5.967091 | -1.260484 | -3.328370 |
| H | 6.378358 | -2.245013 | -3.586281 |
| N | 6.800281 | -0.245510 | -2.900437 |
| H | 7.787001 | -0.417779 | -2.690202 |
| C | 6.054795 | 0.880566 | -2.625523 |
| C | 6.439938 | 2.141859 | -2.135754 |
| H | 7.492242 | 2.365762 | -1.906858 |
| C | 5.436849 | 3.098738 | -1.943023 |
| H | 5.707636 | 4.092036 | -1.557197 |
| C | 4.079144 | 2.813243 | -2.239084 |
| H | 3.319867 | 3.594238 | -2.085755 |

| | | | |
|---|---|---|---|
| C | 3.694809 | 1.560005 | -2.728133 |
| H | 2.640136 | 1.350380 | -2.965233 |
| C | 4.684516 | 0.564707 | -2.922982 |
| C | 3.937498 | -3.305434 | -1.766171 |
| O | 4.277321 | -4.266477 | -2.480729 |
| N | 4.427196 | -3.093528 | -0.510770 |
| H | 3.916666 | -2.378704 | 0.019296 |
| C | 5.064538 | -4.159059 | 0.270559 |
| H | 5.444919 | -3.669010 | 1.192031 |
| C | 4.049098 | -5.251496 | 0.677311 |
| H | 3.653518 | -5.698862 | -0.256518 |
| H | 4.612145 | -6.040422 | 1.211455 |
| C | 2.944267 | -4.674076 | 1.525789 |
| C | 3.052822 | -4.629501 | 2.932000 |
| H | 3.928933 | -5.087926 | 3.417717 |
| C | 2.068995 | -4.023918 | 3.723999 |
| H | 2.148821 | -4.001048 | 4.820589 |
| C | 0.945365 | -3.433495 | 3.111592 |
| O | 0.008438 | -2.849568 | 3.924657 |
| H | -0.718826 | -2.537075 | 3.349558 |
| C | 0.821369 | -3.461313 | 1.710048 |
| H | -0.036254 | -2.987133 | 1.206247 |
| C | 1.811953 | -4.080184 | 0.934337 |
| H | 1.682816 | -4.093075 | -0.158278 |
| C | 6.288565 | -4.779828 | -0.434952 |
| O | 6.578651 | -5.972013 | -0.286086 |
| N | 7.061829 | -3.919524 | -1.161464 |
| H | 6.757608 | -2.957041 | -1.339459 |
| C | 8.113538 | -4.447707 | -2.008206 |
| H | 8.709482 | -5.176334 | -1.415295 |
| C | 7.500382 | -5.225350 | -3.210887 |
| H | 8.315931 | -5.557395 | -3.891875 |
| H | 7.013163 | -6.129965 | -2.785768 |
| O | 6.601665 | -4.436052 | -3.962020 |
| H | 5.743772 | -4.437023 | -3.461549 |
| C | 9.023746 | -3.300215 | -2.457529 |
| O | 8.773914 | -2.109939 | -2.223288 |
| N | 10.141668 | -3.692251 | -3.130290 |
| H | 10.275149 | -4.661701 | -3.416483 |
| H | 10.722847 | -2.970286 | -3.558254 |